REPORT DOCUMENTATION PAGE

AFRL-SR-AR-TR-05-

0028

1. REPORT DATE *(DD-MM-YYYY)*	2. REPORT TYPE	3. DATES COVERED *(From - To)*
3-Jan- 2005	Final	1 Nov 2000 - 30 Nov 2004

4. TITLE AND SUBTITLE

Combined Direct-Adjoint Approximations for Large-Scale Design-Oriented Structural-Acoustics Finite-Element Analysis

5a. CONTRACT NUMBER

5b. GRANT NUMBER

F49620-01-1-0102

5c. PROGRAM ELEMENT NUMBER

6. AUTHOR(S)

Eli Livine
Levent Coskuner

5d. PROJECT NUMBER

5e. TASK NUMBER

5f. WORK UNIT NUMBER

7. PERFORMING ORGANIZATION NAME(S) AND ADDRESS(ES)

Department of Aeronautics and Astronautics
University of Washington
Seattle, WA 98195-2400

8. PERFORMING ORGANIZATION REPORT NUMBER

9. SPONSORING/MONITORING AGENCY NAME(S) AND ADDRESS(ES)

Air Force Office of Scientific Research
4015 Wilson Blvd
Mail Room 713
Arlington, VA 22203

10. SPONSOR/MONITOR'S ACRONYM(S)

AFOSR

11. SPONSOR/MONITOR'S REPORT NUMBER(S)

12. DISTRIBUTION/AVAILABILITY STATEMENT

Distribution Statement A. Approved for public release; distribution is unlimited.

13. SUPPLEMENTARY NOTES

14. ABSTRACT

A second-order approximation method was developed for the design- oriented analysis and sensitivity approximations of large scale structural/acoustic problems. The method is based on combined utilization of low-order approximations of both direct and adjoint problems. A variety of approximation techniques for the first-order model order reduction of the direct and adjoint structural acoustic problems were tested. The overall consistent accuracy level of the second order method over wide frequency ranges and large variations of systems parameters was demonstrated.

15. SUBJECT TERMS

16. SECURITY CLASSIFICATION OF:			17. LIMITATION OF ABSTRACT	18. NUMBER OF PAGES	19a. NAME OF RESPONSIBLE PERSON
a. REPORT	b. ABSTRACT	c. THIS PAGE			Eli Livne
U	U	U	UU		19b. TELEPHONE NUMBER *(Include area code)* 206-543-6643

Combined Direct-Adjoint Approximations for Large-Scale Design-Oriented Structural-Acoustics Finite-Element Analysis

Levent Coskuner

A thesis submitted in partial fulfillment of the requirements for the degree of

Master of Science in Aeronautics and Astronautics

University of Washington

2004

Program Authorized to Offer Degree:

The Department of Aeronautics and Astronautics

University of Washington
Graduate School

This is to certify that I have examined this copy of a master's thesis by

Levent Coskuner

and have found that it is complete and satisfactory in all respects,
and that any and all revisions required by the final
examining committee have been made.

Committee Members:

_____
Eli Livne

_____
Uy-Loi Ly

Date:_____

In presenting this thesis in partial fulfillment of the requirements for a master's degree at the University of Washington, I agree that the Library shall make its copies freely available for inspection. I further agree that extensive copying of this thesis is allowable only for scholarly purposes, consistent with "fair use" as prescribed in the U.S. Copyright Law. Any other reproduction for any purposes or by any means shall not be allowed without my written permission.

Signature_____

Date_____

University of Washington

Abstract

Combined Direct-Adjoint Approximations for Large-Scale Design-Oriented Structural-Acoustics Finite-Element Analysis

Levent Coskuner

Chair of the Supervisory Committee
Dr. Eli Livne
Department of Aeronautics and Astronautics

A second-order combined approximate-direct/approximate-adjoint method for accurate and efficient reduced order calculation of frequency response for a structural acoustic enclosure modeled using finite elements is presented. A design-oriented approach was adopted: not only does the method account for responses itself (such as displacements, stresses and pressure levels) it also accounts for sensitivities of the responses with respect to design variables.

Approximate first order results were obtained using mode-displacement order reduction, reduced-order adjoint solutions based on Ritz vectors, and first order Taylor series. A combined second-order approximation incorporating those first-order approximations was then created for models with modified design variables, and was compared to full order results of a large finite-element problem. Accuracy of the second order method was quantified.

Table of Contents

List of Figures

List of Tables

List of Symbols

$[A]$ Coefficient matrix for a general linear set of equations

$[A_\phi]$ Reduced coefficient matrix for a general linear set of equations

$[C]$ Combined structural-acoustic damping matrix

$[C_s]$ Structural component of the damping matrix

$[K]$ Combined structural-acoustic stiffness matrix

$[K_a]$ Acoustic component of the stiffness matrix

$[K_s]$ Structural component of the stiffness matrix

$[M]$ Combined structural-acoustic mass matrix

$[M_a]$ Acoustic component of the mass matrix

$[M_s]$ Structural component mass matrix

$[R_{as}]$ Structural-acoustic interaction matrix

$[\Phi]$ Reduced order basis matrix obtained using Mode Displacement

$[\Psi]$ Reduced order basis matrix obtained using Ritz Vectors

$\{F\}$ Vector of generalized forces

$\{\overline{F}\}$ Fourier transformed vector of generalized forces

$\{F_\phi\}$ Reduced vector of generalized force

$\{b\}$ Right hand side of a general linear set of equations

$\{c\}$ Response recovery vector

$\{p\}$ Vector of generalized pressures

$\{q_s\}$ Vector of generalized structural displacements

$\{r\}$ Vector of generalized adjoint displacements

$\{u\}$	Displacement vector
$\{x\}$	Direct solution of a general linear set of equations
$\{\tilde{x}\}$	Approximate direct solution of a general linear set of equations
$\{\eta\}$	Adjoint solution vector of a general linear set of equations
$\{\tilde{\eta}\}$	Approximate adjoint solution vector of a general linear set of equations
DV	Design variables
j	The imaginary number $\sqrt{-1}$
y	Scalar response function
$\tilde{y}$	Approximation of a scalar response function
δ	Error entity
ρ_o	Density of the acoustic fluid
ω	Frequency

Acknowledgements

The author wishes to express sincere thanks and appreciation to the Department of Aeronautics and Astronautics at the University of Washington for their support, and especially to Dr. Eli Livne whose extensive knowledge and immense patience has made this work possible.

Support for this research by the U.S. Air Force Office of Scientific Research is gratefully acknowledged with special thanks to Lt. Col. Robert Canfield for his encouragement and support.

Dedication

To my parents, my sister, and my wife, on whose support I could always count on.

Introduction

The examination of large-scale structural-acoustic finite-element models in the time or frequency domain is an important part in the analysis of complex physical structures, especially in the development of design optimization tools (Refs. 4, 7, 9, 12, 14, 15, 17, 25, 27, 29, 32, 36, 41). Such finite-element models often contain tens of thousands or even hundreds of thousands of degree of freedoms, translating to a system of equations of equally formidable size. Solving these systems of equations multiple times for every frequency in the frequency domain is expensive computationally (Ref.16). For design optimization problems where behavior sensitivities are required, and the system of equations have to be solved repetitively to drive the system towards its optimum, the cost of computation becomes prohibitive (Refs. 3, 13).

It is therefore desirable to replace the detailed large-scale models with computationally efficient approximations of reduced order, while preserving the accuracy of the simulation. Commonly used order reduction methods in multidisciplinary design optimization today include first-order Taylor series based direct and reciprocal models, Guyan reduction (Ref. 11), Ritz vectors (Ref. 38), Lanczos coordinates (Ref. 28) and Modal displacement (Refs. 4, 13, 14). These methods seek to create a group of reduced basis vectors from a reduced set of shape functions that will reduce the order of the problem. While accurate in predicting deformations, these methods are often inadequate to accurately predict

stress and sensitivity information, mainly because of the need to capture local effects in such cases. Furthermore, for structural-acoustic problems, methods involving modal approximations face an additional hurdle that in most of the separate structural and acoustic modes that are needed to approximate the problem are often far apart along the frequency band (Ref. 24).

To improve accuracy of approximations obtained using first order sensitivity information, a method combining solutions of the approximate direct and adjoint problems has been shown to accurately predict stresses for airframe structures in the frequency and time domain, as well as unsteady aerodynamic forces on wings in the frequency domain (Refs. 20, 22, 23). It was demonstrated that this combined direct and adjoint approximate approach has second order accuracy (Ref. 34), and is similar to the second-order accuracy shown by the Rayleigh Quotient approximation (Ref. 5).

The Second-Order Approximation (SOA) method presented in this thesis combines two first-order approximations of significantly reduced order to accurately calculate response and design sensitivities of a complex large-scale structural-acoustic problem with thousands of degrees of freedom, while reducing this original large-scale problem into a much more manageable and computationally efficient model of merely tens of equations. In this work, the first-order approximations used are the Modal Displacement (MD) method and the Ritz Vector (RV) method. Performances of these first order methods are compared to that of the SOA method, specifically when dealing with design

sensitivities, for which first-order methods are generally less accurate. Also, problems that arise when using modal approximation methods for models where material properties differ by several orders of magnitude (for example, the density of air compared to that of metal) or where modes of interest are very far apart in frequency range (for example, beam extensional modes compared to bending modes) are discussed.

A goal of the SOA method development presented here is to improve the efficiency of design cycles and contribute to the development of further design optimization tools, especially in cases where structural acoustic-enclosures are of interest such as the design of passenger compartments of cars, airplane cabins, vibration sensitive payloads of space vehicles and other structures where noise and vibration levels are of interest.

Chapter 1: Order Reduction of the Coupled Structural-Acoustic Problem

1.1 Coupled structural-acoustic problem

The Equations of motion for an acoustic enclosure coupled to a flexible structure is written as

$$[M_a]\{\ddot{p}\}+[K_a]\{p\}-\rho_0[R_{as}]\{\ddot{q}_s\}=0 \qquad (1)$$

The Equations for a flexible structure with such an enclosure, including viscous damping and an applied external force, is given by

$$[M_s]\{\ddot{q}_s\}+[C_s]\{\dot{q}_s\}+[K_s]\{q_s\}-[R_{as}]^T\{p\}=\{F\} \qquad (2)$$

where the matrices $[M_a]$ and $[K_a]$ are the acoustic mass and stiffness matrices respectively, and $[M_s],[C_s]$, and $[K_s]$, are the structural mass, damping and stiffness matrices.

The matrix $[R_{as}]$ is the structural-acoustic coupling matrix. The vectors $\{q_s(t)\},\{p(t)\}$, and $\{F(t)\}$ are the vectors of generalized structural displacement, pressures, and structural excitation forces. ρ_o is the density of the acoustic fluid.

Combining equations (1) and (2) in matrix form, the coupled structural-acoustic equations are obtained as

$$\begin{bmatrix} M_s & 0 \\ -\rho_0 R_{as} & M_a \end{bmatrix}\begin{Bmatrix} \ddot{q}_s \\ \ddot{p} \end{Bmatrix}+\begin{bmatrix} C_s & 0 \\ 0 & 0 \end{bmatrix}\begin{Bmatrix} \dot{q}_s \\ \dot{p} \end{Bmatrix}+\begin{bmatrix} K_s & -R^T{}_{as} \\ 0 & K_a \end{bmatrix}\begin{Bmatrix} q_s \\ p \end{Bmatrix}=\begin{Bmatrix} F \\ 0 \end{Bmatrix} \quad (3)$$

1.2 Full-order structural-acoustic model

In equation (3), the coupled structural-acoustic mass matrix is

$$[M]=\begin{bmatrix} M_s & 0 \\ -\rho_0 R_{as} & M_a \end{bmatrix} \quad (4)$$

the coupled structural-acoustic viscous-damping matrix is

$$[C]=\begin{bmatrix} C_s & 0 \\ 0 & 0 \end{bmatrix} \quad (5)$$

and the coupled structural-acoustic stiffness matrix is

$$[K]=\begin{bmatrix} K_s & -R^T{}_{as} \\ 0 & K_a \end{bmatrix} \quad (6)$$

The Fourier-transformed equations for a structural acoustic system in the frequency domain can then be written as

$$\left[-\omega^2[M]+j\omega[C]+[K]\right]\{u(j\omega)\}=\{\overline{F}(j\omega)\} \quad (7)$$

where [*M*], [*C*], and [*K*] are the matrices as shown in (4), (5) and (6), and

$$\{u(j\omega)\}=\begin{Bmatrix} q_s(j\omega) \\ p(j\omega) \end{Bmatrix}$$

$$\{\overline{F}(j\omega)\} = \begin{Bmatrix} F(j\omega) \\ 0 \end{Bmatrix}$$

ω is the frequency in rad/s.

Any linear responses obtained from the solution of equation (7) is

$$y(j\omega) = \{c\}^* \{u(j\omega)\} = \{\eta(j\omega)\}^* \{\overline{F}(j\omega)\} \qquad (8)$$

from which scalar responses such as stress, displacement, and pressure can be calculated.

The full-order adjoint formulation corresponding to equation (7) is

$$\left(-\omega^2[M] + j\omega[C] + [K]\right)^* \{\eta(j\omega)\} = \{c\} \qquad (9)$$

In both equations (8) and (9), the superscript * denotes the complex conjugate transpose of a complex matrix. Note that unlike in pure structural problems where the mass and stiffness matrices $[M]$ and $[K]$ are symmetric, in the coupled structural-acoustic formulation these matrices are non-symmetric. Also, in the adjoint formulation the vector $\{c\}$ is frequency-independent.

1.3 Reduced-order structural-acoustic model

The term "full-order" used in this work describes the complete system of equations corresponding to a finite-element model with a fine mesh and a large number of degrees of freedom. A "reduced-order" system is then a system of

equations with fewer equations used to approximate the "full-order" system. In the Modal Displacement (MD) method, a reduced-order system is obtained by multiplying a subset of modes (shape functions) in a reduced-basis matrix [Φ] with the vector of generalized displacements $\{q(j\omega)\}$ as written below in equation (10).

$$\{u_{MD}(t)\} \cong [\{\phi_1\},\{\phi_2\},\{\phi_3\},...,\{\phi_N\}]\{q(j\omega)\} = [\Phi]\{q(j\omega)\} \tag{10}$$

where N is the number of reduced-basis vectors used.

Similarly we can reduce the full-order equations given in (7). If we write this equation as

$$[A(j\omega)]\{u(j\omega)\} = \{\overline{F}(j\omega)\} \tag{11}$$

then $[A]$ is reduced by pre and post multiplication of $[\Phi]^*$ and $[\Phi]$ such that

$$[A_\Phi] = [\Phi]^*[A][\Phi] \tag{12}$$

and the generalized input force vector $\{F\}$ is also reduced such that

$$\{F_\Phi(j\omega)\} = [\Phi]^*\{\overline{F}(j\omega)\} \tag{13}$$

The complete reduced-order direct problem is then written as

$$[A_\Phi]\{q\{j\omega)\} = \{F_\Phi(j\omega)\} \tag{14}$$

A corresponding reduced-order adjoint frequency response problem can be found by using another reduced basis matrix [ψ] to approximate the full-order adjoint following the same steps used for the direct problem. Starting by reducing the generalized adjoint displacements $\{r(j\omega)\}$, such that

$$\{\tilde{\eta}(t)\} \cong [\{\psi_1\},\{\psi_2\},\{\psi_3\},...,\{\psi_{\hat{N}}\}]\{r(j\omega)\} = [\Psi]\{r(j\omega)\} \tag{15}$$

Simplifying the equation for full-order adjoint equation in (9) as

$$[A]^*\{\eta(j\omega)\} = \{c\} \tag{16}$$

then $[A]^*$ is reduced by pre and post multiplication by the basis matrices [ψ]* and [Ψ] such that

$$[A_\Psi] = [\Psi]^*[A][\Psi] \tag{17}$$

The reduced $\{c\}$ vector is then given by

$$\{c_\Psi\} = [\Psi]^*\{c\} \tag{18}$$

The complete reduced-order adjoint problem can then be written as

$$[A_\Psi]^*\{r(j\omega)\} = \{c_\Psi\} \tag{19}$$

1.4 Selection of reduced-order basis matrices

The reduced-order basis matrices [Φ] and [Ψ] are selected while taking into account such variables as spatial distribution of excitation forces, weights used to determine particular responses (the vector $\{c\}$), frequency oscillation as well as material properties. Utilization of natural modes of structures, "fictitious mass" modes, Ritz vectors and other sub-component modes have been studied over the years in the field of structural-dynamics (Refs. 2, 8, 18, 19, 21, 26, 30, 31, 35, 37). In the general structural-acoustic cases presented here, mode shape matrices (eigenvectors) can be complex.

In this work, the notation [Φ] is used to specifically denote the reduced-order basis matrix created using the Modal Displacement (MD) method while the notation [Ψ] is used to specifically denote the reduced-order basis matrix created using the Ritz Vector (RV) approach.

It is also noteworthy that [Φ] and [Ψ] can be interchanged between either the direct or adjoint formulation as long as it is used consistently. In other words, the direct problem can be reduced by [Φ] and the adjoint problem reduced by [Ψ], or the direct problem can be reduced by [Ψ] and the adjoint problem reduced by [Φ]. The advantages and shortcomings of either approach when it comes to creating first-order approximations to be used for the Second Order Approximation (SOA) will be presented and discussed in following chapters.

Chapter 2: A Second-Order Approximation using Combined Direct and Adjoint Solutions

2.1 Second-order approximation of scalar responses

A linear problem represented as a system of equations in matrix form

$$[A]\{x\} = \{b\} \tag{20}$$

can be solved for $\{x\}$ directly:

$$\{x\} = [A]^{-1}\{b\} \tag{21}$$

This system also has the complementary adjoint problem

$$[A]^{*}\{\eta\} = \{c\} \tag{22}$$

A full-order scalar response y can be found using either the direct or the adjoint solution, such that

$$y = \{c\}^{*}\{x\} = \{c\}^{*}[A]^{-1}\{b\} = \{\eta\}^{*}\{b\} \tag{23}$$

Approximate solutions of the direct (20) and adjoint (22) problems that can be obtained by solving equations (10) and (14) or (15) and (19), and the reduced-order scalar response $\tilde{y}$ can be written as

$$\tilde{y} = \{c\}^{*}\{\tilde{x}\} + \{\tilde{\eta}\}^{*}\{b\} - \{\tilde{\eta}\}^{*}[A]\{\tilde{x}\} \tag{24}$$

The ~ (tilde) symbol here is used to indicate that a quantity is an approximation of the variable named. Variables that do not have the ~ (tilde) symbol are full-order. The errors due to these approximations can be expressed as

$$\begin{aligned} \{\delta x\} &= \{x\} - \{\tilde{x}\} \\ \{\delta \eta\} &= \{\eta\} - \{\tilde{\eta}\} \\ \delta y &= y - \tilde{y} \end{aligned} \tag{25}$$

or

$$\begin{aligned} \{\tilde{x}\} &= \{x\} - \{\delta x\} \\ \{\tilde{\eta}\} &= \{\eta\} - \{\delta \eta\} \\ \tilde{y} &= y - \delta y \end{aligned} \tag{26}$$

Substituting these values into equation (24) shows that the error is second order

$$\delta y = -\delta \eta * A \delta x \tag{27}$$

For a discussion on the second-order nature of this approximation, please consult Appendix D.

2.2 Second order approximation of sensitivities

Design sensitivities are obtained by taking the derivative of the scalar response of interest with respect to the design variable of interest. For the reduced-order scalar response as written in equation (24) then, differentiating with respect to the design variable DV gives

$$\frac{\partial \tilde{y}}{\partial DV} = \frac{\partial}{\partial DV}(\{c\} * \{\tilde{x}\} + \{\tilde{\eta}\} * \{b\} - \{\tilde{\eta}\} * [A]\{\tilde{x}\}) \tag{28}$$

Here, the sensitivities of the approximate direct and approximate adjoint solutions, $\partial\{\tilde{x}\}/\partial DV$ and $\partial\{\tilde{\eta}\}/\partial DV$ are used along with the sensitivities of the full-order vectors and matrices $\partial\{b\}/\partial DV$, $\partial\{c\}/\partial DV$ and $\partial[A]/\partial DV$ to write the second order approximation.

Expanding equation (28),

$$\begin{aligned}\frac{\partial \tilde{y}}{\partial DV} &= \frac{\partial\{c\}^*}{\partial DV}\{\tilde{x}\} + \{c\} * \frac{\partial\{\tilde{x}\}}{\partial DV} + \frac{\partial\{\tilde{\eta}\}^*}{\partial DV}\{b\} + \{\tilde{\eta}\} * \frac{\partial\{b\}}{\partial DV} \\ &- \frac{\partial\{\tilde{\eta}\}^*}{\partial DV}[A]\{\tilde{x}\} - \{\tilde{\eta}\} * \frac{\partial[A]}{\partial DV}\{\tilde{x}\} - \{\tilde{\eta}\} * [A]\frac{\partial\{\tilde{x}\}}{\partial DV}\end{aligned} \tag{29}$$

and collecting terms,

$$\begin{aligned}\frac{\partial \tilde{y}}{\partial DV} &= (\{c\} * - \{\tilde{\eta}\} * [A])\frac{\partial\{\tilde{x}\}}{\partial DV} + \frac{\partial\{\tilde{\eta}\}^*}{\partial DV}(\{b\} - [A]\{\tilde{x}\}) \\ &- \{\tilde{\eta}\} * \frac{\partial[A]}{\partial DV}\{\tilde{x}\} + \frac{\partial\{c\}^*}{\partial DV}\{\tilde{x}\} + \{\tilde{\eta}\} * \frac{\partial\{b\}}{\partial DV}\end{aligned} \tag{30}$$

The term $(\{b\} - [A]\{\tilde{x}\})$ is the error vector of the full order equation (20) when the approximate direct solution is used to replace the exact solution. Likewise the term $(\{c\} * - \{\tilde{\eta}\} * [A])$ is the error vector of the full order equation (22) when the approximate adjoint solution is used instead of the exact solution. If the approximate direct and approximate adjoint solutions are accurate, that is the

quantities $(\{b\}-[A]\{\tilde{x}\})$ and $(\{c\}^{*}-\{\tilde{\eta}\}^{*}[A])$ are small, then the equation for the sensitivity of the second order approximation can be simplified as

$$\frac{\partial \tilde{y}}{\partial DV} \cong -\{\tilde{\eta}\}^{*}\frac{\partial [A]}{\partial DV}\{\tilde{x}\} + \frac{\partial \{c\}^{*}}{\partial DV}\{\tilde{x}\} + \{\tilde{\eta}\}^{*}\frac{\partial \{b\}}{\partial DV} \tag{31}$$

Furthermore, recognizing that in many practical design optimization problems the $\{b\}$ and $\{c\}$ vectors remain independent of the design variables, the equation in (31) can be simplified by realizing that the derivatives

$$\frac{\partial \{c\}^{*}}{\partial DV} = 0 \tag{32}$$

and

$$\frac{\partial \{b\}}{\partial DV} = 0 \tag{33}$$

Thus, equation (31) simplifies to

$$\frac{\partial \tilde{y}}{\partial DV} \cong -\{\tilde{\eta}\}^{*}\frac{\partial [A]}{\partial DV}\{\tilde{x}\} \tag{34}$$

In certain situations where $\{c\}$ does depend on design variables, for instance in the case of stress constraints where $\{c\}$ depends on the element cross-sectional area parameter, a simplified derivative of the 2nd order approximate behavior output is

$$\frac{\partial \tilde{y}}{\partial DV} \cong -\{\tilde{\eta}\} * \frac{\partial [A]}{\partial DV}\{\tilde{x}\} + \frac{\partial \{c\}^*}{\partial DV}\{\tilde{x}\} = \left(\frac{\partial \{c\}^*}{\partial DV} - \{\tilde{\eta}\} * \frac{\partial [A]}{\partial DV}\right)\{\tilde{x}\} \quad (35)$$

2.3 Second order approximations for the structural-acoustic problem

Applications of Order-reduction techniques for structural-acoustic problems are widely in use today (Refs. 26, 29, 35). In most applications, natural modes of the structure are used in the order reduction of the structural model. These are then coupled with a reduced-order acoustic model based on superposition of some acoustic modes in a variant of the substructure modal synthesis method of Structural Dynamics (Ref. 8). Such approaches have often shown accurate structural-displacement responses but failed to provide accurate acoustic pressure responses (Ref 24). This is because in structural-acoustic systems, natural modes of the acoustic system are normally in a much higher frequency range than those of the structural part of the model (Refs. 10, 40). For example, it is desired to create a basis matrix from the first 40 modes of a system to analyze a system's behavior over a range of frequencies. In the case of a coupled structural-acoustic system, let the 40^{th} mode be at 100 Hz. However, the first acoustic mode is at 120 Hz. Clearly then the basis matrix will only contain structural modes and no acoustic modes, resulting in a very poor approximation of any acoustic results. Even if more modes are used, the likely end result is that still a majority of modes selected are structural modes and only a few acoustic modes are included, leading to similarly poor approximations as before. Furthermore,

using more modes also means that the approximation is less efficient as more and more equations are added to the system of equations.

A method proposed here to get around this problem is by creating a pseudo model for which the structural and acoustic modes are closer together to allow more structural and acoustic modes to be used when creating basis-matrices. This is achieved by altering material properties, such as fluid density, to shift the frequency at which natural modes occur. Naturally, this pseudo model is only used for creating basis matrices, and not for the analysis itself. Increasing density of an acoustic fluid means that the fluids modal frequencies move lower in the frequency band towards where the structural modes reside*. Now the basis matrix created will include a significant number of both structural and acoustic mode shapes. A comparison for accuracy between approximations using this method and one where this aspect is ignored is included later in this thesis.

As a final remark, for the structural-acoustic coupled problem when modes to create the basis matrix [Φ] are used, these are then in the present work the coupled modes of the structural-acoustic system. When Ritz vectors are used to create the basis matrix [Ψ] they are made of responses of the coupled full-order structural-acoustic system to various inputs.

*Note: By "structural modes" and "acoustic modes" in the case of a coupled system, we mean coupled modes in which either the structural contributions or acoustic contributions are dominant, respectively.

Chapter 3: The Design-Oriented Structural-Acoustic 2D Finite Element Model

3.1 Finite-element formulation

The design-oriented structural-acoustics finite element model used here for 2D problems is based on beam finite elements for the structural boundaries of an acoustic enclosure, coupled with triangular, linear-pressure elements for the acoustic fluid. A subroutine was written in Fortran 90 to create the necessary matrices, both the coupled structural-acoustic stiffness [K] and mass matrices [M], and also the sensitivity matrices with respect to the design variables of interest. The design variables of interest are the cross-sectional areas of the beams (A) and the moment of inertia (I). Hence the sensitivity matrices created are $[\partial K / \partial A]$, $[\partial K / \partial I]$, $[\partial M / \partial A]$, and $[\partial M / \partial I]$. Detailed derivations for the acoustic equations are presented in Appendix A, while those for the acoustic component of the mass and stiffness matrices are presented in Appendix B. Appendix C outlines the structural-acoustic interaction terms, as well as the combined structural-acoustic formulation.

After these matrices were created, they were imported into MATLAB, which facilitates easier matrix manipulations, for calculation of dynamic deformations, internal stresses in structural elements, pressures at node on the acoustic system. Sensitivities with respect to the above mentioned design variables are also calculated. Direct and adjoint problem solutions are available as

well, both in full-order and approximate order using the various order reduction methods described.

3.2 Description of the finite element model

The test case is a 2-dimensional acoustic enclosure surrounded by flexible walls on 6 sides as shown in Figure 1. The model is inspired by previous work in structural-acoustic finite element analysis (Ref. 33).

For each analysis, a reference structure and a modified structure are created. The reference structure is used to obtain the basis matrices needed to create a reduced-order model. The modified structure is one where the element labeled "Variable Element" is modified due to some changes made to its design variables.

The modified structure is then solved in full order to establish a benchmark solution. This benchmark is then used to evaluate accuracy of the various approximations obtained from order-reduced methods. In design optimization problems, the basis matrices only have to be obtained once from the reference structure, and then can be used to approximate solutions of many modified structures for successive changes in design variables, resulting in significant computational time savings.

3.2.1 Geometry of the finite-element model

The model shown in Figure 1 has 143 acoustic nodes, 44 structural nodes, and a total of 275 degrees of freedom. An additional model, identical in geometry but using a much finer finite element mesh was also created and is shown in Figure 2. This model contains 1147 acoustical nodes, 132 structural nodes and a total of 1543 degrees of freedom, and will be referred to as the large-scale model throughout this work. This large-scale model is used to demonstrate the computational time saving achieved by reducing a 1543 x 1543 system to a much smaller and more manageable system.

As an illustration for the time saving that can be realized, a test case of a large-scale full order system (1543 x 1543 system) requires about 1 hour and 40 minutes to solve on a computer with a 2.66 GHz processor with 512 MB of RAM, for one iteration over 200 steps in the frequency domain. In order to solve this system using the second-order method utilizing Ritz vectors and Mode displacements as the first order approximations, an initial run is necessary to obtain the basis matrices. This initial run takes approximately 2 hours and 20 minutes. However, after this initial investment, the system will be reduced and each additional run only requires 2.5 minutes (in the case of a system reduced to a 40 x 40 system).

Both small-scale and large-scale models represent a 2 dimensional, six-sided acoustic enclosure, where the acoustic fluid is completely enclosed by a

flexible beam wall, and is supported by pivots in 3 corners. The enclosure is 0.508 m wide on the top and bottom, and 0.8763 m high. If the lower left corner of the enclosure is labeled vertex 1 and is located at the origin, then going counter-clockwise, the coordinates of the vertices are as outlined in Table 1.

Table 1: Vertex coordinates of acoustic enclosure

Vertex	*x-coordinate* (m)	*y-coordinate* (m)
1	0	0
2	0.508	0
3	0.8453	0.5842
4	0.508	1.1684
5	0	1.1684
6	-0.506	0.8763

The beams connecting the vertices and surrounding the enclosure are constrained in the x-y direction at vertices 1, 2 and 4, but otherwise are allowed to rotate freely. All other vertices are allowed to move freely. Also, similar to the model in Ref. 33, two point masses of 0.03 kg were attached to the bottom beam panel at x = 0.2032 m and 0.3048 m. The excitation force is a point unit load located at x = 0.3048 m.

3.2.3 Material properties of the reference model

The beams surrounding the enclosure are made of aluminum, with modulus of elasticity (E) of 72 GPa and density of 2600 kg/m^3. The beams have rectangular cross sections with 0.2032 m at the base, and height of 0.003175 m.

Thus they have a cross-sectional area of 6.45 x 10^{-4} m^2 and a moment of inertia of 5.4197 x 10^{-10} m^4. The fluid in the enclosure is air, with density of 1.225 kg/m^3, and speed of sound of 342 m/s.

3.2.4 Material properties of the modified models

The modified models all maintained the same geometrical properties as the reference model. However, in the element marked as "Variable Element" in Figure 1, the design variables of interest were changed. Both the moment of inertia and beam cross-sectional area were increased by 50%, corresponding to I = 8.1296 x 10^{-10} m^4 and A = 9.675 x 10^{-4} m^2. This model was created to represent a design optimization problem where the design variables are changed as the model is driven to the optimum.

Several models were also created with changes in the design variables I and A varying between 10% to 100%, and are used to illustrate how the approximations behave as the modified model moves further away from the reference model.

Finally, two different values of the structural damping factor (g) are used, 0.06 and 0.15. While the value of the damping factor itself does not affect the accuracy of the approximate solution in a fundamental way, a higher damping has the effect of smoothing out sharp peaks in the response curves, which in turn reduces the difference in error calculations caused by small shifts of very narrow frequency response peaks.

Another model that was created is what will be referred to as the pseudo model. This model is created because the difficulties of modal approximation methods in finding proper reduced bases for reducing the order of structural-acoustic models due to the large differences in modal frequencies between the structural and the acoustic modes (Refs 10, 24, 40). This model is used only to obtain the modal basis matrices for the modal approximation methods, as it does not have any physical meaning, other than that it is a model where the structural and acoustic modes are closer together in the frequency range, while the corresponding mode shapes remain the same. To achieve this, the fluid density in this model was increased 100 times, and the cross-sectional areas of the beams were reduced to 0.01 times of the original. (Please see note on page 15).

3.3 Validation of the finite element model

To validate the model used in this work with dedicated codes, two comparison tests were made using a similar model analyzed by the commercial FEM software ANSYS (Ref. 1). The first test is a comparison of natural frequencies between the two models. Table 2, which records the first 12 natural modes of both systems, shows that the natural modes of the two systems are identical, as expected.

Table 2: Comparison of natural frequencies.

Mode	*ANSYS* (Hz)	*FEM Code* (Hz)
1	6.7	6.7
2	18.0	18.1
3	21.4	21.4
4	28.2	28.3
5	31.9	32.0
6	40.4	40.3
7	50.2	50.4
8	68.8	68.0
9	73.5	73.4
10	85.5	85.6
11	91.2	91.2
12	107.0	107.3

The second test is a comparison of sound pressure output in decibels at the node marked in Figure 1. The result again shows very good correlation between the two models and is presented in Figure 2. The sound pressure output calculated from the ANSYS model are virtually identical to that calculated by the FEM program written for this work over the frequency range of 25 Hz to 250 Hz. Based on these two tests, it is shown that the FEM model created for this work is indeed accurate.

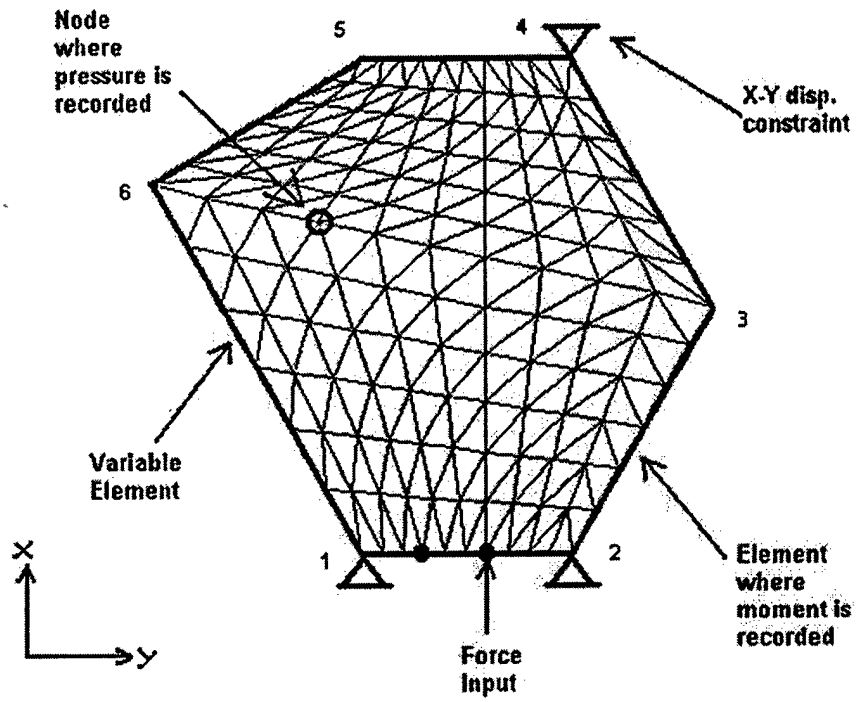

Figure 1: 2D Structural Acoustic System

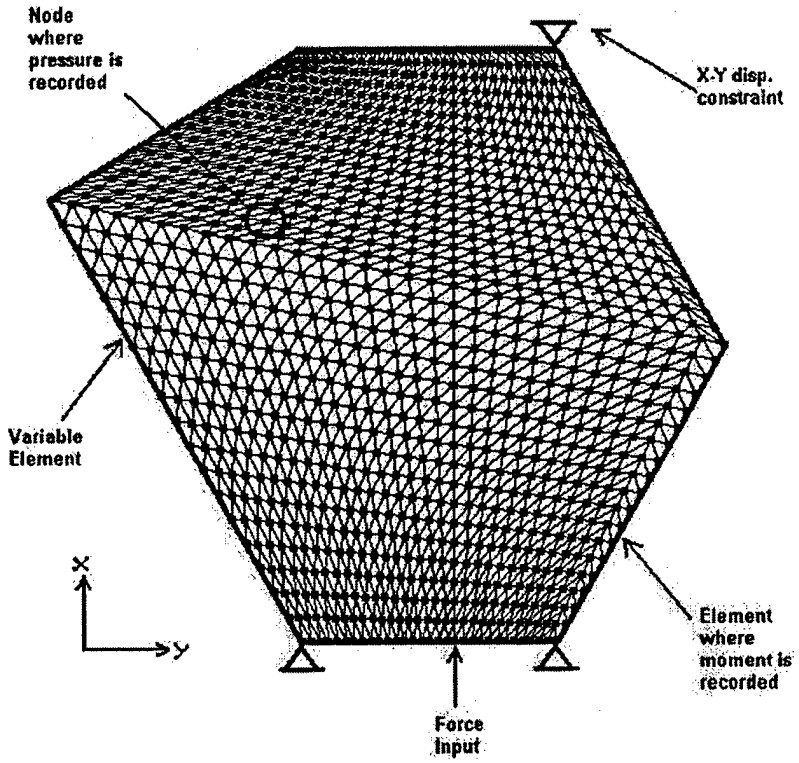

Figure 2: Large-scale 2D Structural Acoustic System

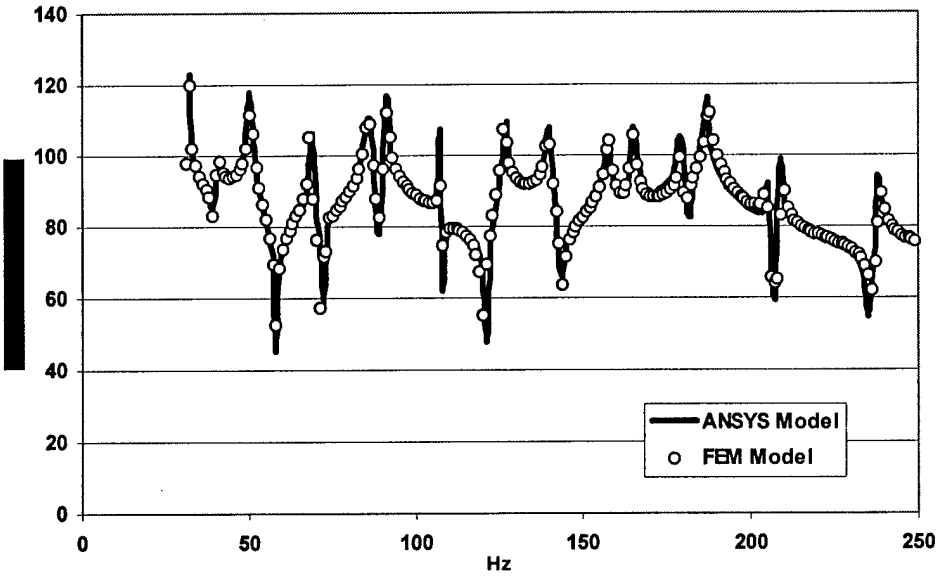

Figure 3: Sound pressure frequency response comparison.

Chapter 4: Numerical Results

4.1 Introduction to the test cases

The Second Order Approximation results were obtained using several different approaches.

In the first approach, the Ritz vector is used to reduce the order of the direct problem written in Eq. 7 corresponds to the force input on the right hand side of the equation. The reduced basis $[\Psi_d]$ is also frequency-dependent and consists of single frequency-dependent vectors each a solution of the full order reference problem. The subscript *d* here is used to denote that this basis vector corresponds to the direct problem. When Ritz vectors were used to reduce the order of the direct problem, then the adjoint problem was reduced by a subset of the left natural modes $[\Phi_d]$.

$$\left[\lambda_i [M]^T + [K]^T\right]\{\psi_i\} = \{0\} \tag{36}$$

In the second approach, a Ritz vector approximation is used for the adjoint problem corresponds to a response $y(j\omega)$ as given in Eq. 8. For this, the reduced basis $[\Psi a]$ used is the solution of Eq. 9. This basis $[\Psi_a]$ is frequency dependent, and varies with frequency. The subscript *a* here is used to denote that this basis vector corresponds to the adjoint problem. The reduced-order Ritz solution is of order 1 x 1 based on a single adjoint solution at each frequency of the reference system. Since Ritz vectors were used to reduce the order of the adjoint problem,

then a low-frequency subset of the right natural modes $[\Phi_a]$ was used to reduce the direct problem.

$$\left(\lambda_i[M]+[K]\right)\{\phi_i\}=\{0\} \tag{37}$$

Since the structural-acoustic mass and stiffness matrices in the formulation used here are non-symmetric, the mode shapes are generally complex. Symmetric formulations for mass and stiffness matrices (Refs 9, 29) can be used, however none of the resulting matrices are positive definite, hence the modes will generally remain complex.

In another approach, the adjoint and direct approximations were using the adjoint and direct solutions of the original reference model. This saves computational time, as there is no need to calculate the first order approximations using reduced order models. A variation of this approach is to use one of the original reference solutions and combine it with a first order approximation (such as the modal approximation) to improve results.

Finally, first order Taylor series approximations were used to create the approximate first order results. In this approach, the approximate first order basis for the second order approximation takes the form

$$[\tilde{\Phi}(j\omega)]=\Phi_0(j\omega)+\sum_i \left.\frac{\partial\Phi(j\omega)}{\partial DV_i}\right|_0 (\Delta DV)_i \tag{38}$$

In this case, the sensitivity derivative $\left.\frac{\partial \Phi}{\partial DV_i}\right|_0$ is the sensitivity of the original reference model. In the following sections, second-order approximation results obtained using various first-order approximations will be presented and evaluated. In all the studies presented here, the following steps were taken. First, analysis and sensitivity results were generated for the reference model, and reduced basis vectors/matrices obtained. Then the model was modified by changing properties of the variable element. A full-order detailed analysis of the modified model was carried out and used to check accuracy of the approximate analysis applied to this modified model. Finally, the modified model was analyzed using a variety of reduced-order techniques and accuracy of the reduced order calculations assessed. In an optimization environment detailed analyses are carried out only a small number of times while most of the optimization search effort is based on approximate analyses.

As can be seen a large number of combinations of first-order methods were used to obtain the second-order approximation. Some combinations are not presented here as they did not add additional insight, or were simply inaccurate. Those that are presented are summarized in Table 3, and are discussed further in the sections that follow.

Table 3: Summary of approximation methods

Case	*First-order Direct*	*First-order Adjoint*	*Scale of Model*
1	Mode Displacement	Ritz Vectors	Small
2	Ritz Vectors	Mode Displacement	Small
3	Original Solution	Original Solution	Small
4	Mode Displacement	Original Solution	Small
5	First-order Taylor	First-order Taylor	Small
6	Mode Displacement	Ritz Vectors	Large
7	Ritz Vectors	Mode Displacement	Large

4.2 Dynamic results of the second order approximation, small scale model

4.2.1 Adjoint based on Ritz Vectors, Direct Based on Modes

In Figure 4 through Figure 9, the reduced order direct solution is based on a single Ritz vector (1 x 1), and the adjoint solution is based on a reduced basis matrix of 41 modes (41 x 41). These numbers of modes chosen were such that it covers at least 2 times the frequency range of interest in the original configuration.

The structure is excited harmonically at the bottom wall, and errors of the reduced approximation presented versus the frequency of excitation, between 20 Hz and 260 Hz.

As can be seen, the Ritz approximation has the least accuracy, relying on only 1 Ritz vector to capture the behavior of the system, since there is only 1 excitation force.

The modal approximation shows better accuracy, especially in the lower ranges of the frequency band, but starts to diverge above the 200 Hz range. This can be attributed to the lack of higher frequency modes in the basis matrix due to only using the first 41 modes. Improvements can be achieved by adding more modes to the basis matrix, but at an increase of computational cost.

By combining the 1 x 1 Ritz approximation with the 40 x 40 modal approximation, the second-order method results show marked improvement of accuracy. It is important to note that while the modal approximation solution plotted was approximated using 41 modes, the second order approximation only used 40 modes, one less mode in order to give a fair comparison since the second order method "gains" one extra approximation vector from the Ritz approximation. This is done to show that the second-order approximation does not gain extra accuracy merely from using more basis vectors.

In Figure 4 errors in the approximate bending moment (stress) are shown for the element shown in Figure 1. Figure 5 shows the error of the different approximation methods compared to the full-order solution when computing pressure at the node indicated in Figure 1. Again the reduced-order direct solution is based on a single Ritz vector (1 x 1), and the adjoint solution is based on a reduced basis matrix of 41 modes (41 x 41). The model is excited with the same load. The Ritz vector approximation was generally not as accurate as the modal approximation, while the second-order approach showed improvement in

accuracy, particularly in the upper frequency range where the modal approximation begins to diverge.

Accuracy of predicting reduced order design sensitivities are examined next. Figure 6 shows errors in the different methods of approximation relative to the full-order solution when predicting sensitivities of bending moment with respect to changes in the beam moment of inertia (dM/dI). Here is where some significant errors in the first-order methods are observable. The error in the approximate direct solution occasionally exceeds 60%, while the error for the approximate adjoint solution exceeds 30% at some point. By contrast, the second order approximation never exceeds 5% in the frequency range shown.

In Figure 7, errors in the different methods of approximation when predicting sensitivities of bending moment with respect to changes in the beam cross-sectional area are presented. It becomes evident here that errors with the direct approximation are uniformly quite large. With only a few exceptions, the error of this method routinely exceeds 40%. In two areas, between 30 Hz and 40 Hz, and between 170 Hz and 175 Hz, the error even exceeds 500%. The adjoint problem approximation behaved better with errors never exceeding 25%. The second-order method however only performs marginally better here. Since it uses information from two first-order approximation methods, if one of them is significantly inaccurate, the second-order method will typically only perform marginally better or equivalent to the more accurate of the two. This pattern is

repeated in all results where one of the first-order approximations has errors far exceeding 100%.

Sensitivities of pressure with respect to design variables were also examined. In Figure 8, errors in the different methods of approximation when predicting sensitivities of pressure with respect to changes in the moment of inertia (*dP/dI*) is shown. As was observed in the *dM/dA* results, the direct approximation solution showed errors larger than 150% throughout the frequency range. The adjoint approximation solution also shows errors of up to 150% in some areas. As noted previously, if one of the first-order approximations shows large errors, then the second-order approximation method will only perform as good as the better first-order approximation. Still, throughout the frequency range, the maximum error of the second-order approximation never exceeds 100%, while both first-order approximations had a maximum error of 150% in the same frequency range.

In Figure 9 we examine errors of the different approximation methods when predicting the sensitivity of the pressure with respect to the beam cross-sectional area (*dP/dA*). Again, despite the large errors in the predictions of the direct approximation, the second-order solution generally is at least as good as the adjoint approximation. The exception being in the regions above 200 Hz where the second-order solution generally had less than half of the error of the adjoint approximation, and significantly more accurate than the direct approximation using Ritz vectors.

4.2.2 Adjoint based on modes, direct based on Ritz vectors

In this approach, a Ritz vector approximation was used for the adjoint problem, while the modal approximation was used for the direct problem. Here the Ritz vector corresponds to a response $y(j\omega)$. That is, each response has its own $\{c\}$ vector (Eq. 19) and it is used as a right-hand side in the adjoint equation to produce the Ritz vector. In Figure 10, it is shown how this approach performs when approximating the bending response. As in previous cases, the second-order bending response approximation has consistently smaller errors when compared to the first-order approximations.

However, a problem that is observed when using this method is that the Ritz vector approximation is simply unable to capture the pressure and pressure related derivatives. This could be due to the response at the acoustic element is relatively an order of magnitude smaller when compared to the response at the beam element. This can be observed in Figure 11. In this approximation, the error due to the adjoint based Ritz vector approximation is so large it is outside of the chart. In cases where one first-order approximation is highly inaccurate, the second-order method performs only as well as the better first-order method, in this case the modal approximation.

4.2.3 Adjoint and direct based on original solution

Here, the original solution, i.e. solution of the unmodified reference model, was used as the first-order approximation for the second-order method. Also, changes in the design variables of the variable element were increased to 100%, and the structural damping factor g is reduced to 0.06. Figure 12 shows the pressure response for the entire range of frequencies, while Figure 13 shows the same for a zoomed area. It can be seen here that the second-order response approaches the modified full-order solution is only somewhat closer than just the original full-order solution alone. Examining the error plot in Figure 14 confirms that the second-order approximation shows some improvement over the original solution.

Examining the sensitivities, Figures 15 and 16 show the errors of the approximate solutions when estimating the sensitivity of the moment and pressure responses with respect to the cross-section Area (A) design variable. In this case, error of the second-order method is in some cases smaller by almost a factor of 4 or more (25% vs. 100%) in various regions of the frequency domain.

4.2.4 Adjoint based on modes, direct based on original solution

Here it is sought to improve on the previous method by using a more accurate first-order basis. Having performed well in the previous approximation methods, the modal basis approximation is used to replace one of the first-order

original solutions. The result is a method that combines the adjoint solution approximation using modal basis vectors with an approximation using the direct solution of the original (unmodified) model. These two approximations are then used to obtain the second-order approximation. From a computational cost perspective this method requires more resources, as the modal basis matrix has to be calculated first. However, as in previous methods, once this basis matrix is calculated, it can be reused for future iterations for all changes in the design variables.

For the case examined, the modified beam cross-sectional area and moment of inertia were increased 100% from the reference model, and a damping factor g=0.06 was used. Figure 17 shows the pressure response around the same region as shown in Figure 13. Comparing these responses shows that the second-order result is now improved over the results previously shown in Figure 13. Examining the error of the second-order pressure response as shown in Figure 18 confirms that over the entire frequency range the second-order method gives significant improvement over the first-order methods. Similarly Figures 19 and 20 show improved second-order approximation results for bending sensitivities, while Figures 21 and 22 show error of the second-order approximation results for pressure sensitivities. In all these sensitivity results, the second-order approximation in general shows less error than any of the first-order methods alone. Also, throughout the range, error of the second-order method is more consistent. For example, in Figure 18, around 200 Hz -220 Hz, the first-order

approximations exhibit large errors to over 80%, while the second-order method never exceeds 20% error throughout the whole frequency band.

As noted before, the second-order method results improve upon the first order method results, and when results from the first order methods become too inaccurate, the second order results typically also become less accurate. This can be observed on Figure 21, particularly in the range between 200 Hz and 250 Hz. As the error in the first-order methods becomes large, the second-order error too becomes large. However, it is important to note that in this particular case, while the second-order error is relatively large, it still improves on the first-order method results.

To see whether the approximation results can be better captured in the case of models with smaller changes to the design variables, the model was solved approximately again with the same method, except the design variables A and I were only changed 50%, compared to 100% previously. Also, the damping coefficient was increased to g = 0.15 to smooth out and widen the resonance frequency peaks. The desired effect of this is to reduce errors due to shifting of the peaks. Figures 23 and 24 contrast the pressure response between these two models. In Figure 23, the pressure response is shown for the model with 100% change in DV and 0.06 damping, and Figure 24 shows the pressure response for the model with 50% change in the two DVs and 0.15 damping. As it can be seen from comparing these two figures, some of the resonance peaks are indeed flattened, as expected.

Figures 25 and 26 show error in the approximations of the pressure and bending responses respectively, in the model with 50% change in the two DVs. As it can be seen the second-order method is now clearly far superior than the first-order methods, showing errors that are less than 2%, compared to up to 12-20% and even higher for the first-order methods.

Examining the response plots also confirms that the second-order method's precision is better than that of each of the first-order methods. Figure 27 shows a segment of the pressure response, and Figure 28 shows a segment of the bending response curves. In both figures the results are magnified for a better comparison.

Errors in approximating the sensitivity of the design variables of interest are also generated. As it can be seen in Figures 29 and 30 for the bending moment sensitivity with respect to the design variables I and A respectively, the second-order approximation produces the most consistently accurate approximations. The same observations can be made for Figures 31 and 32 where the errors in pressure sensitivity approximations are presented. Another observation that can be made is that the magnitude of the errors in the second order approximation is related to the errors in the first order approximation. For example, in Figure 32 near the 100 Hz range, error of both of the first-order approximation is large, so the error in the second-order approximation is also large, even though it is still smaller than each of the first order errors. In Figure 31 at the 200 Hz range, error in the first-order adjoint approximation is large, however the error for the original full-order

solution is not large. Error in the second-order approximation is higher here than at any other point, but still much smaller than the direct first-order.

4.2.5 Adjoint and direct based on Taylor-series approximation

Another attempt at using additional first-order approximations was made using Taylor series to obtain the approximate results. The modified model for this case had only one design variable changed, in this case the moment of inertia (*I*) of the variable element. The design variable was also changed incrementally from 10% to 50% to see the effect of the larger change on the accuracy of the second-order approximation. Figures 33, 34, 35 and 36 show errors in pressure approximation using this method, as the change in design variable is increased by 10%, 20%, 30% and 50% respectively. As it can be seen, the second-order approximation increasingly becomes less accurate as the change is increased. Approximation errors of the sensitivities were also obtained, and in Figures 37, 38, 39 and 40 errors of sensitivity approximation of the pressure with respect to the moment of inertia of the beams (*dP/dI*) are presented. As before, the figures correspond respectively to 10%, 20%, 30% and 50% changes in the design variable. Using the Taylor expansion method, the first-order adjoint and direct approximations for the sensitivities are identical. Similar to previous results, accuracy of the second-order approximation while very good at small changes in design variables, become steadily worse as the changes are increased. When the design variable was changed by more than 50% the second-order solution ceases

to give more accurate results than the best first-order Taylor expansion approximation. The reason is that one of the first-order approximations being highly inaccurate.

4.3 Dynamic results of the second-order approximation, large scale model

4.3.1 Adjoint based on modes, direct based on Ritz vectors

Approximation results for the large-scale model are of great interest, because they test the viability of solving large set of equations with an approximation based on a much smaller sub-set of equations. As already mentioned, the large-scale model has 1543 degrees of freedom. Also for this problem, modes for the modal approximation were obtained from a model for which the density of the fluid was increased 100x and the cross-sectional area of the beams reduced 0.01x. This is to simulate situations where in the process of optimization basis matrices for the approximations are obtained from a model that is very different than the model being solved. This has the advantage of not having to recalculate the modes every time the model changes.

Figure 41 shows error of the different approximation methods compared to the full-order solution when computing pressure at the node of interest. As in the case for the small-scale model, the reduced-order direct solution is based on a single Ritz vector (1 x 1), and the adjoint solution is based on reduced basis matrix of 50 modes (50 x 50). The difference, of course, being that the model

reduced now contains 1543 degrees of freedom, corresponding to a matrix of size 1543 x 1543. As previously in the small model, change in design variables I and A are 50%.

As it can be seen in Figure 41, error of the second-order approach remains consistently the smallest of the three approximations. Figure 42 shows the actual response of the approximations and plots the full-order result along side the 3 approximations in the 20 Hz to 60 Hz range. As can be seen, the second-order approximation solution traces the full-order solution very closely.

In Figure 43, the bending moment approximation errors are presented. The second-order approximation is far more accurate than each of the first-order methods. The largest error recorded for the second-order method in the entire frequency range did not exceed 20% at any time.

Figures 44 and 45 examine the bending moment sensitivity with respect to A and I. For the dM/dA approximations in Figure 44, the second-order method generally performs better than the first-order counterparts. At locations where the first-order direct approximation is grossly inaccurate, the best the second-order approximation can do is match the more accurate of the two first-order approximations, in this case the adjoint approximate solution using modal approximation. An example of this trend can be seen around the 40Hz and 80 Hz points in this figure. For the dM/dI approximation error in Figure 45, neither of the first-order approximations is grossly inaccurate, and hence the second-order

approximation performs well. The sole exception of this is around the 40 Hz point, where the Ritz vector approximation resulted in errors well over 100% and again the second-order approximation was only able to match the better one of the two first-order approximations.

For pressure sensitivity approximations, the second-order approximation is undisputedly the most accurate and most consistent performer. As shown in Figure 46 for the errors in dP/dA approximations and in Figure 47 for the dP/dI approximations, the second-order method consistently outperforms both first-order methods significantly when approximating pressure sensitivities in the given range of frequency. While the errors for one or both the first-order methods exceed 100% in some areas, the second-order method performs far better with maximum error of 40% and 20% for dP/dA and dP/dI respectively, and with average error far lower than that.

4.3.1 Adjoint based on Ritz vectors, direct based on modes

For comparison, the large-scale model was again solved with almost all the same parameters as previously, with one change. In this method the adjoint solution was approximated using a modal basis of 50 modes, while the direct solution uses 1 Ritz vector for approximate basis.

Unfortunately for this method, the Ritz vector approximation was simply unable to approximate the solution, resulting in very large errors for the direct solution approximation. Since the second-order approximation relies on having

two reasonably accurate first-order approximations to further increase accuracy, naturally it would at best be only as accurate as the better one of the first-order approximations if the other one is grossly inaccurate. In extreme cases, where one of the first-order approximations has consistently 1000% or higher errors, the effect of this becomes significant enough that it causes the second-order approximation to show higher inaccuracy than even the alternate first-order approach. An example of this case is illustrated in Figure 48 where large errors in the adjoint approximations result in also large errors in the second-order method. In this case, the first-order direct approximation actually performed better than the second-order approximation.

4.4 Convergence study of the second-order approximation when using a modal basis first-order approximation

In this study, one of the methods for obtaining one of the first-order approximations utilized in the second-order approximation method uses natural mode shapes of the structural-acoustic enclosure model to serve as a basis matrix for the approximation. Typically in first-order approximations using modal basis it is expected that as more modes are used to approximate the model, the more accurate the approximation becomes. The cost of doing this is the increased computational cost involved in solving a larger problem as the reduced basis matrix becomes larger as more modes are used. At the extreme end all natural modes will be used. Then the approximation is then no longer an approximation,

but becomes the exact solution, except that computationally it costs much more to solve, as there are additional computational costs involved in obtaining the mode shapes for the basis matrix (as well as multiplying the basis matrices against the full-order set of equations).

A question then arises. Does this increase in accuracy with increased modes used in the first-order method translate to greater accuracy when using a second-order approximation? To answer this, the same small model that was used in section 4.2.1 was used again with the same experimental parameters except the modes used to approximate the adjoint solution were incrementally increased from 10 modes, 20 modes, and then 40 modes. Figures 49 and 50 respectively show errors of the second-order bending moment and pressure response approximations as the modal basis is increased. For both illustrations it can be seen that an increase in modes used leads to a reduction in error and hence an increase in accuracy. Furthermore, an increase in modes used also gives an increase in the range of frequency where the approximation is accurate. For example it can be seen that in order to get reasonable accuracy past 180 Hz, at least 40 modes are required. This is expected because the lower number of modes prevents mode shapes in the higher frequency ranges to be included in the basis matrix. Care must then be taken to ensure that a significant number of mode shapes are included for the frequency range of interest, but not so many that it unnecessarily affects computational time.

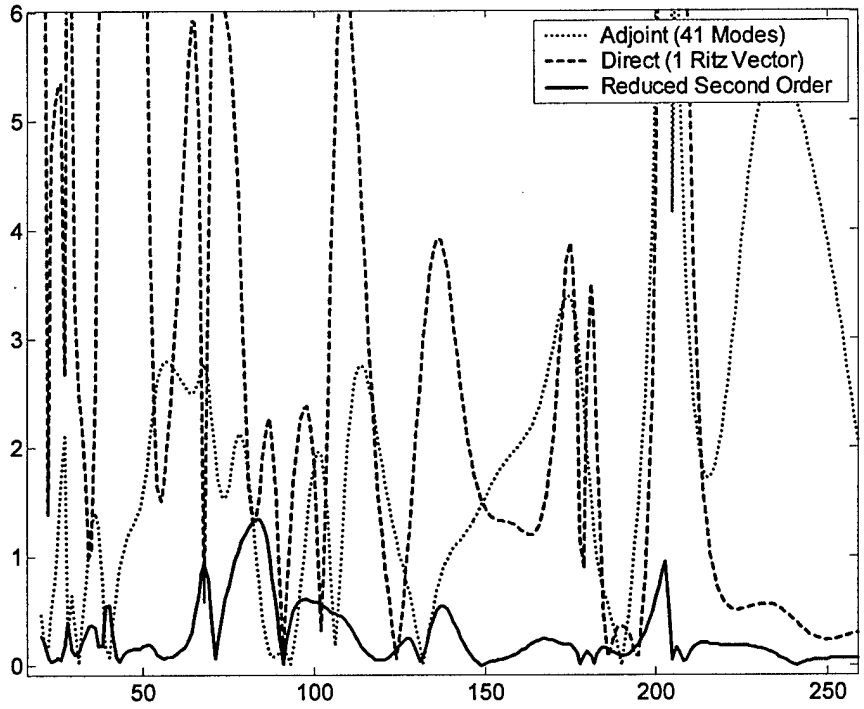

Figure 4: Error (%) in Bending Moment approximation as a function of excitation frequency. Direct solution approximated by 1 Ritz vector, Adjoint solution approximated by 41 modes. Small-scale (275 DOF) model, g=0.15.

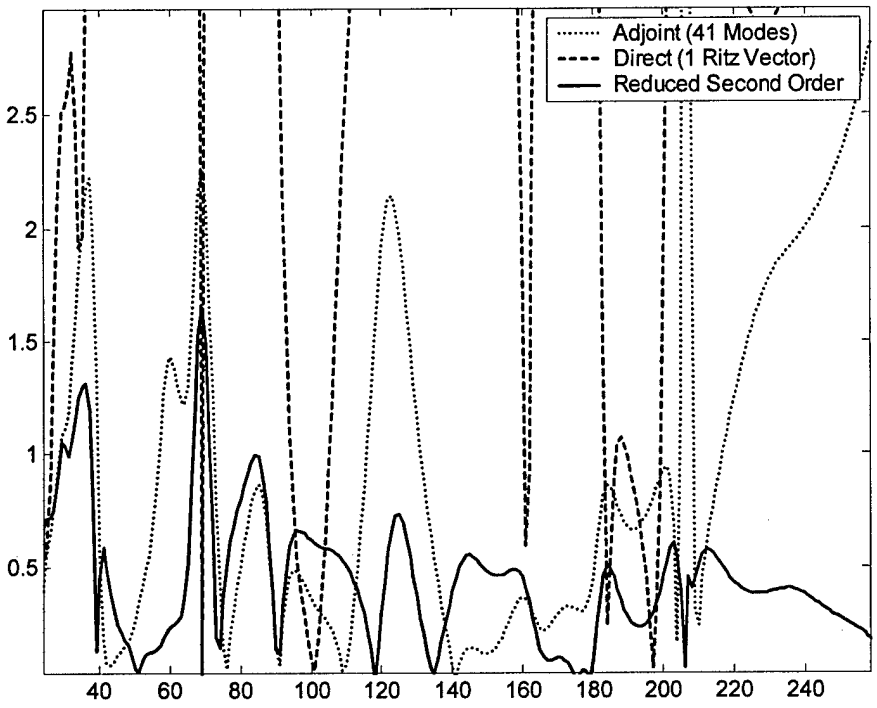

Figure 5: Error (%) in Pressure approximation as a function of excitation frequency. Direct solution approximated by 1 Ritz vector, Adjoint solution approximated by 41 modes. Small-scale (275 DOF) model, g=0.15.

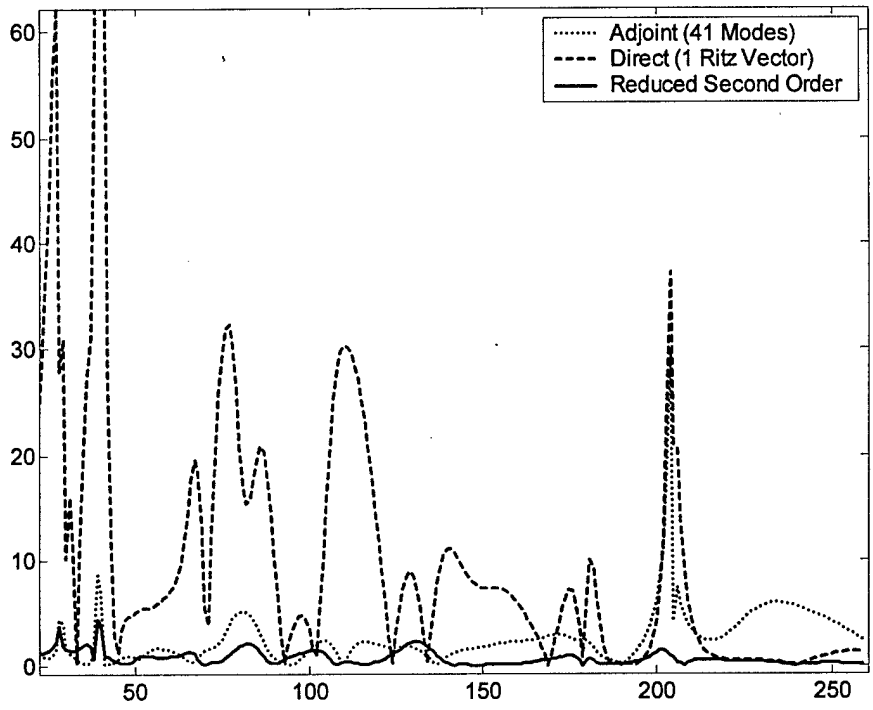

Figure 6: Error (%) in dM/dI approximation as a function of excitation frequency. Direct solution approximated by 1 Ritz vector, Adjoint solution approximated by 41 modes. Small-scale (275 DOF) model, g=0.15.

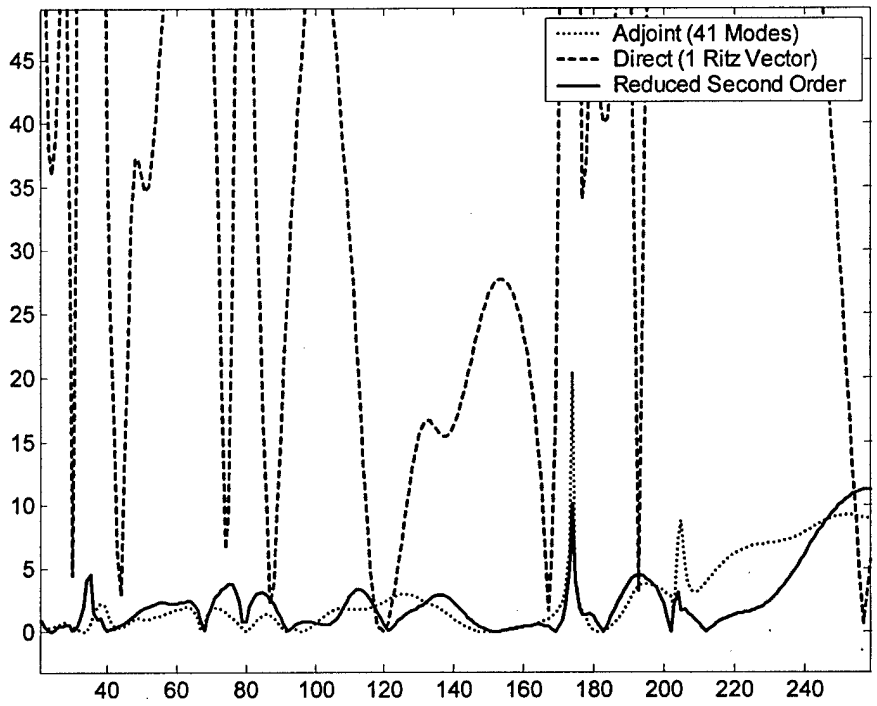

Figure 7: Error (%) in dM/dA approximation as a function of excitation frequency. Direct solution approximated by 1 Ritz vector, Adjoint solution approximated by 41 modes. Small-scale (275 DOF) model, g=0.15.

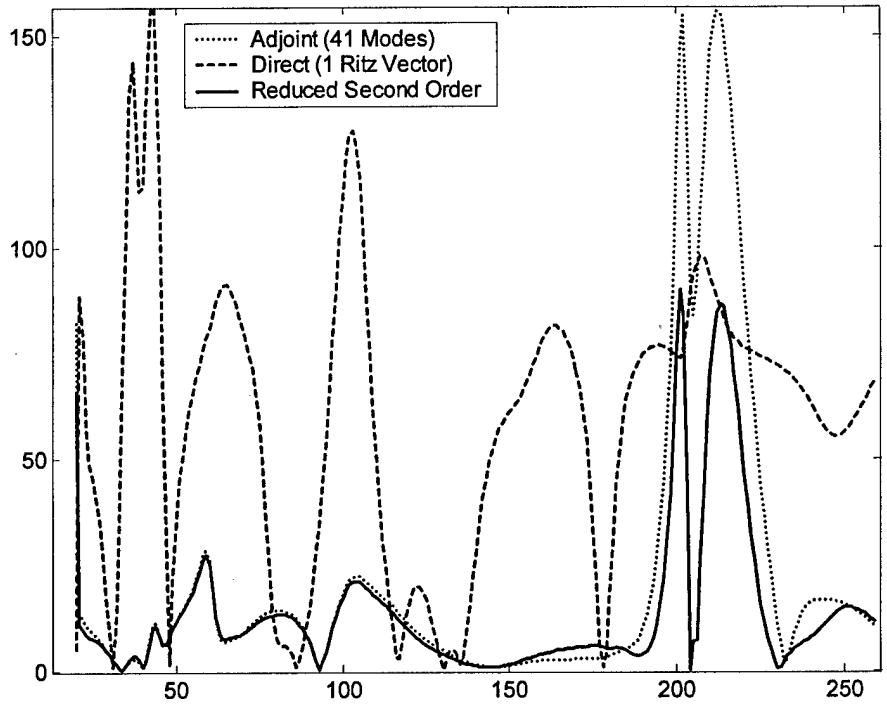

Figure 8: Error (%) in dP/dI approximation as a function of excitation frequency. Direct solution approximated by 1 Ritz vector, Adjoint solution approximated by 41 modes. Small-scale (275 DOF) model, g=0.15.

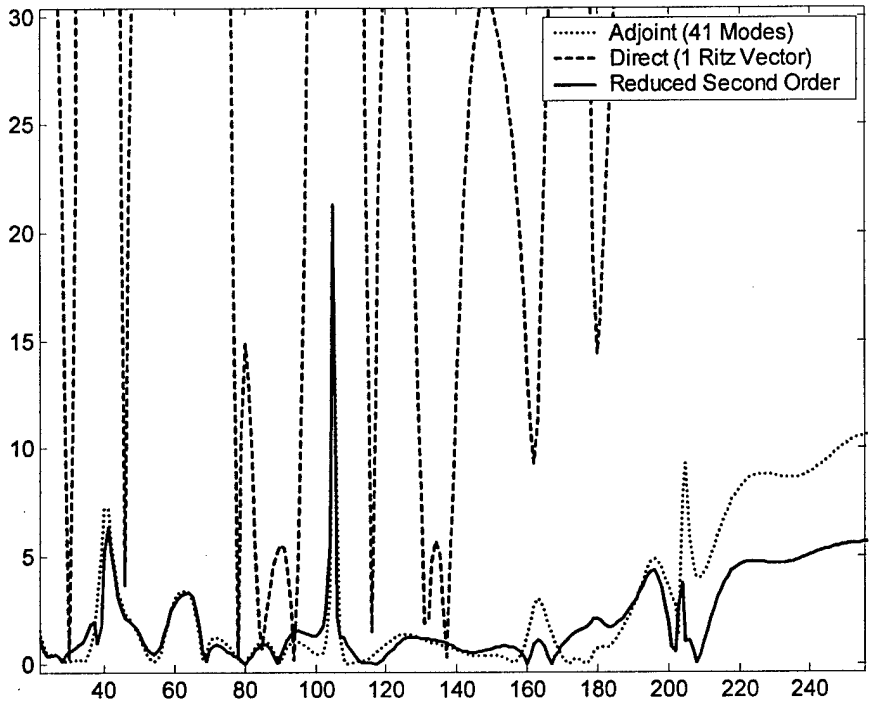

Figure 9: Error (%) in dP/dA approximation as a function of excitation frequency. Direct solution approximated by 1 Ritz vector, Adjoint solution approximated by 41 modes. Small-scale (275 DOF) model, g=0.15.

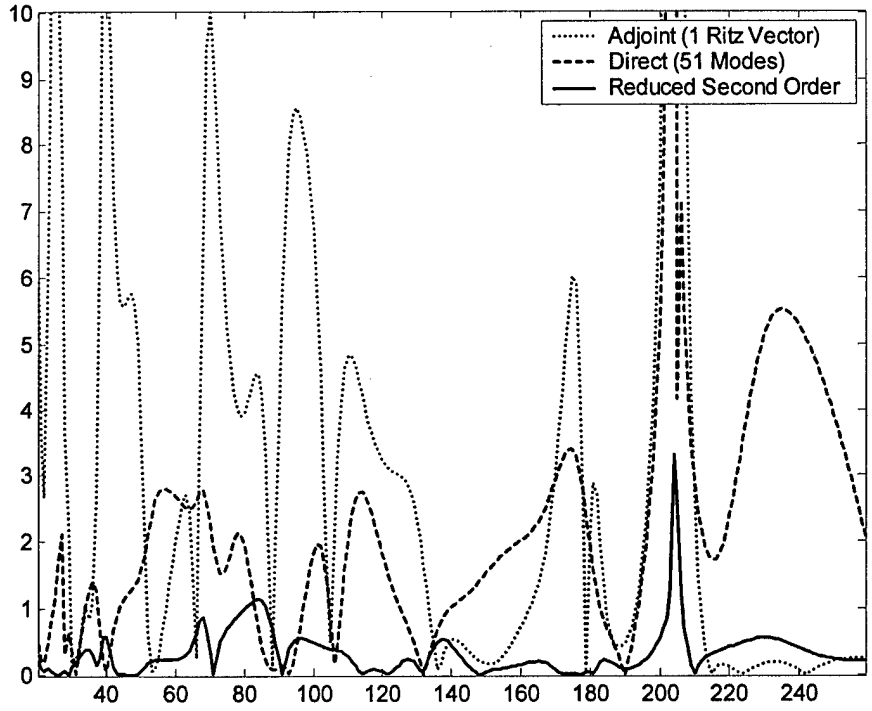

Figure 10: Error (%) in Bending approximation as a function of excitation frequency. Direct solution approximated by 51 modes, Adjoint solution approximated by 1 Ritz Vector. Small-scale (275 DOF) model, g=0.15.

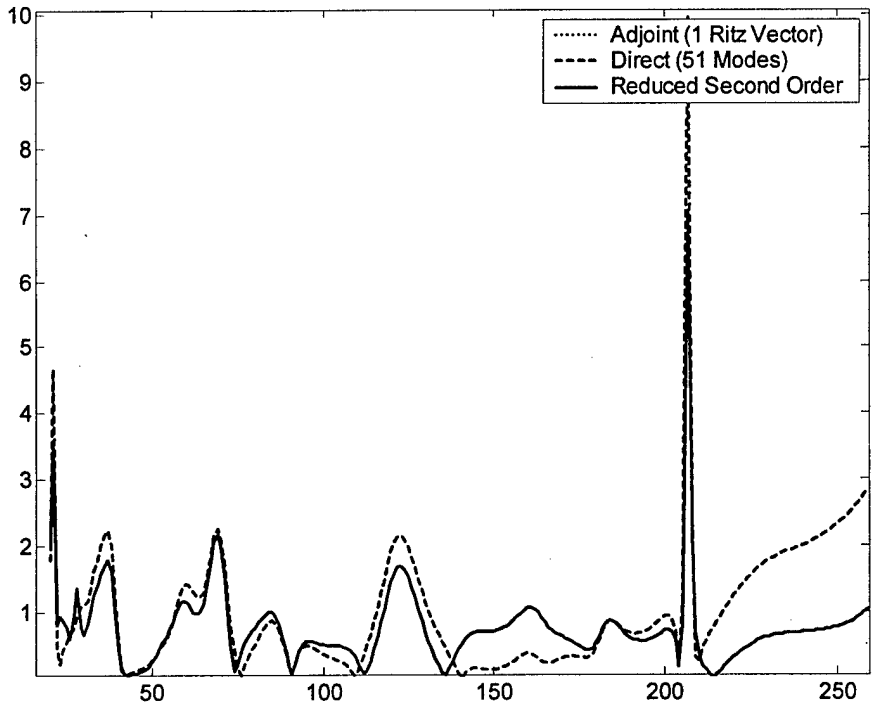

Figure 11: Error (%) in Pressure approximation as a function of excitation frequency. Direct solution approximated by 51 modes, Adjoint solution approximated by 1 Ritz Vector. Small-scale (275 DOF) model, g=0.15. Adjoint Error is off the chart.

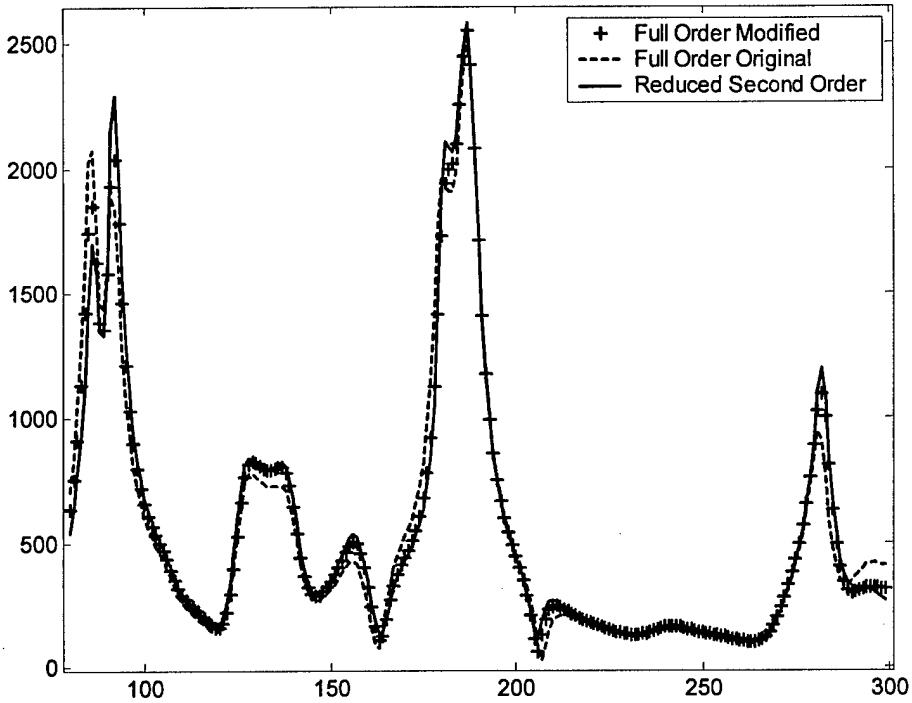

Figure 12: Pressure response approximation as a function of excitation frequency. Approximate direct and adjoint solutions are the original (reference) adjoint and direct solution. Small model, 100% change in design variables of the variable element, g=0.06

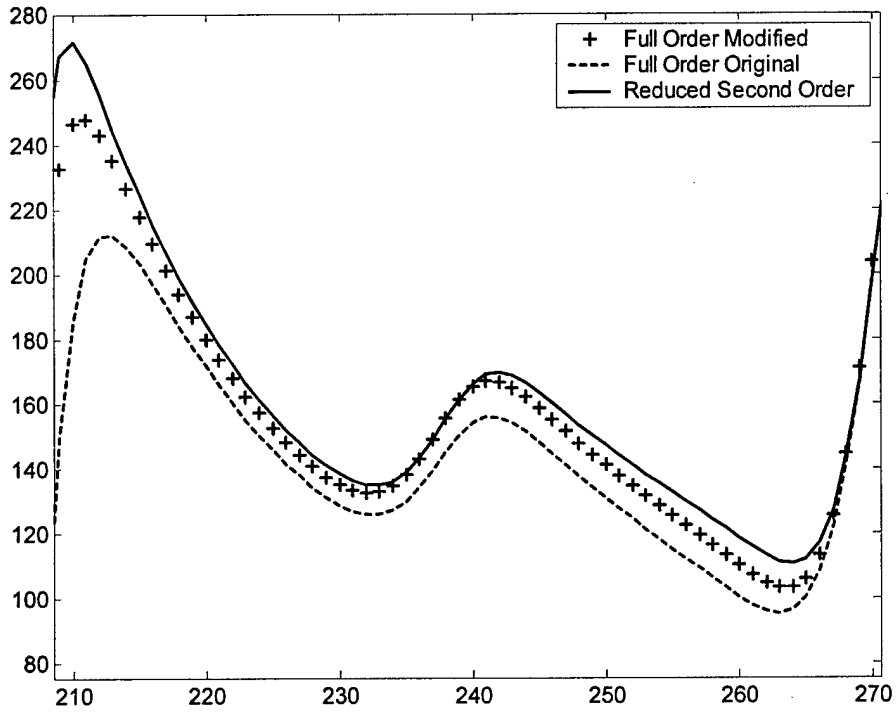

Figure 13: Pressure response approximation as a function of excitation frequency, zoomed to area of interest. Approximate direct and adjoint solutions are the original (reference) adjoint and direct solution. Small model, 100% change in design variables of the variable element, g=0.06

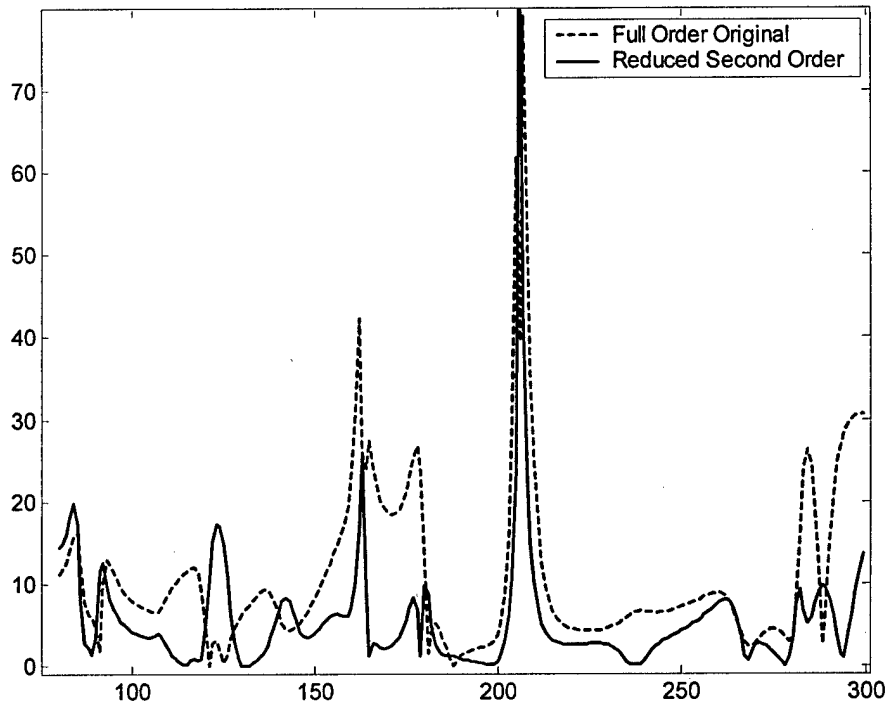

Figure 14: Error (%) in Pressure approximation as a function of excitation frequency. Approximate direct and adjoint solutions are the original (reference) adjoint and direct solution. Small model, 100% change in design variables of the variable element, g=0.06

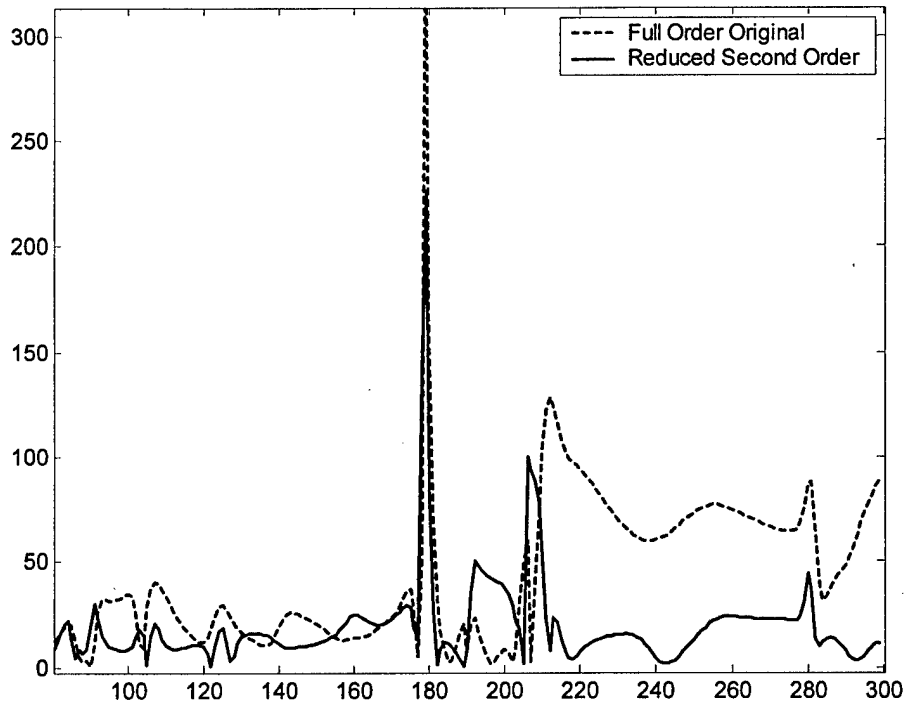

Figure 15: Error (%) in dM/dA approximation as a function of excitation frequency. Approximate direct and adjoint solutions are the original (reference) adjoint and direct solution. Small model, 100% change in design variables of the variable element, g=0.06

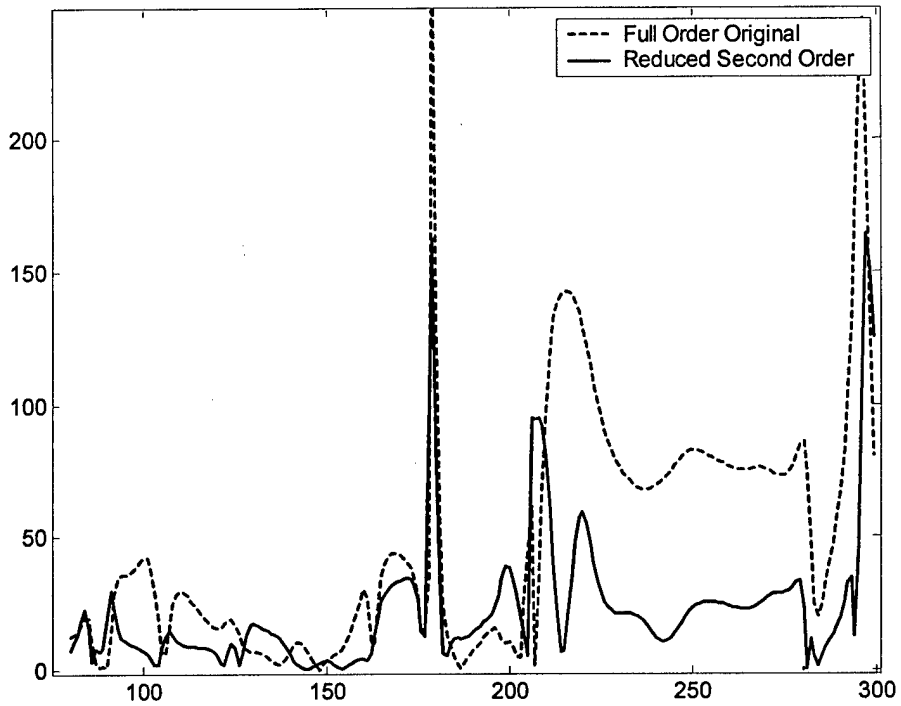

Figure 16: Error (%) in dP/dA approximation as a function of excitation frequency. Approximate direct and adjoint solutions are the original (reference) adjoint and direct solution. Small model, 100% change in design variables of the variable element, g=0.06

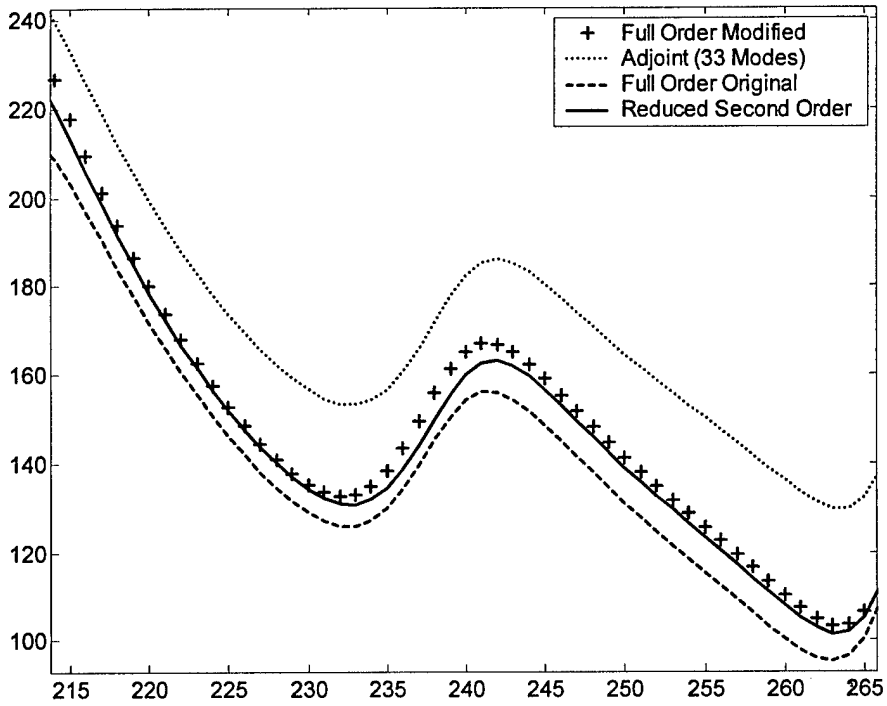

Figure 17: Pressure response as a function of excitation frequency, zoomed to area of interest. Approximate direct solution is the original (reference) direct solution; the adjoint solution is by modal approximation using 33 left and right eigenvectors. Small model, 100% change in design variables of the variable element, g=0.06

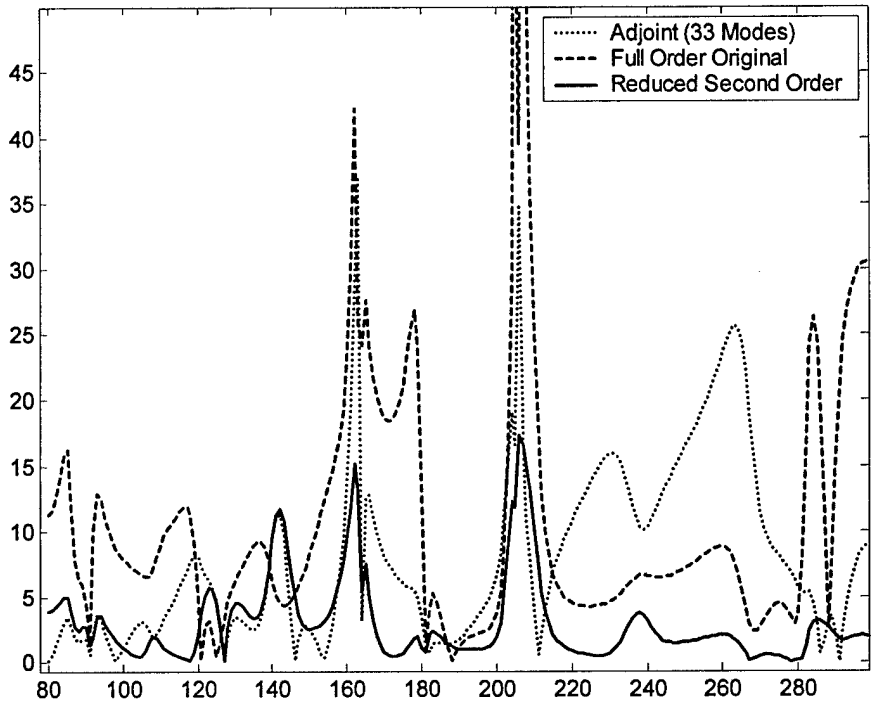

Figure 18: Error in Pressure approximations as a function of excitation frequency. Approximate direct solution is the original (reference) direct solution; the adjoint solution is by modal approximation using 33 left and right eigenvectors. Small model, 100% change in design variables of the variable element, g=0.06

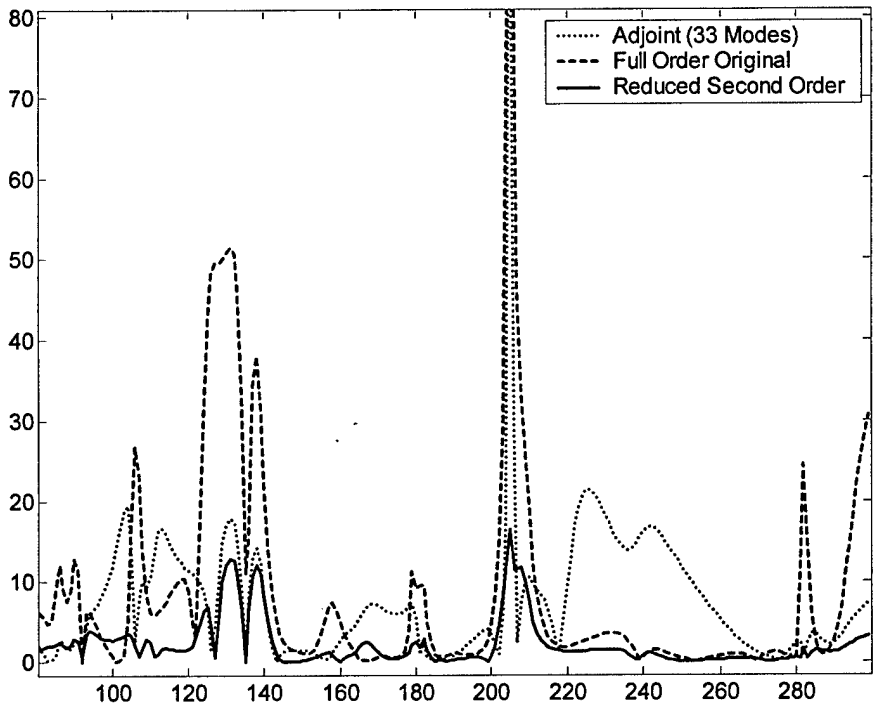

Figure 19: Error in dM/dI approximations as a function of excitation frequency. Approximate direct solution is the original (reference) direct solution; the adjoint solution is by modal approximation using 33 left and right eigenvectors. Small model, 100% change in the design variables of the variable element, g=0.06

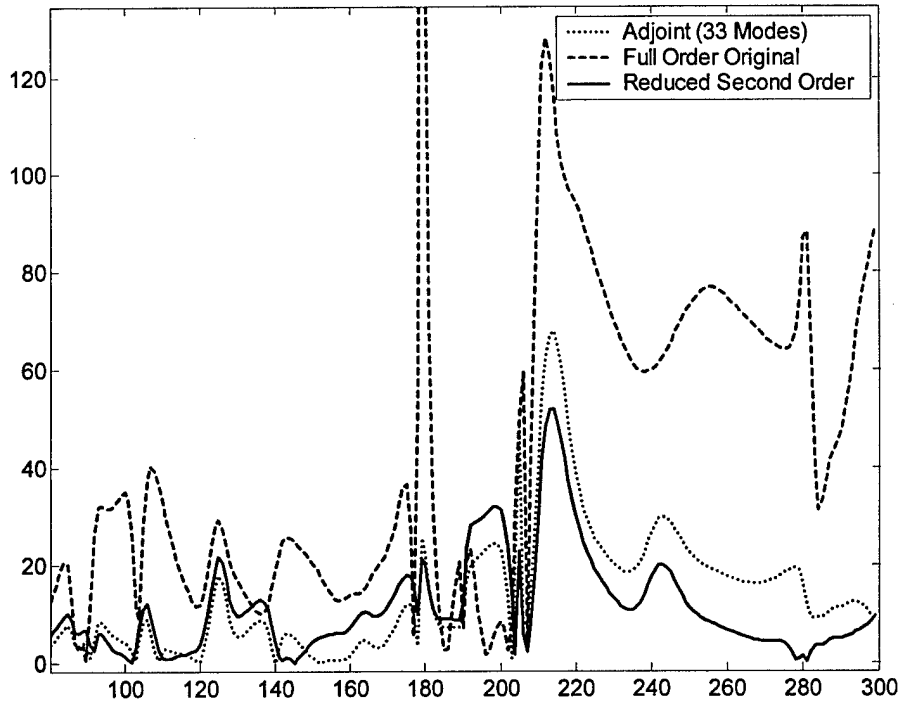

Figure 20: Error in dM/dA approximations as a function of excitation frequency. Approximate direct solution is the original (reference) direct solution; the adjoint solution is by modal approximation using 33 left and right eigenvectors. Small model, 100% change in design variables of the variable element, g=0.06

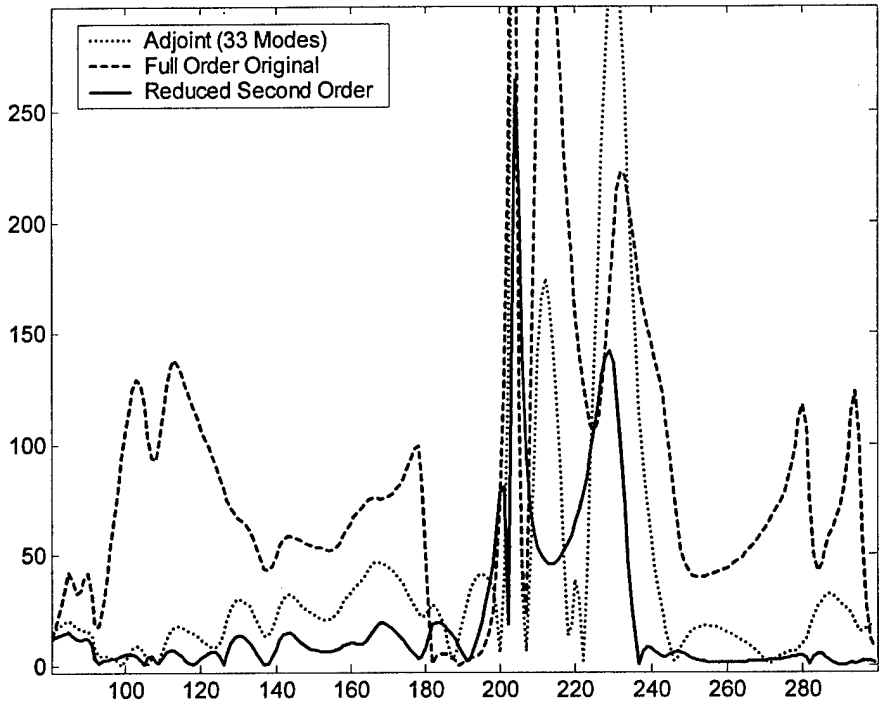

Figure 21: Error in dP/dI approximations as a function of excitation frequency. Approximate direct solution is the original (reference) direct solution; the adjoint solution is by modal approximation using 33 left and right eigenvectors. Small model, 100% change in design variables of the variable element, g=0.06

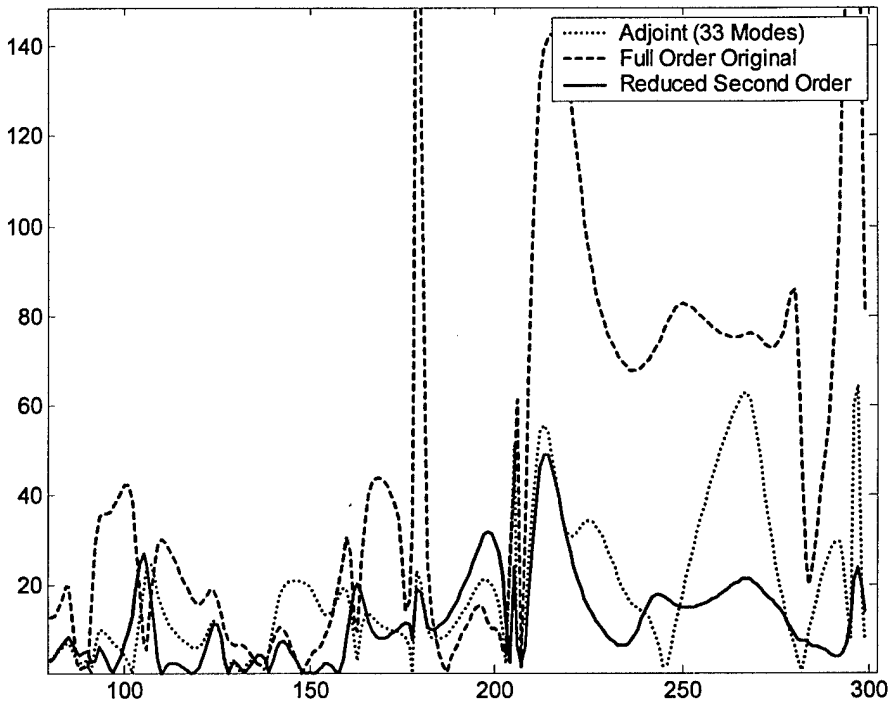

Figure 22: Error in dP/dA approximations as a function of excitation frequency. Approximate direct solution is the original (reference) direct solution; the adjoint solution is by modal approximation using 33 left and right eigenvectors. Small model, 100% change in design variables of the variable element, g=0.06

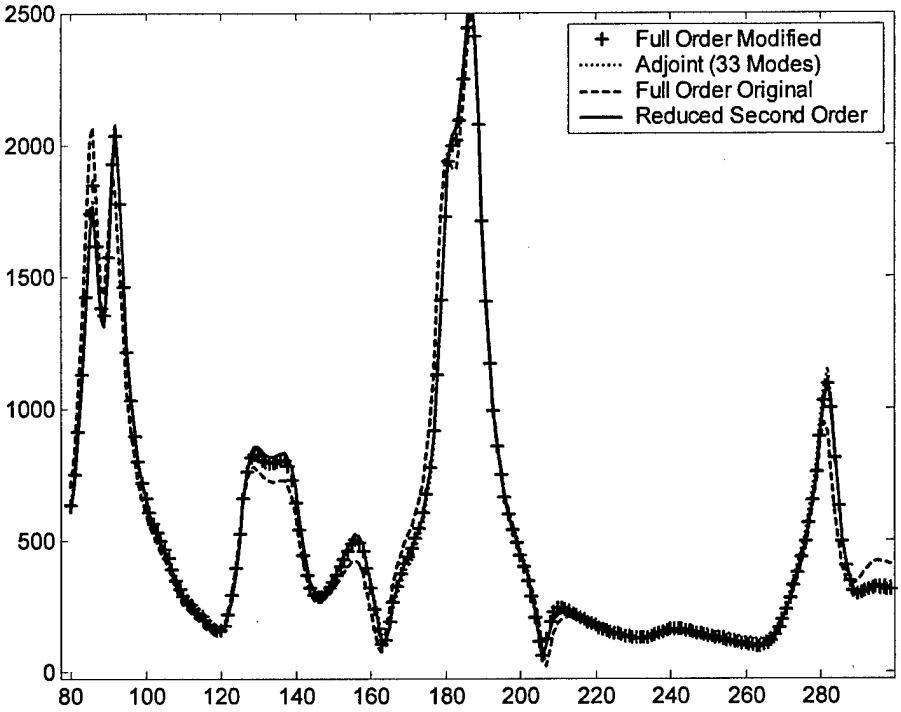

Figure 23: Pressure response approximation as a function of excitation frequency. Approximate direct solution is the original (reference) direct solution; the adjoint solution is by modal approximation using 33 left and right eigenvectors. Small model, 100% change in design variables of the variable element, g=0.06

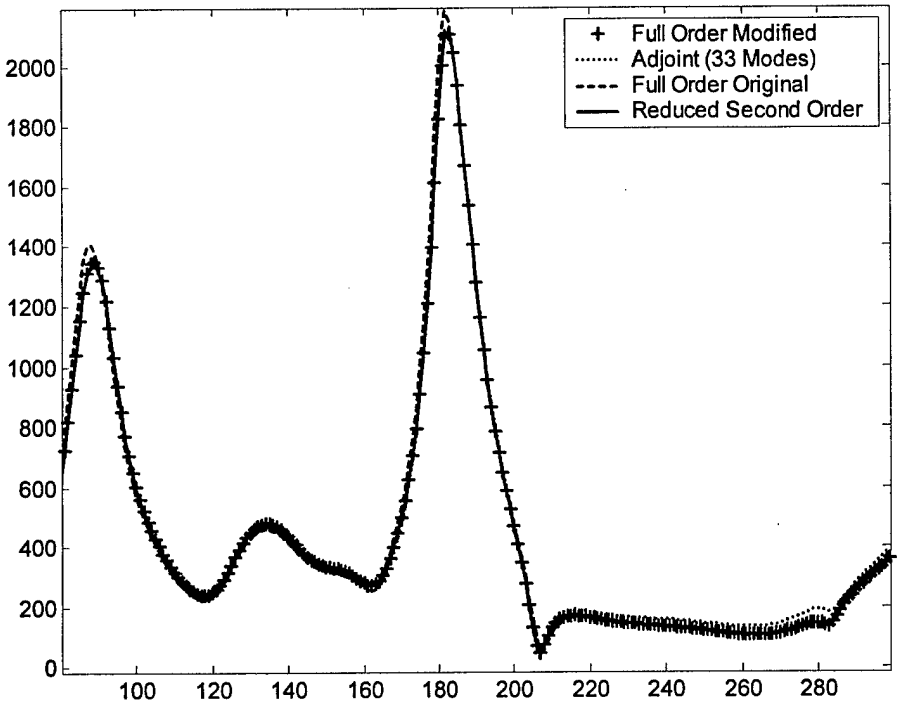

Figure 24: Pressure response approximation as a function of excitation frequency. Approximate direct solution is the original (reference) direct solution; the adjoint solution is by modal approximation using 33 left and right eigenvectors. Small model, 50% change in design variables of the variable element, g=0.15

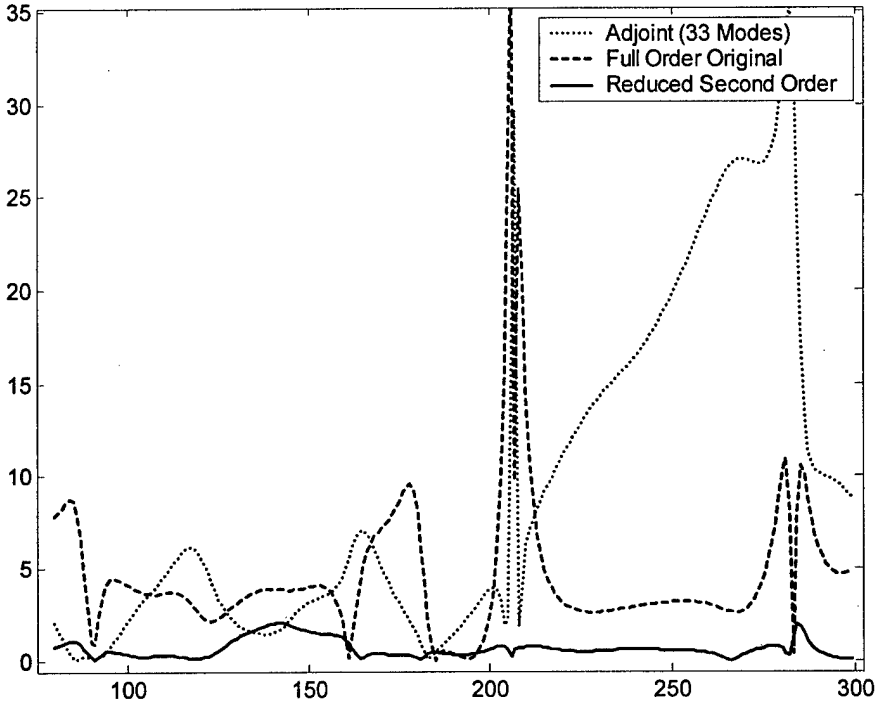

Figure 25: Error in pressure response approximations as a function of excitation frequency. Approximate direct solution is the original (reference) direct solution; the adjoint solution is by modal approximation using 33 left and right eigenvectors. Small model, 50% change in design variables of the variable element, g=0.15

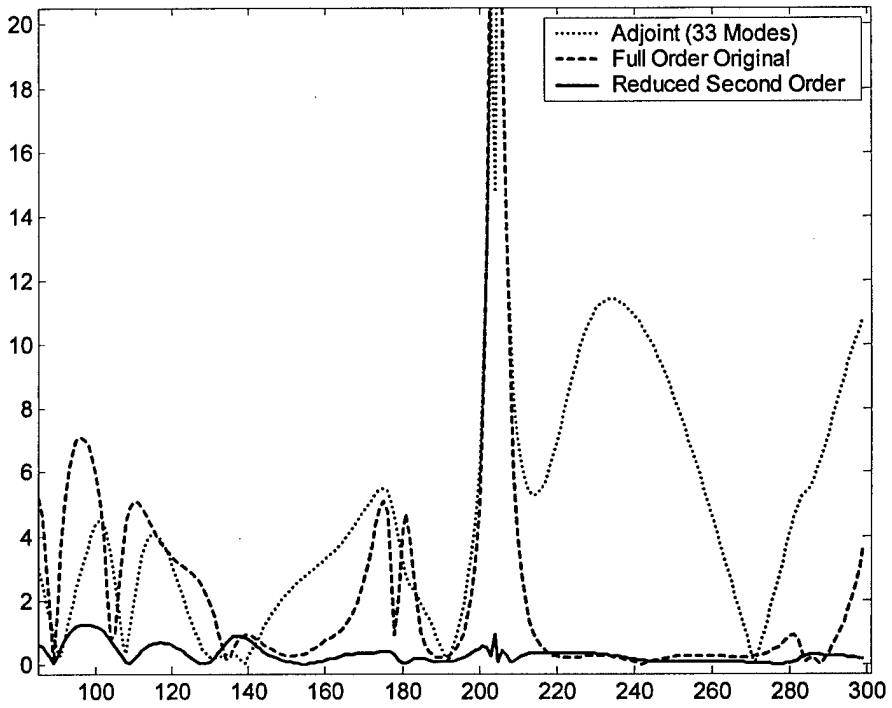

Figure 26: Error in bending moment response approximations as a function of excitation frequency. Approximate direct solution is the original (reference) direct solution; the adjoint solution is by modal approximation using 33 left and right eigenvectors. Small model, 50% change in design variables of the variable element, g=0.15

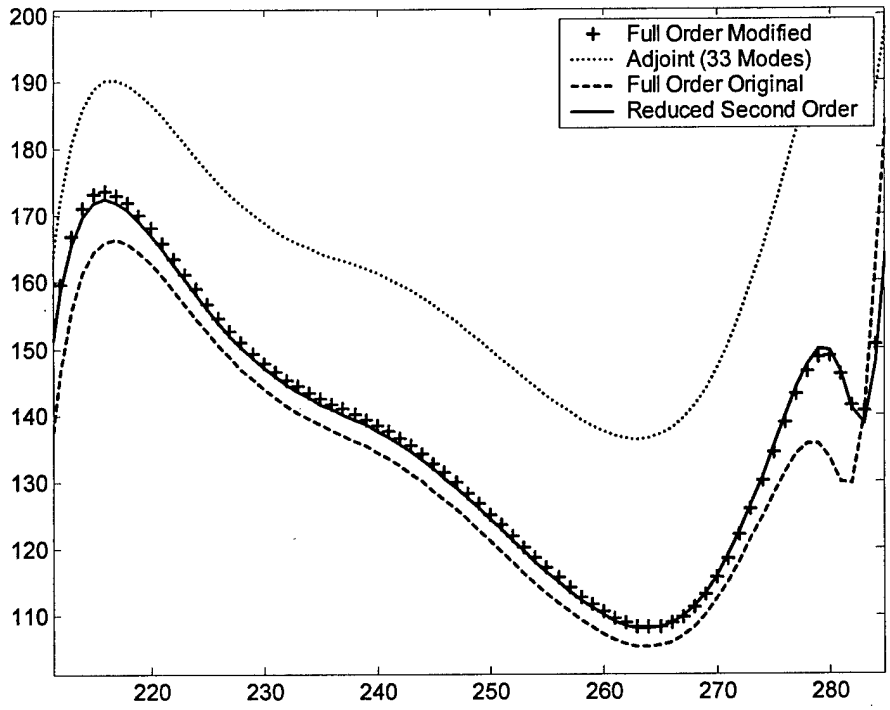

Figure 27: Pressure response approximation as a function of excitation frequency. Approximate direct solution is the original (reference) direct solution; the adjoint solution is by modal approximation using 33 left and right eigenvectors. Zoomed to area of interest. Small model, 50% change in design variables of the variable element, g=0.15

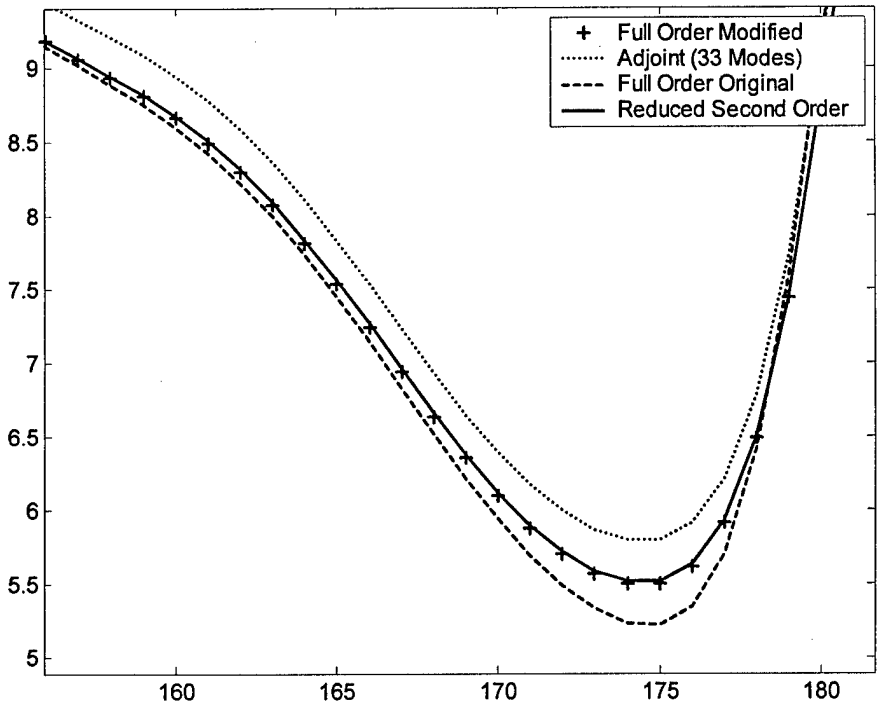

Figure 28: Bending response approximation as a function of excitation frequency. Approximate direct solution is the original (reference) direct solution; the adjoint solution is by modal approximation using 33 left and right eigenvectors. Zoomed to area of interest. Small model, 50% change in design variables of the variable element, g=0.15

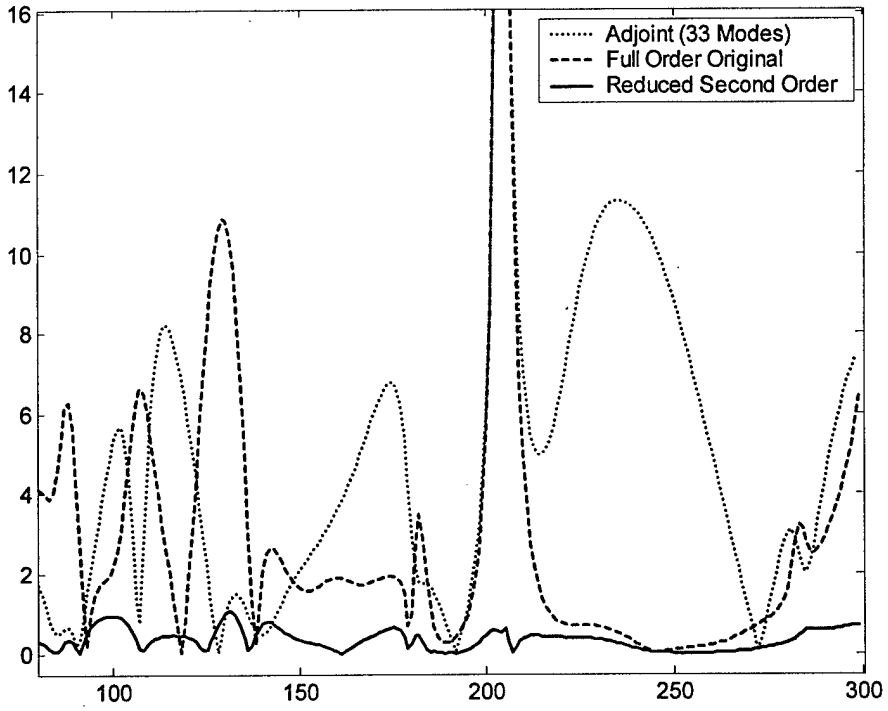

Figure 29: Error in dM/dI approximations as a function of excitation frequency. Approximate direct solution is the original (reference) direct solution; the adjoint solution is by modal approximation using 33 left and right eigenvectors. Small model, 50% change in design variables of the variable element, g=0.15

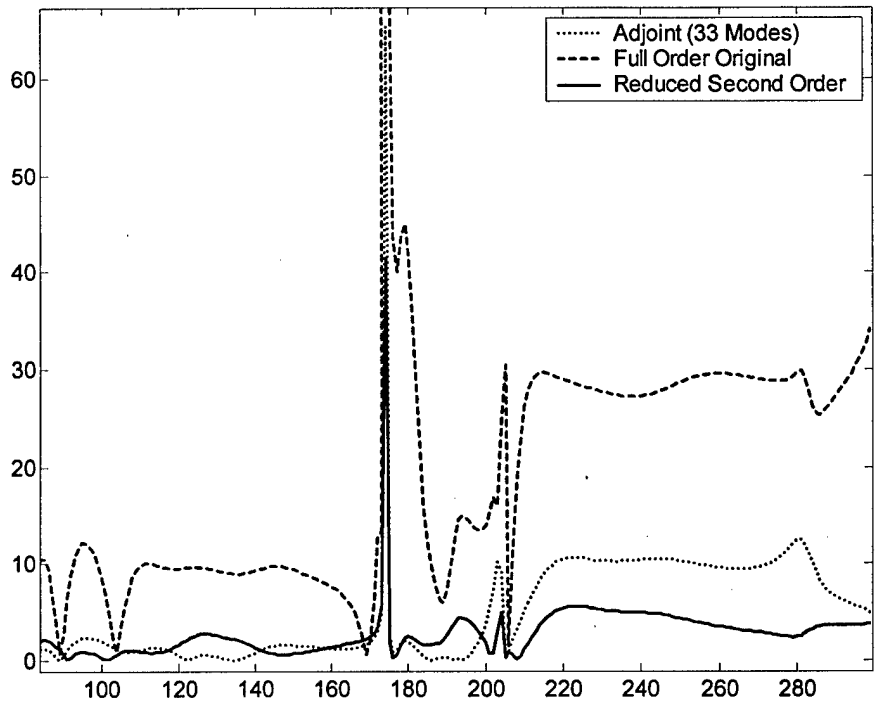

Figure 30: Error in dM/dA approximations as a function of excitation frequency. Approximate direct solution is the original (reference) direct solution; the adjoint solution is by modal approximation using 33 left and right eigenvectors. Small model, 50% change in design variables of the variable element, g=0.15

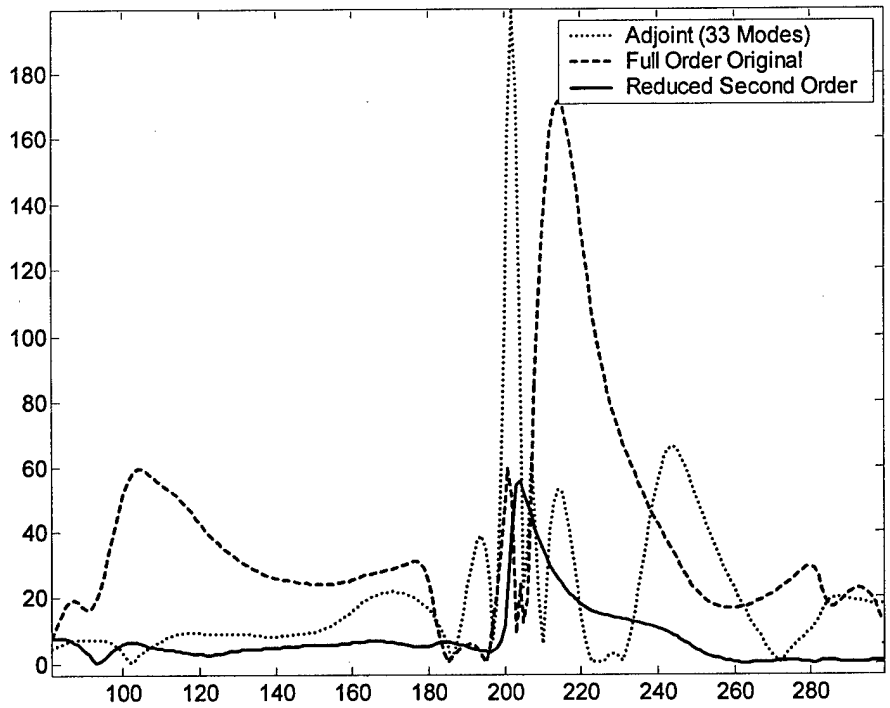

Figure 31: Error in dP/dI approximations as a function of excitation frequency. Approximate direct solution is the original (reference) direct solution; the adjoint solution is by modal approximation using 33 left and right eigenvectors. Small model, 50% change in design variables of the variable element, g=0.15

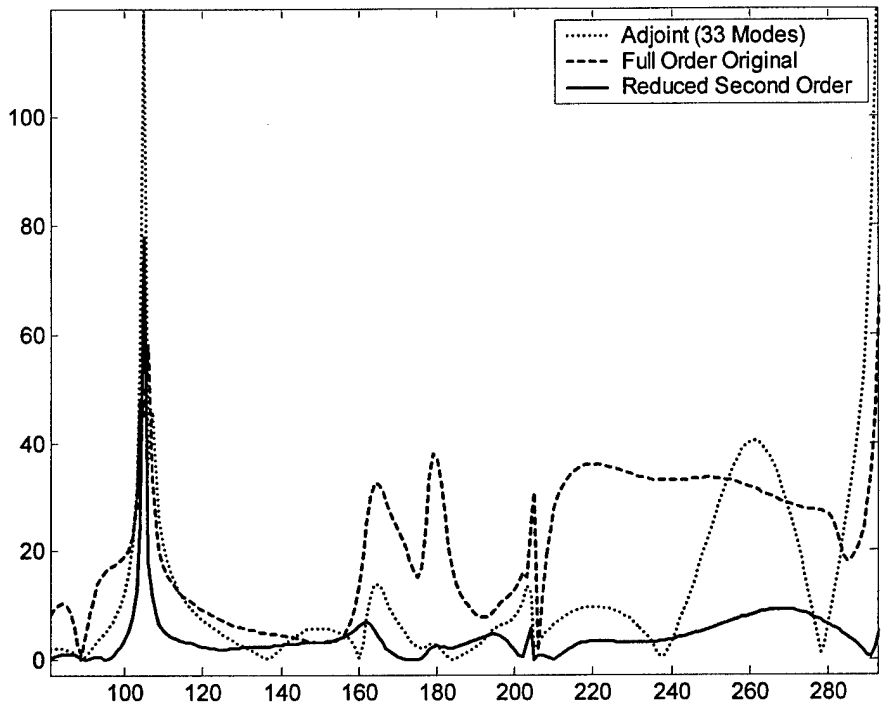

Figure 32: Error in dP/dA approximations as a function of excitation frequency. Approximate direct solution is the original (reference) direct solution; the adjoint solution is by modal approximation using 33 left and right eigenvectors. Small model, 50% change in design variables of the variable element, g=0.15

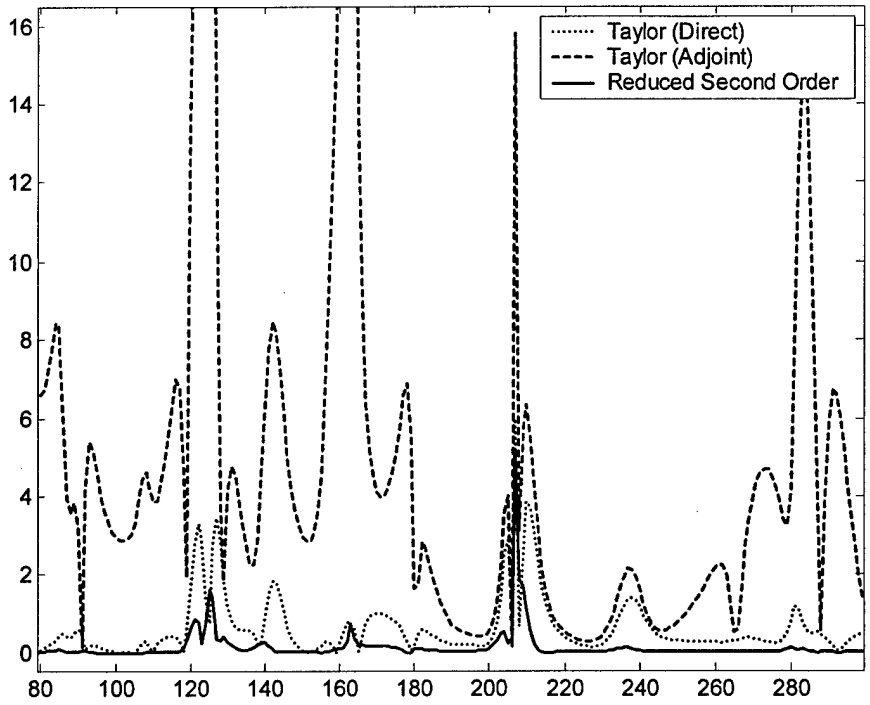

Figure 33: Error in Pressure approximations as a function of excitation frequency. Approximate direct solution and adjoint solution is by first order Taylor expansion. Small model, 10% change in design variable I of the variable element, g=0.06

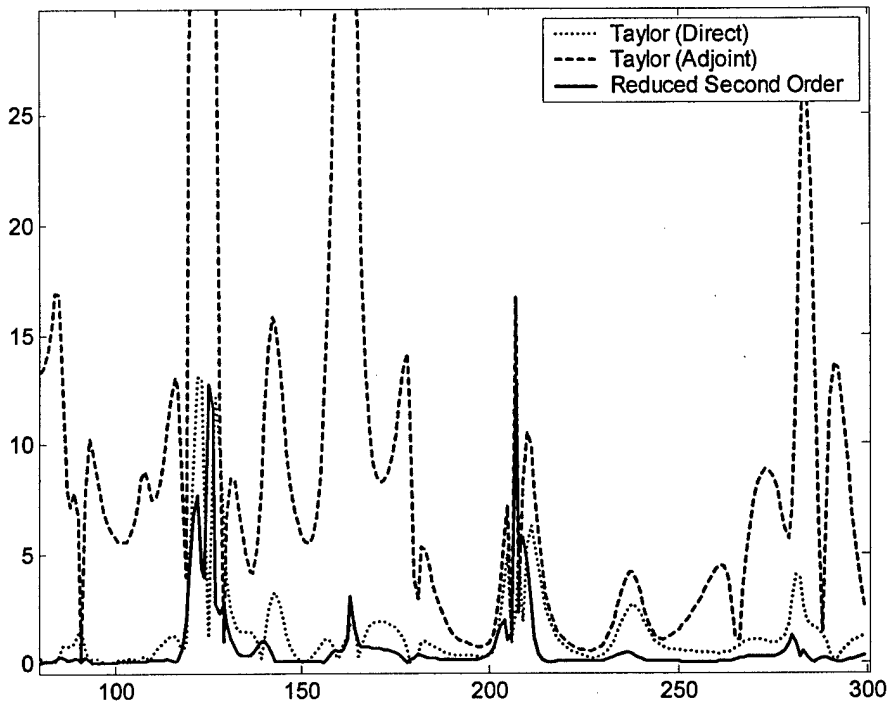

Figure 34: Error in Pressure approximations as a function of excitation frequency. Approximate direct solution and adjoint solution is by first order Taylor expansion. Small model, 20% change in design variable I of the variable element, g=0.06

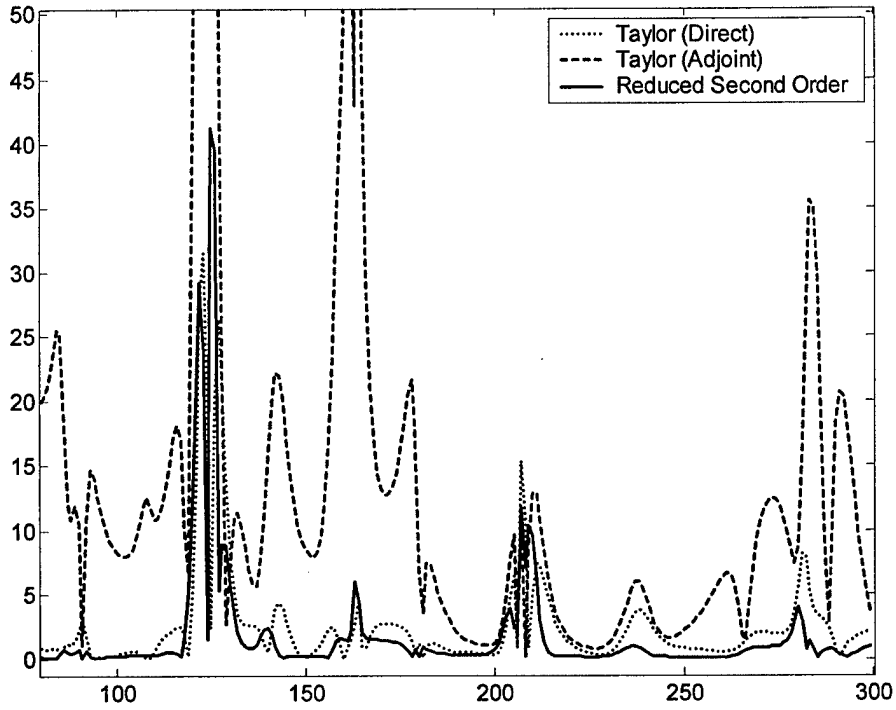

Figure 35: Error in Pressure approximations as a function of excitation frequency. Approximate direct solution and adjoint solution is by first order Taylor expansion. Small model, 30% change in design variable I of the variable element, g=0.06

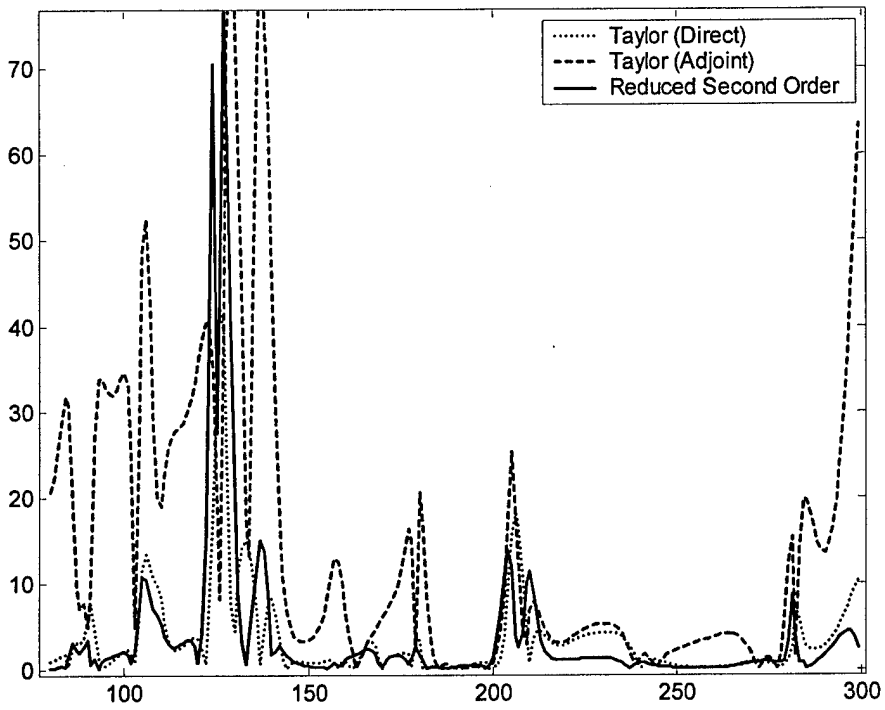

Figure 36: Error in Pressure approximations as a function of excitation frequency. Approximate direct solution and adjoint solution is by first order Taylor expansion. Small model, 50% change in design variable I of the variable element, g=0.06

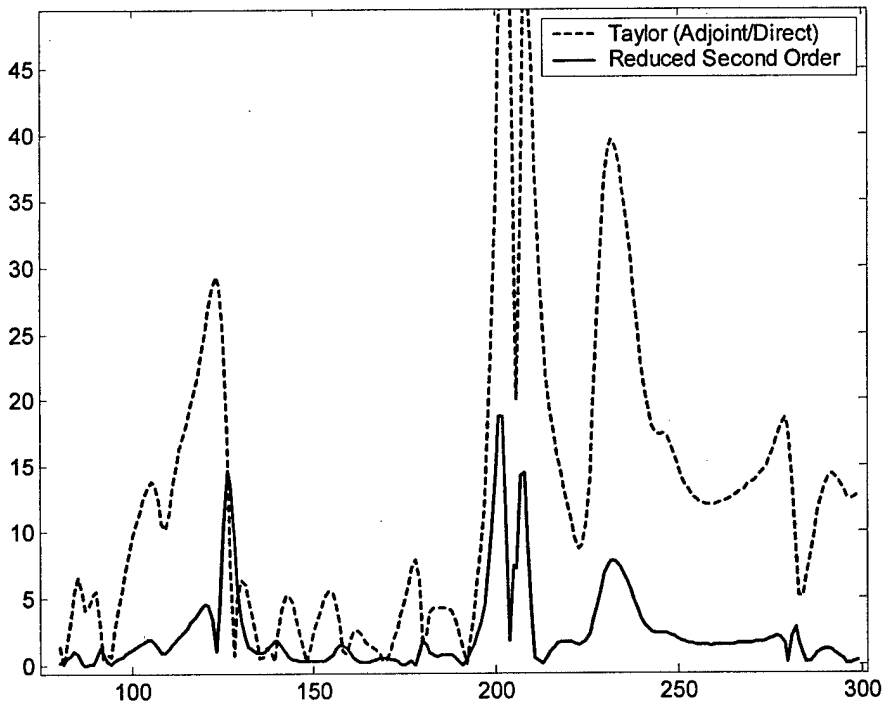

Figure 37: Error in dP/dI approximations as a function of excitation frequency. Approximate direct solution and adjoint solution is by first order Taylor expansion. Small model, 10% change in design variable I of the variable element, g=0.06

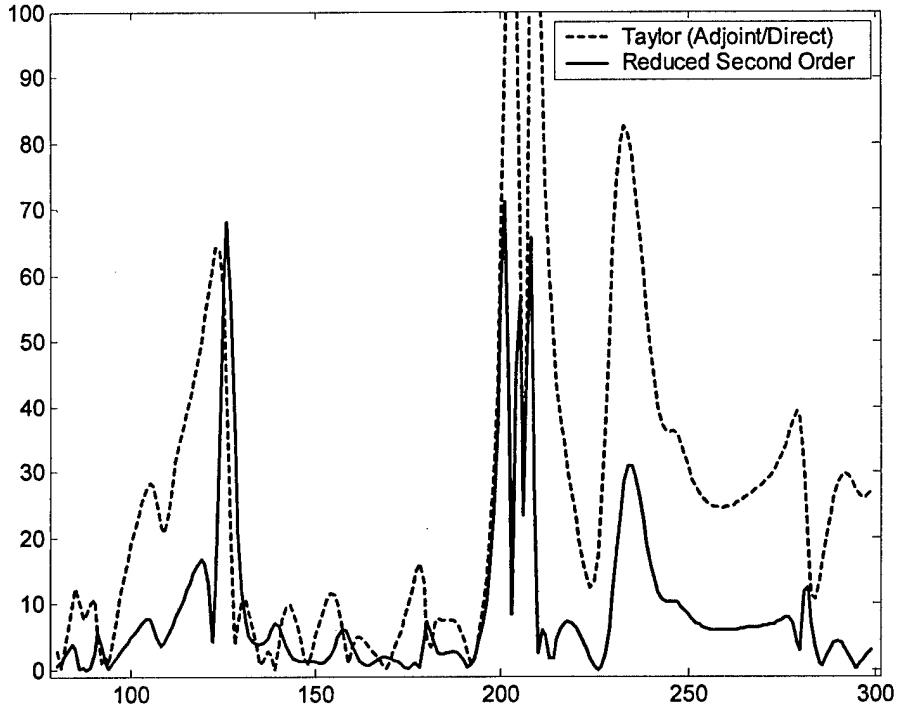

Figure 38: Error in dP/dI approximations as a function of excitation frequency. Approximate direct solution and adjoint solution is by first order Taylor expansion. Small model, 20% change in design variable I of the variable element, g=0.06

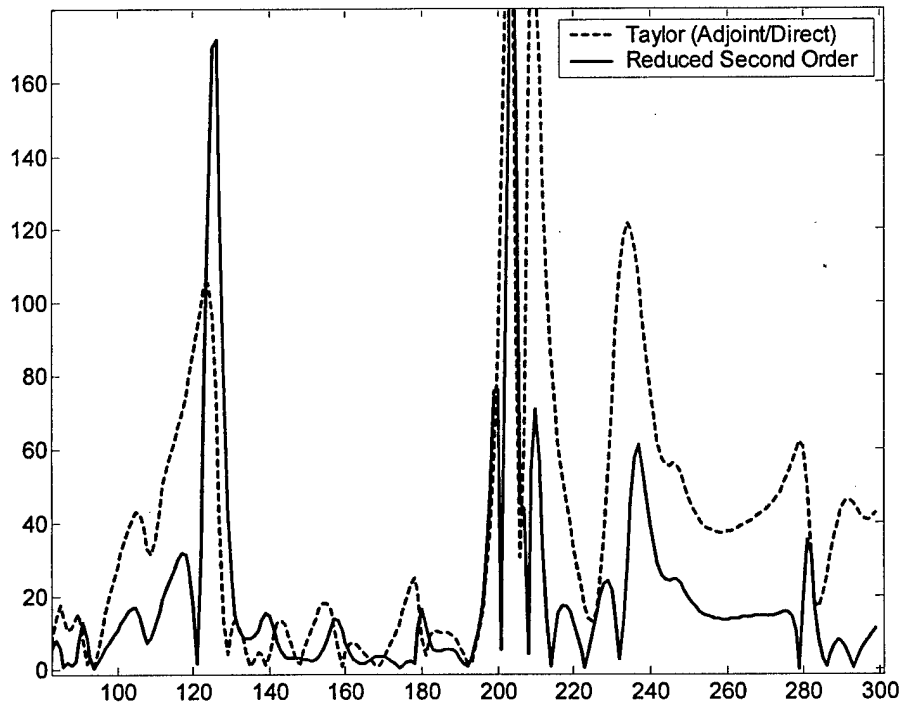

Figure 39: Error in dP/dI approximations as a function of excitation frequency. Approximate direct solution and adjoint solution is by first order Taylor expansion. Small model, 30% change in design variable I of the variable element, g=0.06

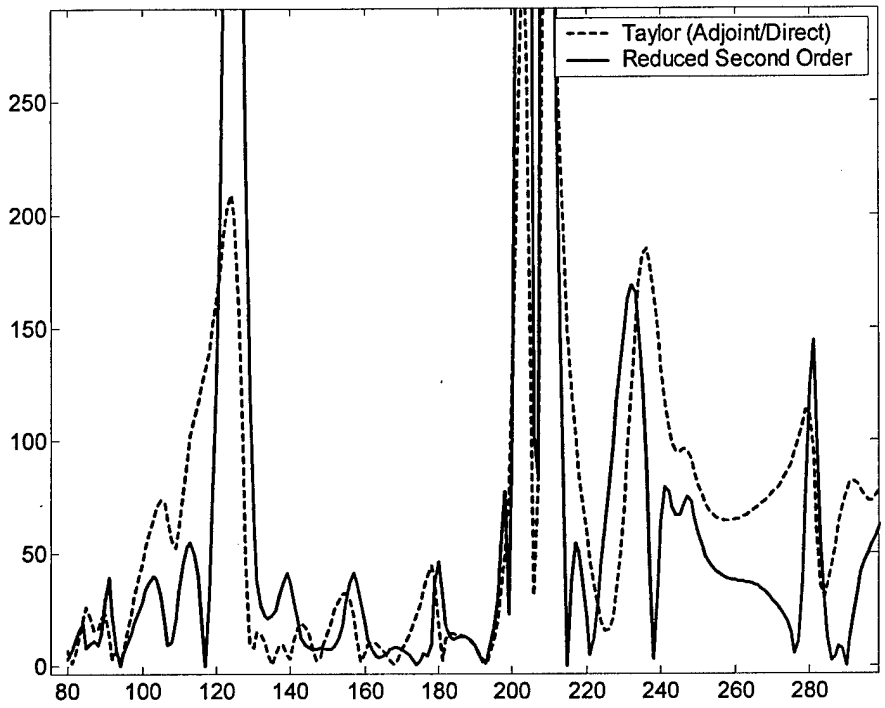

Figure 40: Error in dP/dI approximations as a function of excitation frequency. Approximate direct solution and adjoint solution is by first order Taylor expansion. Small model, 50% change in design variable I of the variable element, g=0.06

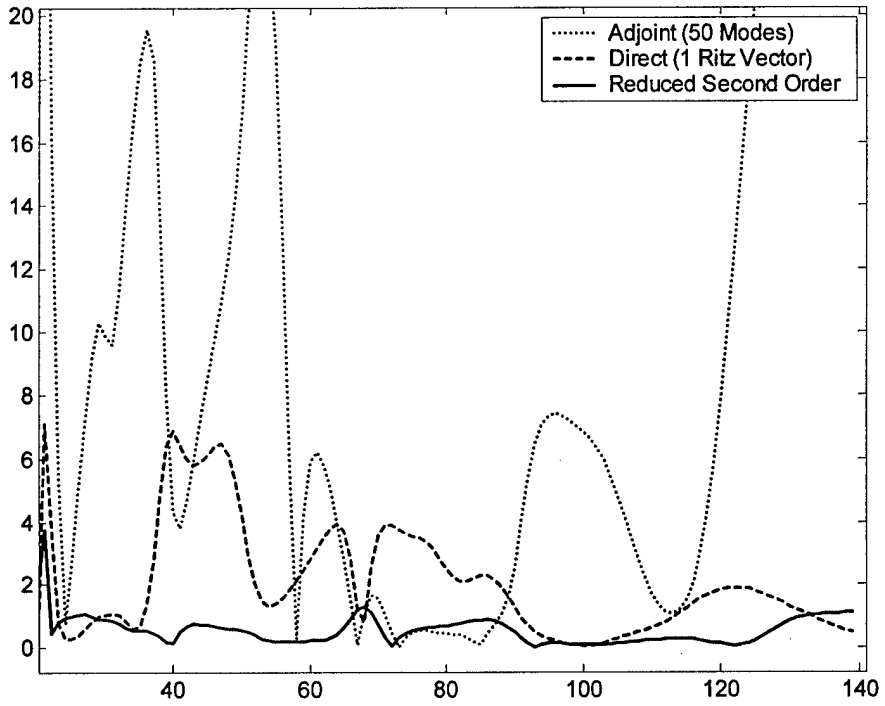

Figure 41: Error in dP/dI approximations as a function of excitation frequency. Approximate direct solution and adjoint solution is by first order Taylor expansion. Small model, 50% change in design variable I of the variable element, g=0.06

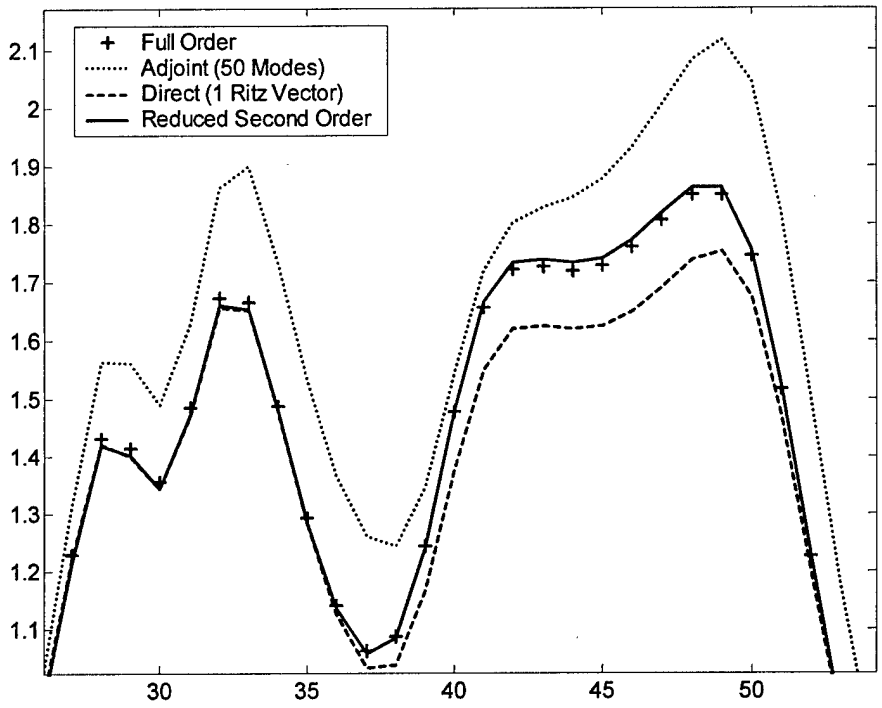

Figure 42: Pressure response approximation as a function of excitation frequency. Adjoint solution approximated by 50 modes, Direct solution approximated by 1 Ritz Vector. Large-scale (1543 DOF) model. Zoomed to area of interest.

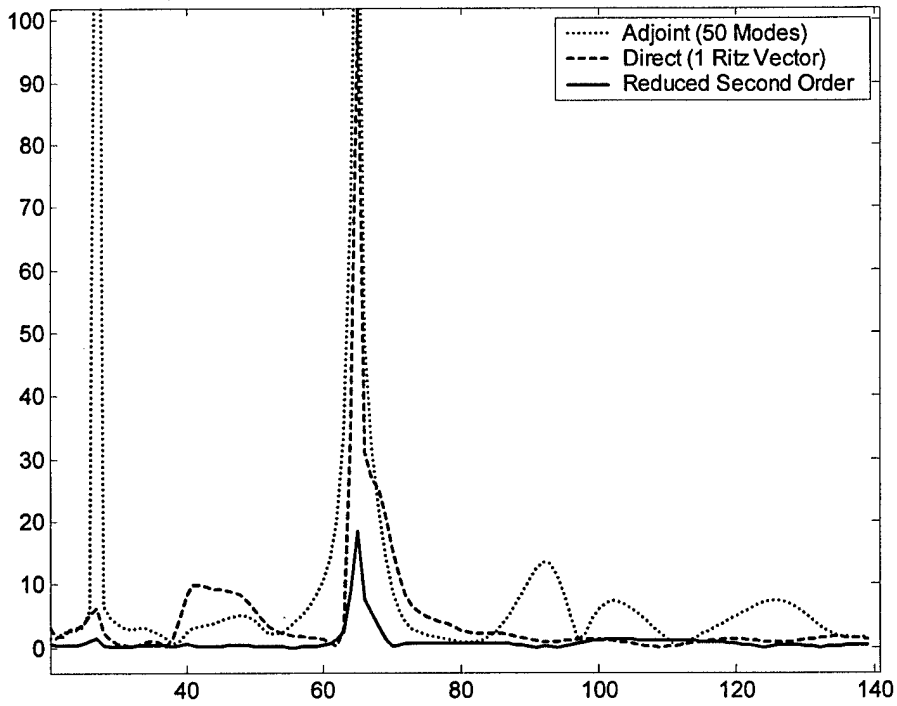

Figure 43: Error (%) in Bending Moment approximations as a function of excitation frequency. Adjoint solution approximated by 50 modes, Direct solution approximated by 1 Ritz Vector. Large-scale (1543 DOF) model.

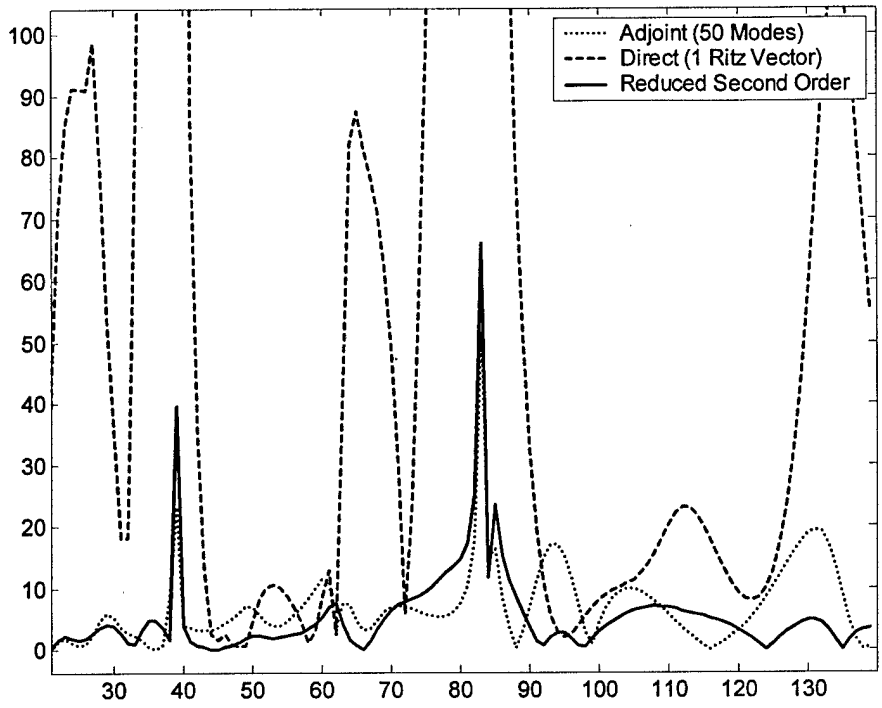

Figure 44: Error (%) in dM/dA approximations as a function of excitation frequency. Adjoint solution approximated by 50 modes, Direct solution approximated by 1 Ritz Vector. Large-scale (1543 DOF) model.

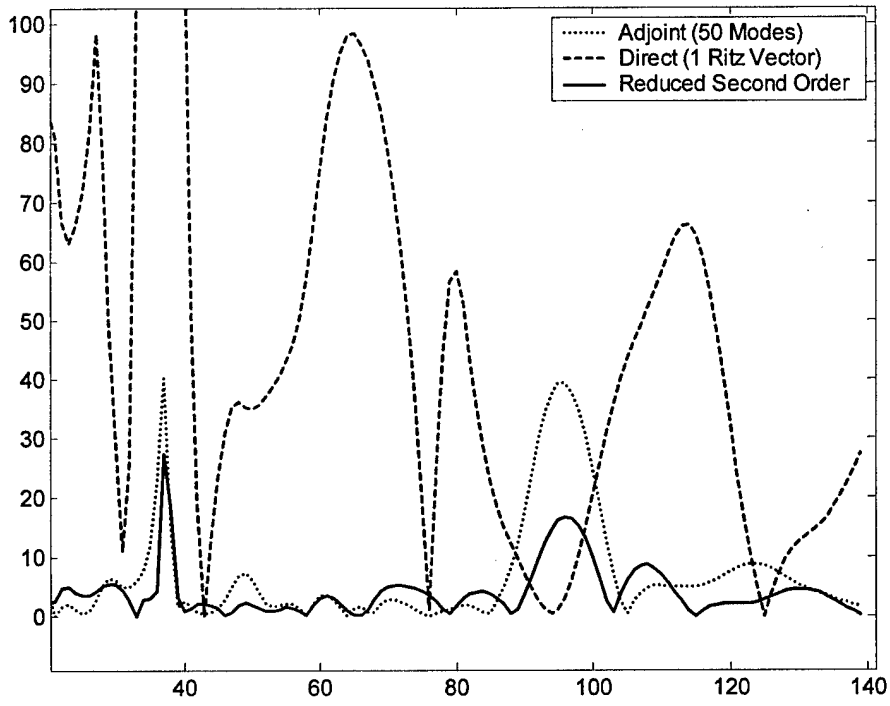

Figure 45: Error (%) in dM/dA approximations as a function of excitation frequency. Adjoint solution approximated by 50 modes, Direct solution approximated by 1 Ritz Vector. Large-scale (1543 DOF) model.

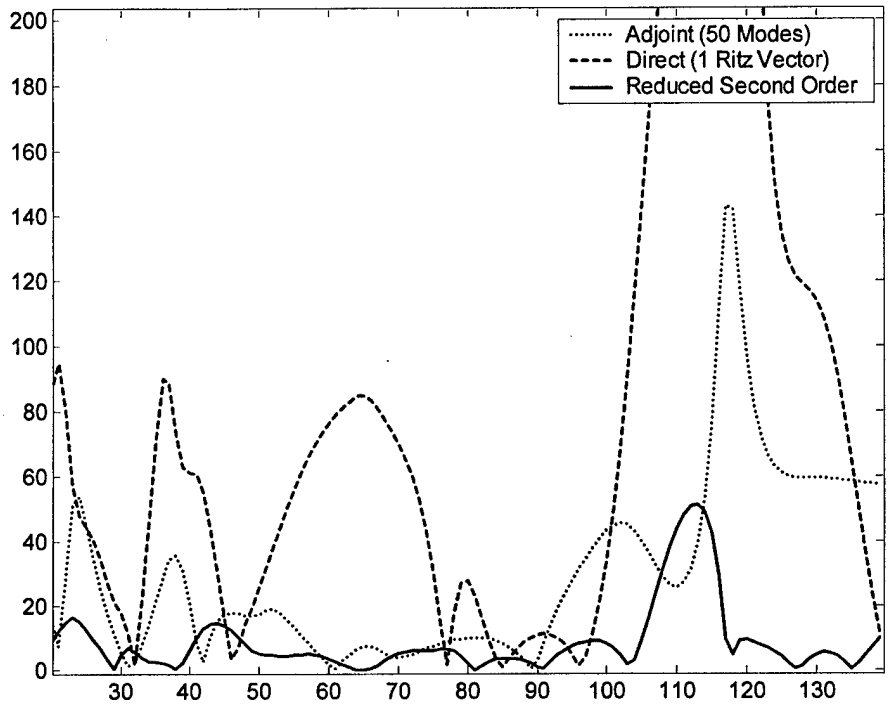

Figure 46: Error (%) in dP/dA approximations as a function of excitation frequency. Adjoint solution approximated by 50 modes, Direct solution approximated by 1 Ritz Vector. Large-scale (1543 DOF) model.

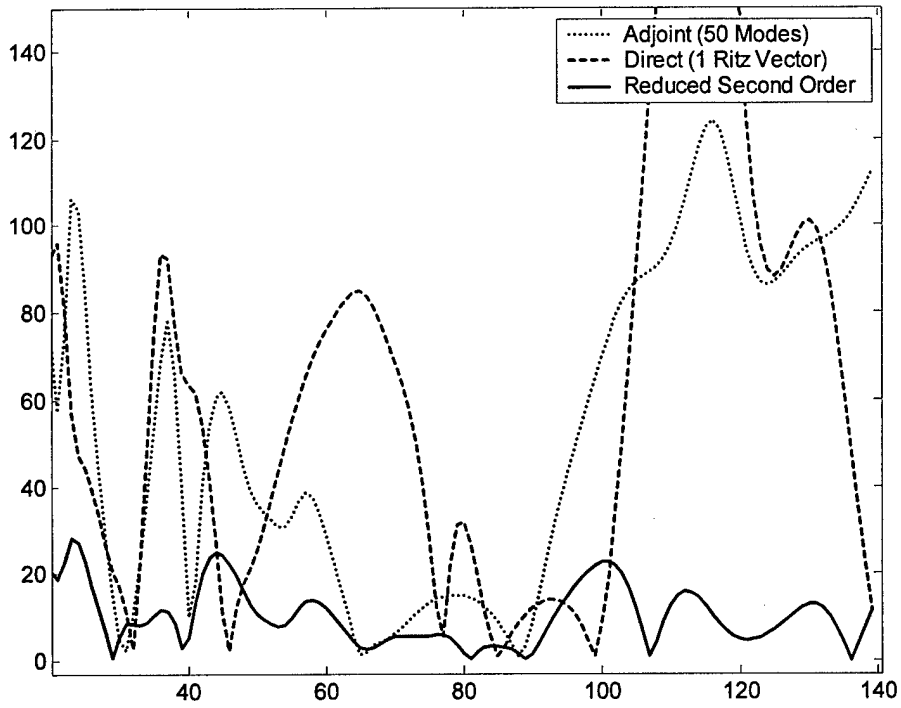

Figure 47: Error (%) in dP/dA approximations as a function of excitation frequency. Adjoint solution approximated by 50 modes, Direct solution approximated by 1 Ritz Vector. Large-scale (1543 DOF) model.

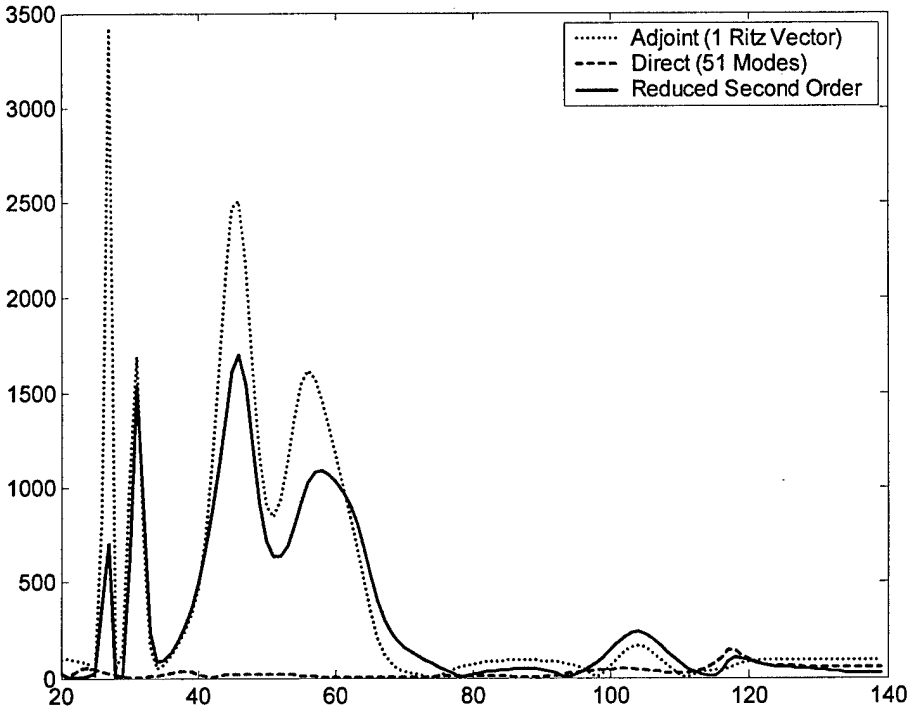

Figure 48: Error (%) in dP/dI approximations as a function of excitation frequency. Adjoint solution approximated by 1 Ritz vector, Direct solution approximated by 51 modes. Large-scale (1543 DOF) model.

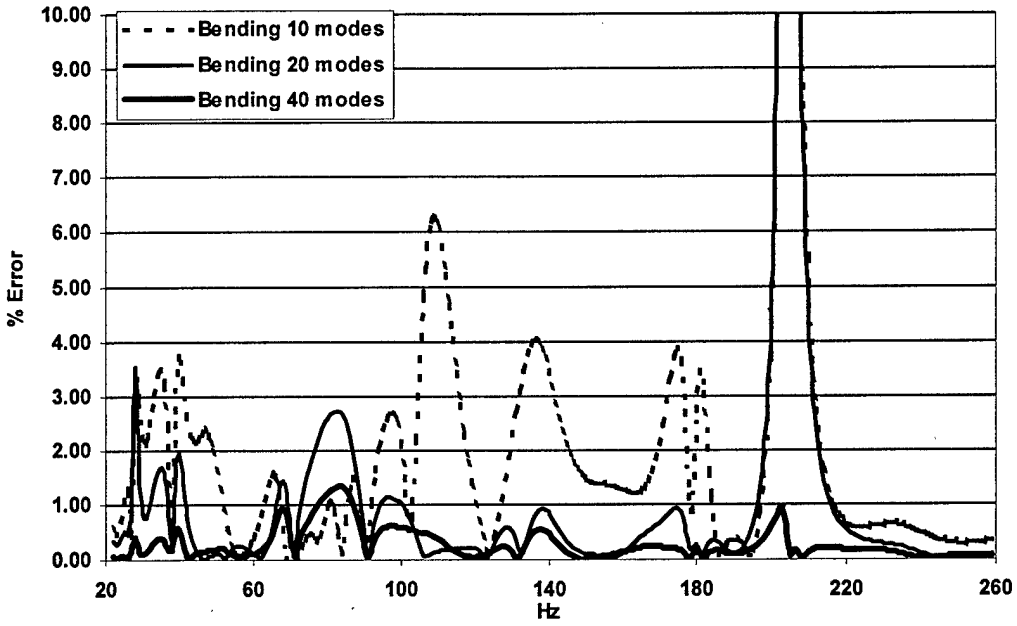

Figure 49: Reduction in error of the second order bending moment approximation as a function of excitation frequency, as modal basis is increased. Direct solution approximated by 1 Ritz vector, Adjoint solution approximated by 10, 20 and 40. Small-scale (275 DOF) model, g=0.15

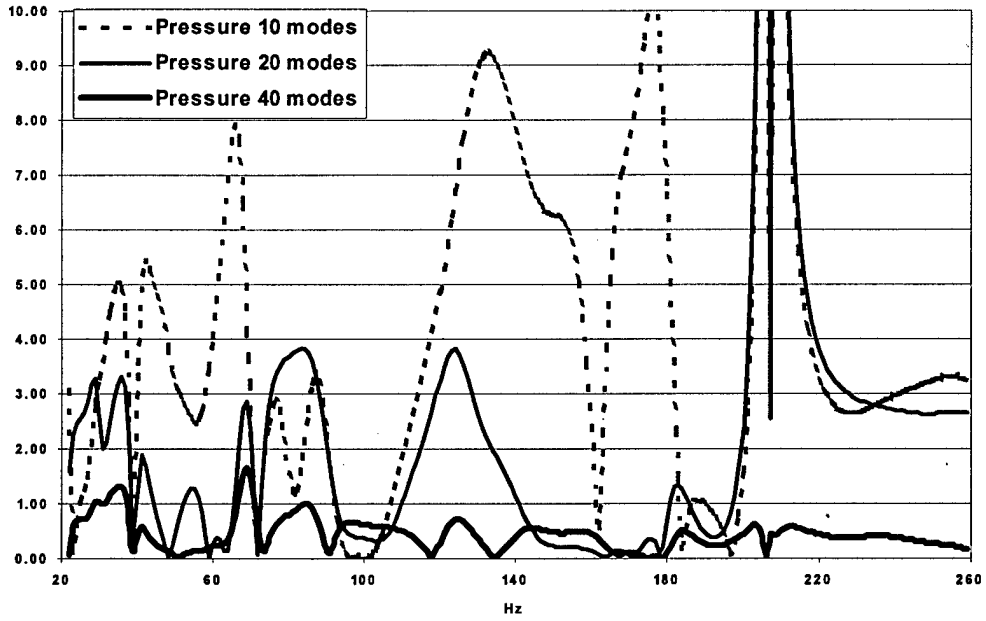

Figure 50: Reduction in error of the second order pressure approximation as a function of excitation frequency, as modal basis is increased. Direct solution approximated by 1 Ritz vector, Adjoint solution approximated by 10, 20 and 40. Small-scale (275 DOF) model, g=0.15

Chapter 5: Conclusions

Results were presented for various approximation studies using the second order approximation method for a coupled structural-acoustic finite element enclosure surrounded by flexible walls. Application of the combined direct-adjoint solution for second order approximation was extended from structural dynamic models to coupled structural-acoustic models, and a variety of first order approximation methods for the direct and adjoint problems were explored. Bending moment/stress and pressure frequency response and sensitivity to design variables, critical for optimization techniques, were studied, and improvements were quantified for the accuracy of the combined direct/adjoint second order approximation when compared to first order approximation techniques. A system where the design variables evolve relative to a reference system, as is typical in the optimization process, was examined. Finally, the effects of increasing the modal basis for the second order approximation method were also presented.

It was shown that the second order approximation method was able to significantly improve accuracy over first order methods provided that two reasonably accurate first order adjoint and direct approximations are available. In cases where only one was accurate and the other was grossly inaccurate, the second order approximation would only be as good as the better one of the two first order approximations. Some first order approximations can be as simple as using the actual direct and adjoint solution for the reference model, which costs

nothing computationally to obtain beyond the reference analysis. More sophisticated approximations such as using Ritz Vectors, Taylor expansion, or modal approximation could be employed. A large part of this work has been an effort in finding a reliable combination of adjoint and direct approximations for use in the second order method.

The combination that gave the most consistently accurate results was the adjoint solution approximated using the modal approximation with the direct solution approximated with using the Ritz vector method. Conversely, the worst performing approximation was the adjoint solution approximated using the Ritz vector method with the direct solution using modal approximation. This was primarily due to the inability of one single Ritz vector (obtained for one configuration) to capture the behavior of approximate pressure responses when the natural mode frequencies were shifted even slightly due to changes in design variables.

Where the second order approximation method has been shown to improve accuracy it also offers significant computational time savings by reducing large sized problems in the order of hundreds of thousands of degrees of freedom to a much smaller problem of mere tens of equations. For the purposes of optimization techniques, these computational time savings are compounded as the optimizer recalculates the problem many times in the optimization process.

Further investigation of this method (particularly the ways for finding more reliable and cost efficient first order approximations to be used in the combined direct/adjoint second order approximation method) can potentially further increase accuracy while maintaining the cost and time saving advantage.

It is hoped that this work contributes to the efficiency of solving design oriented structural-acoustic problems by providing an additional practical numerical computing tool, as well as point to additional avenues of research in the field of order reduction of large-scale design oriented finite element modeling.

References

1. ANSYS Theory Reference, 001099, Ninth Edition, SAS IP, Inc., Chapter 8.

2. Arnold, R.R., Citerley, R.L., Chargin, M., Galant, D., "Application of Ritz Vectors for Dynamic Analysis of Large Structures", Computers and Structures, Vol. 21, No. 5, pp. 901-908, 1985. Vol. 21, No. 3, pp. 461-467, 1985.

3. Barthelemy, J.-F.M. and Haftka, R.T. Approximation concepts for optimum structural design - a review. *Structural Optimization*, 5, 129-144, 1993

4. Bisplinghoff, R.L., Ashley, H., and Halfman, R.L., Aeroelasticity, Addison-Wesley, Reading, Massachusetts, 1955, pp.641-650.

5. Canfield, R.A., "Design of Frames Against Buckling Using a Rayleigh Quotient Approximation", AIAA Journal, Vol. 31, No. 6, June 1993, pp. 1143-1149.

6. Canfield, R. A., "High Quality Approximation of Eigenvalues in Structural Optimization", AIAA Journal, Vol. 28, No. 6, 1990, pp. 1116-1122.

7. Choi, K.K., Shim, I., Lee, J., and Kulkami, H.T., " Design Sensitivity Analysis of Dynamic Frequency Responses of Acousto-Elastic Built-Up Structures", in Optimization of Large Structural Systems, G.I.N. Rozvany, editor, Vol. I, pp. 329-343, Kluwer Academic Publishers, the Netherlands, 1993.

8. Craig, R.R., Structural Dynamics, John Wiley & Sons, New York, 1981.

9. Everstine, G.C., "Finite Element Formulations of Structural Acoustics Problems", Computers & Structures, Vol. 65, No. 3, 1997, pp. 307-321.

10. Flanigan, D.L., and Borders, S.G., "Application of Acoustic Modeling for Vehicle Boom Analysis", Society of Automotive Engineers Paper 840744, 1984.

11. Guyan, R.J., "Reduction of Stiffness and Mass Matrices", AIAA Journal, Vol. 3, No. 2, p. 380. 1965.

12. Habault, D., (editor), Fluid-Structure Interactions in Acoustics, Springer Verlag, Wien New York, 1999, ISBN 3-211-83147-9.

13. Haftka, R.T., and Gurdal, Z., Elements of Structural Optimization, Third revised and expanded addition, Kluwer Academic Publishers, Dordrecht, The Netherlands, 1992.

14. Hurty, W.C., and Rubinstein, M.F., "Dynamics of Structures", Prentice Hall Inc., Englewood Cliffs, New Jersey, 1964, pp. 299-307.

15. Ihlenburg, F., Finite Element Analysis of Acoustic Scattering, Springer Verlag, New York, 1998.

16. Johnson, E.H., "Adjoint Sensitivity Analysis in MSC/NASTRAN", MSC NASTRAN World Users Conference 1997.

17. Kardestuncer, H., and Norrie, D.H., "Finite Element Handbook", McGraw-Hill, 1987, section 7.4.

18. Karpel, M., and Raveh, D., "Fictitious Mass Element in Structural Dynamics", AIAA Journal, Vol. 34, No. 3, 1996, pp. 607-613.

19. Kline, K.A., "Dynamic Analysis using a Reduced Basis of Exact Modes and Ritz Vectors", AIAA Journal, Vol. 24, No. 12, December 1986, pp. 2022-2029.

20. Li, W-L., and Livne, E., "Analytic Sensitivities and Approximations in Supersonic and Subsonic Wing / Control Surface Unsteady Aerodynamics", Journal of Aircraft, Vol. 34, No. 3, pp. 370-379, May-June 1997.

21. Livne, E., "Accurate Calculation of Control Augmented Structural Eigenvalue Sensitivities Using Reduced-Order Models", AIAA Journal, Vol. 27, No. 7, 1989, pp. 947-954.

22. Livne, E., and Blando, G.D., "Reduced Order Design-Oriented Stress Analysis Using Combined Direct and Adjoint Solutions", AIAA Journal, Vol. 38, No. 5, 2000, pp. 898-909.

23. Livne, E., and Blando, G.D., "Structural Dynamic Frequency Response Using Combined Direct and Adjoint Reduced-Order Approximation", AIAA Journal, Vol. 41, No. 7, July 2003, pp. 1377-1385.

24. Ma, Z.D., and Hagiwara, I., "Improved Mode-Superposition Technique for Modal Frequency Response Analysis of Coupled Acoustic-Structural Systems", AIAA Journal, Vol 29, No. 10, 1991, pp. 1720-1726.

25. Morand, H., J.P., and Ohayon, R., "Fluid-Structure Interaction: Applied Numerical Methods", John Wiley & Sons, 1995.

26. Morand, H., and Ohayon, R., "Substructure Variational Analysis of the Vibrations of Coupled Fluid-Structure Systems. Finite Element Results, International Journal for Numerical Methods in Engineering, Vol. 14, 1979, pp. 741-755.

27. Nefske, D. J.; Sung, S. H. , "Vehicle Interior Acoustic Design Using Finite Element Methods, Int. J. of Vehicle Design", Vol. 6, No. 1, pp. 24-40, 1985.

28. Nour-Omid, B., and Clough, R.W., "Dynamic Analysis of Structures Using Lanczos Coordinates", International Journal of Earthquake Engineering and Structural Dynamics, Vol. 12, No. 4., pp. 565-577. 1984.

29. Ohayon, R., and Soize, C., "Structural Acoustics and Vibrations", Academic Press 1998.

30. Sandridge, C. A., and Haftka, R. T., "Accuracy of Eigenvalue Derivatives from Reduced Order Structural Models," Journal of Guidance, Control and Dynamics, 12, 6, pp. 822-829, 1989.

31. Sandridge, C. A., and Haftka, R. T., ` `Modal Truncation, Ritz Vectors and Damping-Ratio Derivatives in Structural Control," Journal of Guidance, Control and Dynamics, Vol. 14, No. 4, pp. 785-790, 1991.

32. Sung, S. H.; Nefske, D. J., "A Coupled Structural-Acoustic Finite Element Model for Vehicle Interior Noise Analysis", Trans. of the ASME, J. of Vibration, Acoustics, Stress and Reliability in Design, Vol. 106, pp. 314-318, 1984.

33. Unruh, J.F., "Finite Element Subvolume Technique for Structural-Borne Interior Noise Prediction", Journal of Aircraft, Vol.17, No. 6, 1980, pp. 434-441.

34. Van-Niekerk, B., "Computation of Second Order Accurate Unsteady Aerodynamic Generalized Forces", AIAA Journal, Vol. 24, No. 3, 1986, pp. 492-498.

35. Wang, X., "On a Mode Superposition Method for Fluid-Structure Interaction Problems", Paper DAS-RH-P07, ASME DE-Vol. 98, Dynamics, Acoustics, and Simulations, ASME 1998, pp. 71-77.

36. Wenigwieser, C., and Haeusler, S., "Finite Element Application to Interior Noise Prediction in Aircraft Fuselage", ICAS-90-4.2R, Proceeding of the 17th Congress of the International Council of the Aeronautical Sciences, Stockholm, 19-24 September 1990, pp. 2094-2104.

37. Wilson, E.L., "A New Method of Dynamic Analysis for Linear and Non-Linear Systems", Finite Element in Analysis and Design, Vol.1, 1985, pp 21-23.

38. Wilson, E.L., Yuan, M. W., and Dickens, J.M., "Dynamic Analysis by Direct Superposition of Ritz Vectors", International Journal of Earthquake Engineering and Structural Dynamics, Vol. 10, pp. 813-821, 1982.

39. Wolf Jr., J.A., Nefske, D. J., and Howell, L.J., "Structural-Acoustic Finite Element Analysis of the Automobile Passenger Compartment", Transactions of the Society of Automotive Engineers, Vol. 85, pp. 857-864, 1976.

40. Yashiro, H., Suzuki, K., Kaijo, Y., Hagiwara, I., and Arai, A., "An Application of Structural-Acoustic Analysis to Car Body Structures," SAE 1985 Transactions Section, Vol. 4, 1985, pp. 777-784.

41. Zienkiewicz, O.C., and Taylor, R.L., "The Finite Element Method", Fourth Edition, Volume 2, 1991, McGraw-Hill, London, New York, Chapter 11.

Appendix A: Derivation of Acoustic Equations

Assuming a compressible homogeneous fluid, the homogeneous initial pressure field (uniform, constant),

$$p_0, \rho_0, \overline{U}_0 = 0 \tag{A.1}$$

For small disturbances:

$$p << p_0, \rho << \rho_0, \overline{u} << 1 \tag{A.2}$$

The Thermodynamic and state relations:

For an isentropic process (adiabatic, no change in entropy),

$$\frac{p_0 + p}{(\rho_0 + \rho)^\gamma} = \frac{p_{total}}{(\rho_{total})^\gamma} = C \tag{A.3}$$

$$dp = \left.\frac{dp_{total}}{d\rho_{total}}\right|_0 d\rho \Rightarrow p = \left.\frac{dp_{total}}{d\rho_{total}}\right|_0 \rho \tag{A.4}$$

$$p = c_\infty{}^2 \rho \left.\frac{dp_{total}}{d\rho_{total}}\right|_0 = \gamma C(\rho_{total})^{\gamma-1} = \gamma C \frac{(\rho_{total})^\gamma}{\rho_{total}} = \gamma \left.\frac{p_{total}}{\rho_{total}}\right|_0 = c_\infty{}^2 \tag{A.5}$$

where c_∞ is the speed of sound in the undisturbed fluid.

Hence, for the pressure and density perturbations,

$$p = c_\infty{}^2 \rho \tag{A.6}$$

Equations of motion

Continuity:

$$\frac{\partial \rho_{total}}{\partial t} + \nabla \cdot \left(\rho_{total} \bar{V}\right) = 0 \tag{A.7}$$

For small perturbations:

$$\rho_{total} = \rho_0 + \rho \tag{A.8}$$

$$\bar{V} = \bar{v} \tag{A.9}$$

Neglecting second order terms,

$$\frac{\partial \rho}{\partial t} + \rho_0 \nabla \cdot \bar{v} = 0 \tag{A.10}$$

Momentum

Euler equations:

$$\frac{D\bar{V}}{DT} = -\frac{\nabla p_{total}}{\rho_{total}} \tag{A.11}$$

For small perturbations:

$$\left(\rho_0 + \rho\right)\frac{D\bar{v}}{Dt} = -\nabla\left(p_0 + p\right) = -\nabla p \tag{A.12}$$

$$\left(\rho_0 + \rho\right)\left(\frac{\partial \bar{v}}{\partial t} + \left(\bar{v} \cdot \nabla\right)\bar{v}\right) = -\nabla p \tag{A.13}$$

where

$$\left(\bar{v} \cdot \nabla\right)\bar{v} = \left(v_1 \frac{\partial}{\partial x_1} + v_2 \frac{\partial}{\partial x_2} + v_3 \frac{\partial}{\partial x_3}\right)\bar{v} \tag{A.14}$$

This results in a second-order term and can be neglected. The perturbation momentum (Euler) equation is:

$$\rho_0 \frac{\partial \bar{v}}{\partial t} = -\nabla p \tag{A.15}$$

Combining the continuity and momentum equations,

$$\frac{\partial \rho}{\partial t} + \rho_0 \nabla \cdot \bar{v} = 0 \tag{A.16}$$

$$\rho_0 \frac{\partial \bar{v}}{\partial t} = -\nabla p \tag{A.17}$$

Single-field formulations

Pressure Formulation:

Differentiating momentum equation with respect to time (interchanging the order of differentiations):

$$\frac{\partial^2 \rho}{\partial t^2} + \rho_0 \nabla \cdot \left(\frac{\partial \bar{v}}{\partial t} \right) = 0 \tag{A.18}$$

Substituting from the continuity equation,

$$\frac{\partial^2 \rho}{\partial t^2} + \rho_0 \nabla \cdot \left(\frac{\nabla p}{\rho_0} \right) = 0 \Rightarrow \frac{\partial^2 \rho}{\partial t^2} + \nabla^2 p = 0 \tag{A.19}$$

and express $\frac{\partial^2 \rho}{\partial t^2}$ in terms of p:

$$\frac{\partial \rho}{\partial t} = \frac{\partial \rho}{\partial p} \frac{\partial p}{\partial t} = \frac{1}{c_\infty} \frac{\partial p}{\partial t} \Rightarrow \frac{\partial^2 \rho}{\partial t^2} = \frac{1}{c_\infty^{\,2}} \frac{\partial^2 p}{\partial t^2} \tag{A.20}$$

Thus, the acoustic pressure equation is:

$$\frac{1}{c_\infty^{\,2}} \frac{\partial^2 p}{\partial t^2} = \nabla^2 p \tag{A.21}$$

with boundary conditions (from the Euler equation):

$\nabla p = -\rho_0 \frac{\partial \bar{v}}{\partial t}$ on the boundary, when velocity perturbations are known (moving boundary walls in an enclosure). Alternatively, the pressure disturbance $p(x_1, x_2, x_3, t)$ can be defined on the boundary.

A velocity potential formulation:

Starting with the perturbations and continuity equations again we apply the curl operator to the Euler equation:

$$\frac{\partial \rho}{\partial t} + \rho_0 \nabla \cdot \bar{v} = 0 \tag{A.22}$$

$$\nabla \times \left(\rho_0 \frac{\partial \bar{v}}{\partial t} = -\nabla p \right) \Rightarrow \rho_0 \frac{\partial (\nabla \times \bar{v})}{\partial t} = -\nabla \times \nabla p = 0 \tag{A.23}$$

Thus,

$$\frac{\partial (\nabla \times \bar{v})}{\partial t} = 0 \Rightarrow (\nabla \times \bar{v}) = 0 \tag{A.24}$$

The perturbation velocity field is irrotational.

The zero constant value for the curl of the velocity perturbation vector is due to the fact that at time zero, before any excitation is applied, there are no perturbations, and the perturbation velocities are zero.

If $\nabla \times \bar{v} = 0$

Then the velocity vector can be expressed as a gradient of some potential function:

$\bar{v} = \nabla \phi$

The scalar function $\phi(x_1, x_2, x_3, t)$ is defined as the velocity potential.

Substitution into the continuity equation,

$$\frac{\partial \rho}{\partial t} + \rho_0 \nabla^2 \phi = 0 \tag{A.25}$$

$$\rho_0 \frac{\partial(\nabla \phi)}{\partial t} = -\nabla p \Rightarrow \nabla\left(\rho_0 \frac{\partial \phi}{\partial t} + p\right) = 0 \tag{A.26}$$

Recall that the reference density is constant throughout the fluid before perturbations. Before perturbations begin, the perturbation pressure and velocity are zero. Hence,

$$\rho_0 \frac{\partial \phi}{\partial t} + p = 0 \Rightarrow p = -\rho_0 \frac{\partial \phi}{\partial t} \tag{A.27}$$

Returning to the continuity equation, expressing the density perturbation in terms of pressure perturbation, and then substitute the previous relationship for the pressure in terms of velocity potential.

$$\frac{\partial \rho}{\partial t} = \frac{\partial \rho}{\partial p}\frac{\partial p}{\partial t} = -\rho_0 \frac{1}{c_\infty{}^2}\frac{\partial^2 \phi}{\partial t^2} \tag{A.28}$$

substitution into the continuity equation leads to

$$\frac{1}{c_\infty{}^2}\frac{\partial^2 \phi}{\partial t^2} = \nabla^2 \phi \tag{A.29}$$

Boundary conditions:

When velocity on the boundary is known (due to motion of the boundary)

$\bar{v} = \nabla\phi$ on the boundary, or alternatively, if pressure disturbance is given on the boundary, then

$$\frac{\partial\phi}{\partial t} = -\frac{p}{\rho_0} \tag{A.30}$$

Weak forms – the basis for Finite Element Analysis

The differential equation,

$$\frac{1}{c_\infty^{\,2}}\frac{\partial^2 p}{\partial t^2} = \nabla^2 p \qquad \rightarrow \quad \nabla^2 p - \frac{1}{c_\infty^{\,2}}\frac{\partial^2 p}{\partial t^2} = 0 \tag{A.31}$$

multiply by a scalar function $\delta p(x_1, x_2, x_3, t)$ and integrate over the volume of the fluid,

$$\iiint_\Omega \delta p \nabla^2 p \cdot d\Omega - \frac{1}{c_\infty^{\,2}} \iiint_\Omega \delta p \frac{\partial^2 p}{\partial t^2} d\Omega = 0 \tag{A.32}$$

Review of some vector integral relations:

Gauss Theorem (for a vector field $\bar{A}$ in a volume Ω with surface (boundary) Σ):

$$\iiint_\Omega \nabla \cdot \bar{A} d\Omega = \iint_\Sigma \bar{A} \cdot \bar{n} d\Sigma \tag{A.33}$$

where $\bar{n}$ is a unit vector normal to the boundary surface and pointing out of the enclosed volume of fluid.

To integrate $\iiint_\Omega \delta p \nabla^2 p \cdot d\Omega$ using Gauss Theorem, we can define a vector field:

$$\bar{A} = \delta p \cdot \nabla p \tag{A.34}$$

In this case

$$\nabla \cdot \overline{A} = \nabla \delta p \cdot \nabla p + \delta p \cdot \nabla^2 p \tag{A.35}$$

Thus, from Gauss's Theorem

$$\iiint_{\Omega} \left(\nabla \cdot \overline{A}\right) d\Omega = \iiint_{\Omega} \left(\nabla \delta p \cdot \nabla p + \delta p \cdot \nabla^2 p\right) d\Omega = \iint_{\Sigma} \delta p \nabla p \cdot \overline{n} d\Sigma \tag{A.36}$$

Then

$$\iiint_{\Omega} \left(\delta p \cdot \nabla^2 p\right) d\Omega = \iint_{\Sigma} \delta p \nabla p \cdot \overline{n} d\Sigma - \iiint_{\Omega} \nabla \delta p \cdot \nabla p d\Omega \tag{A.37}$$

Note that the directional derivative:

$$\nabla p \cdot \overline{n} = \frac{\partial p}{\partial n}$$

substituting into the integral equation above we get the final weak form:

$$\iint_{\Sigma} \delta p \frac{\partial p}{\partial n} d\Sigma - \iiint_{\Omega} \nabla \delta p \cdot \nabla p d\Omega - \frac{1}{c_{\infty}^{\ 2}} \iiint_{\Omega} \delta p \frac{\partial^2 p}{\partial t^2} d\Omega = 0 \tag{A.38}$$

Note the symmetry in this form if we use the same spatial functions $N_i(x_1, x_2, x_3)$ to approximate the two fields p and δp.

If we use any approximation of the form

$$p(x_i, t) = \{N_1(x_i) \quad N_2(x_i) \quad \ldots \quad N_n(x_i)\} \begin{Bmatrix} q_1(t) \\ q_2(t) \\ \vdots \\ q_n(t) \end{Bmatrix} = \{N\}^T \{q\} \tag{A.39}$$

$$\delta p(x_i,t) = \{N_1(x_i) \quad N_2(x_i) \quad \cdots \quad N_n(x_i)\} \begin{Bmatrix} \delta q_1(t) \\ \delta q_2(t) \\ \vdots \\ \delta q_n(t) \end{Bmatrix} = \{N\}^T \{\delta q\} \tag{A.40}$$

The gradients:

$$\nabla p(x_i,t) = \begin{bmatrix} \dfrac{\partial \{N\}^T}{\partial x_1} \\ \dfrac{\partial \{N\}^T}{\partial x_2} \\ \dfrac{\partial \{N\}^T}{\partial x_3} \end{bmatrix} \{q(t)\} \tag{A.41}$$

$$\nabla \delta p(x_i,t) = \begin{bmatrix} \dfrac{\partial \{N\}^T}{\partial x_1} \\ \dfrac{\partial \{N\}^T}{\partial x_2} \\ \dfrac{\partial \{N\}^T}{\partial x_3} \end{bmatrix} \{\delta q(t)\} \tag{A.42}$$

In the volume integral, then

$$\nabla \delta p \cdot \nabla p = \{\delta q\}^T \begin{bmatrix} \dfrac{\partial \{N\}}{\partial x_1} & \dfrac{\partial \{N\}}{\partial x_2} & \dfrac{\partial \{N\}}{\partial x_3} \end{bmatrix} \begin{bmatrix} \dfrac{\partial \{N\}^T}{\partial x_1} \\ \dfrac{\partial \{N\}^T}{\partial x_2} \\ \dfrac{\partial \{N\}^T}{\partial x_3} \end{bmatrix} \{q(t)\} \tag{A.43}$$

which leads to

$$\nabla \delta p \cdot \nabla p =$$
$$\{\delta q\}^T \left[\frac{\partial \{N\}}{\partial x_1} \frac{\partial \{N\}^T}{\partial x_1} + \frac{\partial \{N\}}{\partial x_2} \frac{\partial \{N\}^T}{\partial x_2} + \frac{\partial \{N\}}{\partial x_3} \frac{\partial \{N\}^T}{\partial x_3} \right] \{q(t)\}$$
$$= \{\delta q\}^T [k] \{q(t)\} \tag{A.44}$$

where $[k]$ is a symmetric matrix.

Similarly,

$$\delta p \frac{\partial^2 p}{\partial t^2} = \{\delta q(t)\}^T \{N\} \{N\}^T \{\ddot{q}(t)\} = \{\delta q(t)\}^T [m] \{\ddot{q}(t)\} \tag{A.45}$$

where $[m]$ is symmetric.

Appendix B: The Triangular Acoustic Finite Element

For a linear C^0 acoustic triangle, with nodes 1, 2, and 3 in counter-clockwise cyclic order

The area coordinates are,

$$x = \{N_1(\xi,\eta) \quad N_2(\xi,\eta) \quad N_3(\xi,\eta)\}\begin{Bmatrix} x_1 \\ x_2 \\ x_3 \end{Bmatrix} \tag{B.1}$$

$$y = \{N_1(\xi,\eta) \quad N_2(\xi,\eta) \quad N_3(\xi,\eta)\}\begin{Bmatrix} y_1 \\ y_2 \\ y_3 \end{Bmatrix} \tag{B.2}$$

where

$$\begin{aligned} N_1(\xi,\eta) &= 1-\xi-\eta \\ N_2(\xi,\eta) &= \xi \\ N_3(\xi,\eta) &= \eta \end{aligned} \tag{B.3}$$

The Jacobian of the transformation is then

$$J = \begin{bmatrix} \frac{\partial x}{\partial \xi} & \frac{\partial x}{\partial \eta} \\ \frac{\partial y}{\partial \xi} & \frac{\partial y}{\partial \xi} \end{bmatrix} \tag{B.4}$$

Using equations B.1 through B.3,

$$\frac{\partial x}{\partial \xi} = -x_1 + x_2 \tag{B.5}$$

$$\frac{\partial y}{\partial \xi} = -y_1 + y_2$$

$$\frac{\partial x}{\partial \eta} = -x_1 + x_3$$

$$\frac{\partial y}{\partial \eta} = -y_1 + y_3 \tag{B.6}$$

Thus

$$J = \begin{bmatrix} x_2 - x_1 & y_2 - y_1 \\ x_3 - x_1 & y_3 - y_1 \end{bmatrix} \tag{B.7}$$

and

$$\det J = \left((x_2 - x_1)(y_3 - y_1) - (x_3 - x_1)(y_2 - y_1)\right) = 2A \tag{B.8}$$

where A is the area of the triangle.

Two area integrals have to be evaluated for the triangle:

$$\iint_A \delta\dot{p}(x,y) \cdot p(x,y)dxdy \tag{B.9}$$

and

$$\iint_A \nabla\delta p(x,y) \cdot \nabla p(x,y)dxdy \tag{B.10}$$

Let

$$p = \{N_1(\xi,\eta) \quad N_2(\xi,\eta) \quad N_3(\xi,\eta)\}\begin{Bmatrix} p_1 \\ p_2 \\ p_3 \end{Bmatrix} \tag{B.11}$$

and

$$\delta p = \{N_1(\xi,\eta) \quad N_2(\xi,\eta) \quad N_3(\xi,\eta)\}\begin{Bmatrix} \delta p_1 \\ \delta p_2 \\ \delta p_3 \end{Bmatrix} \tag{B.12}$$

Then

$$\iint_A \delta p(x,y)\cdot \ddot{p}(x,y)dxdy =$$

$$\iint_A \{\delta p_1 \quad \delta p_2 \quad \delta p_3\}\begin{Bmatrix} N_1 \\ N_2 \\ N_3 \end{Bmatrix}\{N_1 \quad N_2 \quad N_3\}\begin{Bmatrix} \ddot{p}_1 \\ \ddot{p}_2 \\ \ddot{p}_3 \end{Bmatrix}\det J\cdot d\xi d\eta$$

(B.13)

$$\iint_A \delta p(x,y)\cdot p(x,y)dxdy = \{\delta p_1 \quad \delta p_2 \quad \delta p_3\}[m]\begin{Bmatrix} \ddot{p}_1 \\ \ddot{p}_2 \\ \ddot{p}_3 \end{Bmatrix} =$$

$$\{\delta p_1 \quad \delta p_2 \quad \delta p_3\}\iint_A \begin{Bmatrix} N_1 \\ N_2 \\ N_3 \end{Bmatrix}\{N_1 \quad N_2 \quad N_3\}\det J\cdot d\xi d\eta \begin{Bmatrix} \ddot{p}_1 \\ \ddot{p}_2 \\ \ddot{p}_3 \end{Bmatrix} \qquad \text{(B.14)}$$

where

$$[m] = \iint_A \begin{bmatrix} N_1N_1 & N_1N_2 & N_1N_3 \\ N_1N_2 & N_2N_2 & N_2N_3 \\ N_1N_3 & N_2N_3 & N_3N_3 \end{bmatrix}\det J\cdot d\xi d\eta \qquad \text{(B.15)}$$

Note that in (B.13) through (B.15), N is a function of (ξ,η).

The following integration formula for integrals over triangles using area coordinates can be used,

$$\iint_A \xi^a\eta^b d\xi d\eta = \frac{a!b!}{(a+b+2)!}2A \qquad \text{(B.16)}$$

Integration of the terms of the $[m]$ matrix for the element leads to

$$[m] = \begin{bmatrix} 1/6 & 1/12 & 1/12 \\ & 1/6 & 1/12 \\ Sym & & 1/6 \end{bmatrix} \qquad \text{(B.17)}$$

The area integral

$$\iint_A \nabla \delta p(x,y) \cdot \nabla p(x,y) dx dy \tag{B.18}$$

for a triangular linear pressure element is obtained as follows,

First converting from x, y coordinates to area ξ, η coordinates,

$$\nabla p = \begin{Bmatrix} \frac{\partial p}{\partial x} \\ \frac{\partial p}{\partial y} \end{Bmatrix} = \begin{Bmatrix} \frac{\partial p}{\partial \xi}\frac{\partial \xi}{\partial x} + \frac{\partial p}{\partial \eta}\frac{\partial \eta}{\partial x} \\ \frac{\partial p}{\partial \xi}\frac{\partial \xi}{\partial y} + \frac{\partial p}{\partial \eta}\frac{\partial \eta}{\partial y} \end{Bmatrix} = \begin{bmatrix} \frac{\partial \xi}{\partial x} & \frac{\partial \eta}{\partial x} \\ \frac{\partial \xi}{\partial y} & \frac{\partial \eta}{\partial y} \end{bmatrix} \begin{Bmatrix} \frac{\partial p}{\partial \xi} \\ \frac{\partial p}{\partial \eta} \end{Bmatrix} = J^{-1} \begin{Bmatrix} \frac{\partial p}{\partial \xi} \\ \frac{\partial p}{\partial \eta} \end{Bmatrix} \tag{B.19}$$

and expressing the area coordinates as functions of x and y,

$$\begin{aligned} N_1(x,y) &= \frac{1}{2A}\{(y_2 - y_3)x + (x_3 - x_2)y + (y_3 x_2 - x_3 y_2)\} \\ N_2(x,y) &= \frac{1}{2A}\{(y_3 - y_1)x + (x_1 - x_3)y + (y_1 x_3 - x_1 y_3)\} \\ N_3(x,y) &= \frac{1}{2A}\{(y_1 - y_2)x + (x_2 - x_1)y + (y_2 x_1 - x_2 y_1)\} \end{aligned} \tag{B.20}$$

where from B.8,

$$2A = (x_3 - x_2)(y_1 - y_2) - (x_1 - x_2)(y_3 - y_2)$$

To express $\nabla p = \begin{Bmatrix} \frac{\partial p}{\partial x} \\ \frac{\partial p}{\partial x} \end{Bmatrix}$ in local area coordinates, chain-rule differentiation has to be used

$$\frac{\partial p}{\partial x} = \frac{\partial p}{\partial \xi}\frac{\partial \xi}{\partial x} + \frac{\partial p}{\partial \eta}\frac{\partial \eta}{\partial x} \tag{B.21}$$

Since

$$\xi = N_2(x,y) \tag{B.22}$$

and

$$\eta = N_3(x,y) \tag{B.23}$$

$$\nabla p = \begin{Bmatrix} \frac{\partial p}{\partial x} \\ \frac{\partial p}{\partial y} \end{Bmatrix} = \frac{1}{2A}\begin{bmatrix} (y_3 - y_1) & (y_1 - y_2) \\ (x_1 - x_3) & (x_2 - x_1) \end{bmatrix} \begin{Bmatrix} \frac{\partial p}{\partial \xi} \\ \frac{\partial p}{\partial \eta} \end{Bmatrix} \tag{B.24}$$

Since

$$p = \begin{Bmatrix} 1-\xi-\eta & \xi & \eta \end{Bmatrix} \begin{Bmatrix} p_1 \\ p_2 \\ p_3 \end{Bmatrix} \tag{B.25}$$

and

$$\delta p = \begin{Bmatrix} 1-\xi-\eta & \xi & \eta \end{Bmatrix} \begin{Bmatrix} \delta p_1 \\ \delta p_2 \\ \delta p_3 \end{Bmatrix} \tag{B.26}$$

then

$$\begin{Bmatrix} \frac{\partial p}{\partial \xi} \\ \frac{\partial p}{\partial \eta} \end{Bmatrix} = \begin{bmatrix} -1 & 1 & 0 \\ -1 & 0 & 1 \end{bmatrix} \begin{Bmatrix} p_1 \\ p_2 \\ p_3 \end{Bmatrix} \tag{B.27}$$

$$\begin{Bmatrix} \frac{\partial \delta p}{\partial \xi} \\ \frac{\partial \delta p}{\partial \eta} \end{Bmatrix} = \begin{bmatrix} -1 & 1 & 0 \\ -1 & 0 & 1 \end{bmatrix} \begin{Bmatrix} \delta p_1 \\ \delta p_2 \\ \delta p_3 \end{Bmatrix} \tag{B.28}$$

Finally substituting into equation B.18, it is shown that for a triangular element

$$\iint_A \nabla \delta p(x,y) \cdot \nabla p(x,y) dx dy =$$

$$\begin{Bmatrix}\delta p_1\\ \delta p_2\\ \delta p_3\end{Bmatrix}^T \cdot \frac{1}{2A}\iint_A \begin{bmatrix}-1 & -1\\ 1 & 0\\ 0 & 1\end{bmatrix}\begin{bmatrix}(y_3-y_1) & (x_1-x_3)\\ (y_1-y_2) & (x_2-x_1)\end{bmatrix}\cdot$$

$$\begin{bmatrix}(y_3-y_1) & (y_1-y_2)\\ (x_1-x_3) & (x_2-x_1)\end{bmatrix}\begin{bmatrix}-1 & 1 & 0\\ -1 & 0 & 1\end{bmatrix} d\xi d\eta \cdot \begin{Bmatrix}p_1\\ p_2\\ p_3\end{Bmatrix}$$

(B.29)

Thus, for a triangular element,

$$\iint_A \nabla \delta p(x,y)\cdot \nabla p(x,y)dxdy = \begin{Bmatrix}\delta p_1\\ \delta p_2\\ \delta p_3\end{Bmatrix}[k]\begin{Bmatrix}p_1\\ p_2\\ p_3\end{Bmatrix} \tag{B.30}$$

where

$$[k]=\frac{1}{2}\begin{bmatrix}-1 & -1\\ 1 & 0\\ 0 & 1\end{bmatrix}\begin{bmatrix}(y_3-y_1) & (x_1-x_3)\\ (y_1-y_2) & (x_2-x_1)\end{bmatrix}\begin{bmatrix}(y_3-y_1) & (y_1-y_2)\\ (x_1-x_3) & (x_2-x_1)\end{bmatrix}\begin{bmatrix}-1 & 1 & 0\\ -1 & 0 & 1\end{bmatrix} \tag{B.31}$$

It is also noted that

$$(y_3-y_1)^2+(x_1-x_3)^2 = {L_{13}}^2 \tag{B.32}$$

$$(y_1-y_2)^2+(x_2-x_1)^2 = {L_{12}}^2 \tag{B.33}$$

$$(y_3-y_1)(y_1-y_2)+(x_1-x_3)(x_2-x_1)=\frac{1}{2}({L_{23}}^2-{L_{13}}^2-{L_{12}}^2) \tag{B.34}$$

where

L_{ij} is the distance between vertex i and vertex j on the triangle.

For a triangular acoustic element with nodes 1,2, and 3 counter-clockwise at its vertices, the vertex coordinates being $x_1, y_1, x_2, y_2, x_3, y_3$ then

$$L_{13}^{\ 2} = (y_3 - y_1)^2 + (x_1 - x_3)^2$$
$$L_{12}^{\ 2} = (y_1 - y_2)^2 + (x_2 - x_1)^2$$
$$L_{23}^{\ 2} = (y_3 - y_2)^2 + (x_2 - x_3)^2$$
(B.35)

and

$$A = \frac{1}{2}((x_2 - x_1)(y_3 - y_1) - (x_3 - x_1)(y_2 - y_1)) \tag{B.37}$$

Performing the matrix multiplication in B.31 and substituting the identities in B.32-34, the stiffness matrix [k] can then be written as

$$[k] = \frac{1}{2}\begin{bmatrix} L_{23}^{\ 2} & \frac{1}{2}(-L_{13}^{\ 2} - L_{23}^{\ 2} + L_{12}^{\ 2}) & \frac{1}{2}(-L_{23}^{\ 2} + L_{13}^{\ 2} - L_{12}^{\ 2}) \\ & L_{13}^{\ 2} & \frac{1}{2}(L_{23}^{\ 2} - L_{13}^{\ 2} - L_{12}^{\ 2}) \\ symm. & & L_{12}^{\ 2} \end{bmatrix} \tag{B.38}$$

and the mass matrix as given in B.17 is then

$$[m] = \frac{A}{c_\infty^2}\begin{bmatrix} 1/6 & 1/12 & 1/12 \\ & 1/6 & 1/12 \\ Symm. & & 1/6 \end{bmatrix}$$

with c_∞^2 being the speed of sound of the fluid concerned.

Appendix C: The Structural-Acoustic Coupling Terms

The weak form of the acoustic field problem is

$$\iint_{\Sigma} \delta p \frac{\partial p}{\partial n} d\Sigma - \iiint_{\Omega} \nabla \delta p \cdot \nabla p d\Omega - \frac{1}{c_{\infty}^{\ 2}} \iiint_{\Omega} \delta p \frac{\partial^2 p}{\partial t^2} d\Omega = 0 \tag{C.1}$$

On the boundary between the acoustic enclosure and structure that surrounds it the surface integral is

$$\iint_{\Sigma} \delta p \frac{\partial p}{\partial n} d\Sigma \tag{C.2}$$

The Euler equation for small perturbations is

$$\rho_0 \frac{\partial \overline{u}}{\partial t} = -\nabla p \tag{C.3}$$

Equation C.3 makes it possible to relate the normal derivative of pressure on the boundary $\partial p/\partial n$ to the motion of that boundary. Multiplying by a direction vector normal to the surface (and pointing outwards),

$$\rho_0 \frac{\partial \overline{u}}{\partial t} \cdot \overline{n} = -\nabla p \cdot \overline{n} = -\frac{\partial p}{\partial n} \tag{C.4}$$

thus

$$\frac{\partial p}{\partial n} = -\rho_0 \frac{\partial u_n}{\partial t} \tag{C.5}$$

where $\overline{u} \cdot \overline{n} = u_n$ is the velocity component normal to the surface in the outwards direction. (u here denotes velocity, not displacement as in the structural finite element formulations).

For a triangular acoustic element with nodes 1-2-3 (counter clockwise) touching a beam element A-B, the derivation here will be limited to the case where the nodes A,B and the nodes 1,2 coincide, respectively.

The surface integral in this 2D case becomes a line integral from A to B (1 to 2)

$$\iint_{\Sigma} \delta p \frac{\partial p}{\partial n} d\Sigma = -\rho_0 \int_{1}^{2} \delta p \frac{\partial u_n}{\partial t} d\hat{x} \tag{C.6}$$

For a 2D beam element in local coordinates ξ, η, standard FE interpolation for the transverse displacement is given by

$$w(\xi) = \begin{Bmatrix} N_1^s(\xi) & N_2^s(\xi) & N_3^s(\xi) & N_4^s(\xi) \end{Bmatrix} \begin{Bmatrix} w_1 \\ L\theta_1 \\ w_2 \\ L\theta_2 \end{Bmatrix} \tag{C.7}$$

where for $\frac{\hat{x}}{L} = \xi \in [0,1]$:

$$\begin{aligned} N_1^s(\xi) &= 1 - 3\xi^2 + 2\xi^3 \\ N_2^s(\xi) &= \xi - 2\xi^2 + \xi^3 \\ N_3^s(\xi) &= 3\xi^2 - 2\xi^3 \\ N_4^s(\xi) &= -\xi^2 + \xi^3 \end{aligned} \tag{C.8}$$

Along the same line (1,2) the acoustic pressure disturbance is linear

$$\delta p(\xi) = \begin{Bmatrix} 1-\xi & \xi \end{Bmatrix} \begin{Bmatrix} \delta p_1 \\ \delta p_2 \end{Bmatrix} = \begin{Bmatrix} N_1^a(\xi) & N_1^a(\xi) \end{Bmatrix} \begin{Bmatrix} \delta p_1 \\ \delta p_2 \end{Bmatrix} = \begin{Bmatrix} \delta p_1 & \delta p_2 \end{Bmatrix} \begin{Bmatrix} N_1^a(\xi) \\ N_2^a(\xi) \end{Bmatrix} \tag{C.9}$$

Using

$$d\hat{x} = L \cdot d\xi \tag{C.10}$$

we have

$$\iint_{\Sigma} \delta p \frac{\partial p}{\partial n} d\Sigma = -\rho_0 \int_1^2 \delta p \frac{\partial u_n}{\partial t} d\hat{x} = \{\delta p_1 \quad \delta p_2\} \cdot \rho_0 L \cdot$$

$$\int_0^1 \begin{Bmatrix} N_1^a(\xi) \\ N_2^a(\xi) \end{Bmatrix} \{N_1^s(\xi) \quad N_2^s(\xi) \quad N_3^s(\xi) \quad N_4^s(\xi)\} d\xi \cdot \begin{Bmatrix} \ddot{w}_1 \\ L\ddot{\theta}_1 \\ \ddot{w}_2 \\ L\ddot{\theta}_2 \end{Bmatrix} \tag{C.11}$$

Note that there is a change of sign due to the fact that the transverse displacements *w* are given here as pointing into the acoustic enclosure, while the surface integral takes as positive displacements pointing out.

For a beam element oriented with respect to the global x-axis by an angle Λ, and including both axial and transverse deformations, transformation from local to global displacements leads to

A direction vector along the axis of the beam

$$\begin{Bmatrix} \cos\Lambda \\ \sin\Lambda \end{Bmatrix} \tag{C.12}$$

where

$$\cos\Lambda = \frac{x_B - x_A}{L}$$
$$\cos\Lambda = \frac{y_B - y_A}{L} \tag{C.13}$$

and

$$L = \sqrt{(x_B - x_A)^2 + (y_B - y_A)^2} \tag{C.14}$$

In global coordinates the contributions of the transverse motion w to motions u_x, u_y is

$$\begin{Bmatrix} u_x \\ u_y \end{Bmatrix} = \begin{bmatrix} c\Lambda & -s\Lambda \\ s\Lambda & c\Lambda \end{bmatrix} \begin{Bmatrix} u \\ w \end{Bmatrix} \Rightarrow \begin{Bmatrix} u \\ w \end{Bmatrix} = \begin{bmatrix} c\Lambda & s\Lambda \\ -s\Lambda & c\Lambda \end{bmatrix} \begin{Bmatrix} u_x \\ u_y \end{Bmatrix} \tag{C.15}$$

Then,

$$\begin{Bmatrix} w_1 \\ L\theta_1 \\ w_2 \\ L\theta_2 \end{Bmatrix} = \begin{bmatrix} -s\Lambda & c\Lambda & 0 & 0 & 0 & 0 \\ 0 & 0 & L & 0 & 0 & 0 \\ 0 & 0 & 0 & -s\Lambda & c\Lambda & 0 \\ 0 & 0 & 0 & 0 & 0 & L \end{bmatrix} \begin{Bmatrix} u_{x1} \\ u_{y1} \\ \theta_1 \\ u_{x2} \\ u_{y2} \\ \theta_2 \end{Bmatrix} \tag{C.16}$$

Returning to equation C.11, we now have,

$$\iint_{\Sigma} \delta p \frac{\partial p}{\partial n} d\Sigma = \{\delta p_1 \quad \delta p_2\} \cdot \rho_0 L \int_0^1 \begin{Bmatrix} N_1^a(\xi) \\ N_2^a(\xi) \end{Bmatrix} \{N_1^s(\xi) \quad N_2^s(\xi) \quad N_3^s(\xi) \quad N_4^s(\xi)\} d\xi \cdot$$

$$\begin{bmatrix} -s\Lambda & c\Lambda & 0 & 0 & 0 & 0 \\ 0 & 0 & L & 0 & 0 & 0 \\ 0 & 0 & 0 & -s\Lambda & c\Lambda & 0 \\ 0 & 0 & 0 & 0 & 0 & L \end{bmatrix} \begin{Bmatrix} \ddot{u}_{x1} \\ \ddot{u}_{y1} \\ \ddot{\theta}_1 \\ \ddot{u}_{x2} \\ \ddot{u}_{y2} \\ \ddot{\theta}_2 \end{Bmatrix} \tag{C.17}$$

Expanding the term from C.17 above,

$$\int_0^1 \begin{Bmatrix} N_1^a(\xi) \\ N_2^a(\xi) \end{Bmatrix} \{N_1^s(\xi) \quad N_2^s(\xi) \quad N_3^s(\xi) \quad N_4^s(\xi)\} d\xi$$

we arrive at

$$\int_0^1 \begin{bmatrix} (1-\xi)(1-3\xi^2+2\xi^3) & (1-\xi)(\xi-2\xi^2+\xi^3) & (1-\xi)(3\xi^2-2\xi^3) & (1-\xi)(-\xi^2+\xi^3) \\ \xi(1-3\xi^2+2\xi^3) & \xi(\xi-2\xi^2+\xi^3) & \xi(3\xi^2-2\xi^3) & \xi(-\xi^2+\xi^3) \end{bmatrix} d\xi$$

Solving the integral gives

$$\int_0^1 \begin{Bmatrix} N_1^a(\xi) \\ N_2^a(\xi) \end{Bmatrix} \{ N_1^s(\xi) \quad N_2^s(\xi) \quad N_3^s(\xi) \quad N_4^s(\xi) \} d\xi = \begin{bmatrix} 7/20 & 1/20 & 3/20 & -1/30 \\ 3/20 & 1/30 & 7/20 & -1/20 \end{bmatrix}$$

And the matrix multiplication

$$\begin{bmatrix} 7/20 & 1/20 & 3/20 & -1/30 \\ 3/20 & 1/30 & 7/20 & -1/20 \end{bmatrix} \begin{bmatrix} -s\Lambda & c\Lambda & 0 & 0 & 0 & 0 \\ 0 & 0 & L & 0 & 0 & 0 \\ 0 & 0 & 0 & -s\Lambda & c\Lambda & 0 \\ 0 & 0 & 0 & 0 & 0 & L \end{bmatrix}$$

gives

$$\begin{bmatrix} -7s\Lambda/20 & 7c\Lambda/20 & L/20 & -3s\Lambda/20 & 3c\Lambda/20 & -L/30 \\ -3s\Lambda/20 & 3c\Lambda/20 & L/30 & -7s\Lambda/20 & 7c\Lambda/20 & -L/20 \end{bmatrix}$$

Then, the contribution to the surface integral of a beam and an acoustic element touching it is

$$\iint_\Sigma \delta p \frac{\partial p}{\partial n} d\Sigma =$$

$$\{ \delta p_1 \quad \delta p_2 \} \cdot \rho_0 L \begin{bmatrix} -7s\Lambda/20 & 7c\Lambda/20 & L/20 & -3s\Lambda/20 & 3c\Lambda/20 & -L/30 \\ -3s\Lambda/20 & 3c\Lambda/20 & L/30 & -7s\Lambda/20 & 7c\Lambda/20 & -L/20 \end{bmatrix} \begin{Bmatrix} \ddot{u}_{x1} \\ \ddot{u}_{y1} \\ \ddot{\theta}_1 \\ \ddot{u}_{x2} \\ \ddot{u}_{y2} \\ \ddot{\theta}_2 \end{Bmatrix} \tag{C.18}$$

Or simply,

$$\iint_\Sigma \delta p \frac{\partial p}{\partial n} d\Sigma = \{ \delta p \}^T \cdot \rho_0 [R_{as}] \{ \ddot{q}_s \} \cdot L \tag{C.19}$$

where $\{ \dot{q}_s \}$ is the vector of structural degrees of freedom, and $\{ \delta p \}$ is the vector of virtual changes in the pressure degrees of freedom.

Combining Structural-Acoustic terms.

Recalling from Appendix B that for the area integrals for a single acoustic element are

$$\iint_A \nabla \delta p(x,y) \cdot \nabla p(x,y) dxdy = \begin{Bmatrix} \delta p_1 \\ \delta p_2 \\ \delta p_3 \end{Bmatrix}^T [k] \begin{Bmatrix} p_1 \\ p_2 \\ p_3 \end{Bmatrix}$$

$$\iint_A \delta p(x,y) \cdot \ddot{p}(x,y) dxdy = \{\delta p_1 \quad \delta p_2 \quad \delta p_3\} [m] \begin{Bmatrix} \ddot{p}_1 \\ \ddot{p}_2 \\ \ddot{p}_3 \end{Bmatrix}$$

Assembling contributions from all elements we get the integrals for the complete acoustic cavity

$$\iint_A \nabla \delta p(x,y) \cdot \nabla p(x,y) dxdy = \{\delta p\}^T [K_a] \{p\}$$

$$\frac{1}{c_\infty^2} \iint_A \delta p(x,y) \cdot \ddot{p}(x,y) dxdy = \{\delta p\}^T [M_a] \{\ddot{p}\}$$

FE discretization of the acoustic equations in weak form (from C.1),

$$\iint_\Sigma \delta p \frac{\partial p}{\partial n} d\Sigma - \iiint_\Omega \nabla \delta p \cdot \nabla p d\Omega - \frac{1}{c_\infty^2} \iiint_\Omega \delta p \frac{\partial^2 p}{\partial t^2} d\Omega = 0$$

now leads to

$$\{\delta p\}^T [[M_a] \{\ddot{p}\} + [K_a] \{p\} - \rho_0 [R_{as}] \{\ddot{q}_s\}] = 0 \qquad \text{(C.20)}$$

Then

$$[[M_a] \{\ddot{p}\} + [K_a] \{p\} - \rho_0 [R_{as}] \{\ddot{q}_s\}] = 0 \qquad \text{(C.21)}$$

For the structural part (the beams, assuming viscous damping in the structure and applied external forces) we have

$$\left[[M_s]\{\ddot{q}_s\}+[C_s]\{\dot{q}_s\}+[K_s]\{q_s\}-[R_{as}]^T\{p\}\right]=\{F\} \tag{C.22}$$

The pressure contributions to the structural equations are obtained by integration of pressures over the length of each beam, pressures providing the applied transverse load on the beam.

Thus the final coupled structural–acoustics equations are

$$\begin{bmatrix} M_s & 0 \\ -\rho_0 R_{as} & M_a \end{bmatrix}\begin{Bmatrix} \ddot{q}_s \\ \ddot{p} \end{Bmatrix}+\begin{bmatrix} C_s & 0 \\ 0 & C_a \end{bmatrix}\begin{Bmatrix} \dot{q}_s \\ \dot{p} \end{Bmatrix}+\begin{bmatrix} K_s & -R^T{}_{as} \\ 0 & K_a \end{bmatrix}\begin{Bmatrix} q_s \\ p \end{Bmatrix}=\begin{Bmatrix} F \\ 0 \end{Bmatrix} \tag{C.23}$$

Appendix D: The Second Order Approximation

The second-order approximation is derived from a process comparable to central-differencing second-order derivative approximations. The key idea is to eliminate first-order error terms by manipulating alternative expressions for the desired response.

Let the direct and adjoint solutions of a linear matrix equation be

$$[A]\{x\} = \{b\} \tag{D.1}$$

$$[A]^* \{\eta\} = \{c\} \tag{D.2}$$

where response y can be calculated from either the direct solution $\{x\}$ or the adjoint solution $\{\eta\}$ by

$$y = \{c\}^* \{x\} = \{c\}^* [A]^{-1} \{b\} = \{\eta\}^* \{b\} \tag{D.3}$$

An error $\{\delta x\}$ in the direct solution will result in a corresponding error in the calculated response

$$\delta y_1 = \{c\}^* \{\delta x\} \tag{D.4}$$

and likewise, an error $\{\delta\eta\}$ in the adjoint solution will result in a corresponding error

$$\delta y_2 = \{\delta\eta\}^* \{b\} \tag{D.5}$$

If there are no errors in Eqs. (D.1) and (D.2) and their solution $\{x\}$ and $\{\eta\}$, then the {b} and {c} vectors in Eqs. (D.4) and (D.5) can be replaced by

$$\delta y_1 = \{\eta\}^* [A]\{\delta x\} \tag{D.6}$$

$$\delta y_2 = \{\delta\eta\}^* [A]\{x\} \tag{D.7}$$

Adding (D.6) and (D.7),

$$\delta y_1 + \delta y_2 = \{\eta + \delta\eta\}^T [A]\{x + \delta x\} - \{\eta\}^* [A]\{x\} - \{\delta\eta\}^* [A]\{\delta x\} \tag{D.8}$$

The first two terms are the error in the expression $\{\eta\}^* [A]\{x\}$ when the exact $\{x\}$ and $\{\eta\}$ are replaced by approximate $\{x\} + \{\delta x\}$ and $\{\eta\} + \{\delta\eta\}$. Based on equations D.4-D.8,

$$\delta(\{c\}^* \{x\}) + \delta(\{\eta\}^* \{b\}) - \delta(\{\eta\}^* [A]\{x\}) = -\{\delta\eta\}^* [A]\{\delta x\} \tag{D.9}$$

Equation D.9 is the error in the expression

$$\{c\}^* \{x\} + \{\eta\}^* \{b\} - \{\eta\}^* [A]\{x\} \tag{D.10}$$

when the exact direct and adjoint solutions are replaced by approximate ones. The expression in D.10, when exact direct and adjoint solutions are used together is just the response y because with exact solution Eqs. (D.1) or (D.2) can be substituted into Eq. (D.10) to cancel either $\{\eta\}^* \{b\} - \{\eta\}^* [A]\{x\}$ or $\{c\}^* \{x\} - \{\eta\}^* [A]\{x\}$.